Flavocytochrome b_2:Molecular recognition

Fraser E. Welsh

Thesis presented for the degree of
Doctor of Philosophy
The University of Edinburgh
October 1998

Acknowledgements.

There are a number of people who I would like to thank for their help and support during my three years at Edinburgh University. Professor Stephen Chapman and Dr Graeme Reid for their excellent supervision and encouragement. Dr Alexis Balme for his guidance during my first months in the lab and Dr Stuart Rivers for teaching me everything I know about the "art" of Molecular Biology. I would also like to thank all the members of the Reid-Chapman groups past and present for unreserved help, entertainment, coffee and biscuits!

During my studies I have utilised a number of techniques and I would like to thank the people who helped with experiments and analysis namely, Dr Andrew Munro (University of Edinburgh, fluorimetry and CD), Dr Sharon Kelly and Prof Nick Price (University of Stirling, circular dichroism facility), Dr Alan Cooper (University of Glasgow, calorimetry facility), Prof Malcolm Walkinshaw and Rhiannon Macfie (ICMB, University of Edinburgh) for the molecular modelling studies. I would also like to thank Prof Scott Mathews (Washington University, St Louis, USA) and his group for an excellent crash course in protein crystallography and X-ray diffraction. I should also like to mention the EPSRC for funding throughout the three years.

Finally I would like to thank my fiancée, Ali, and my family without whom I am unlikely to have made it this far.

Abstract.

Flavocytochrome b_2 from *Saccharomyces cerevisiae* is an L-lactate:cytochrome *c* oxidoreductase found in the mitochondrial intermembrane space. The crystal structure has been solved to 2.4 Å showing the enzyme to be a homotetramer of M_r 230 000. Each subunit comprises 511 amino acids and two domains. A cytochrome domain contains protohaem IX and comprises residues 1-100. Residues 101-488 constitute a flavodehydrogenase domain, FDH, which contains FMN. The two domains are tethered by a "hinge" region (residues 92-103). The hinge allows the domains enough movement with respect to each other for efficient intra-protein electron transfer. In the crystal structure residues 295-311 are highly disordered and so not visible. This is a proteolytically sensitive loop for which a function has not been determined. The enzyme has been fully characterised and shown to be a "biological transformer" accepting electrons from strictly 2-electron donor molecules such as L-lactate and passing them one at a time to 1-electron acceptors such as cytochrome *c*. FDH has been independently expressed in *E. coli* allowing accurate characterisation of its properties without interference from the intense absorbance of the cytochrome domain. This has shown that although FDH remains an efficient L-lactate dehydrogenase it has negligible cytochrome *c* reductase activity. This is intriguing as the thermodynamic driving force for electron transfer from FDH to cytochrome *c* , as determined from redox potentials, is greater than $^1/_3$ V. We believe a lack of inter-protein recognition between the two prevents them forming an effective electron transfer complex. The aim of this work was to improve inter-protein recognition by engineering a negatively charged binding site on FDH specific for positively charged molecules such as cytochrome *c*. This was accomplished using Site directed mutagenesis to exchange hydrophobic and positively charged residues for negatively charged or neutral residues. The following mutants were constructed; K201E, L199E, F325E, L199E/K201E, L199E/K296E, K201E/K324A/F325E and L199E/K201E/K324A/F325E. These mutants were characterised using the inorganic molecules $[Co(phen)_3]^{3+}$ and $[Fe(CN)_6]^{3-}$ as artificial electron acceptors. Wild type

FDH has second-order rate constants for $[Fe(CN)_6]^{3-}$ and $[Co(phen)_3]^{3+}$ of $1x10^6$ $M^{-1}s^{-1}$ and $3x10^4$ $M^{-1}s^{-1}$ respectively indicating a preference for negatively charged molecules. However, the triple mutant, K201E/K324A/F325E, has a second-order rate constant with $[Co(phen)_3]^{3+}$ of $8x10^4$ $M^{-1}s^{-1}$. It also has no concentration dependence for $[Fe(CN)_6]^{3-}$ and a maximum rate of only 10 s^{-1}. Thus the specificity of FDH for small inorganic electron acceptors has been altered to favour positively charged molecules. However, these mutants show no improvement in cytochrome *c* reductase activity. Experiments using circular dichroism, fluorescence and isothermal titrations show little improvement in the binding between cytochrome *c* and the mutants. This suggests that something else is preventing electron transfer. The most obvious possibility is steric hindrance caused by the aforementioned loop. It was undertaken to attain the crystal structure of FDH to ascertain the position of the loop. Data sets have been obtained and refinements are ongoing. In the absence of a crystal structure molecular modelling studies were performed to investigate the position of the loop and its effect on the docking of electron acceptors. Results show that the loop is likely to fold over the FMN face of FDH. Modelling the docking of electron acceptors on FDH indicates that smaller inorganic molecules can get to within 7 Å of the FMN. However, the haem of cytochrome *c* can only get to within ~20 Å of the FMN due to the position of the modelled loop. This explains the very slow rates of electron transfer with cytochrome *c* and the much faster rates of electron transfer with $[Fe(CN)_6]^{3-}$ and $[Co(phen)_3]^{3+}$. Further modelling studies have indicated that it may be feasible to replace the loop with 7 glycine residues such that FDH should fold normally but the steric bulk of the loop is removed allowing cytochrome *c* a clear approach to the FMN.

Index.

Figures.

Abbreviations.

Amino acids.

	Code.	symbol.
Alanine	Ala	A
Arginine	Arg	R
Asparagine	Asn	N
Aspartic acid	Asp	D
Cysteine	Cys	C
Glutamic acid	Glu	E
Glutamine	Gln	Q
Glycine	Gly	G
Histidine	His	H
Isoleucine	Ile	I
Leucine	Leu	L
Lysine	Lys	K
Methionine	Met	M
Phenylalanine	Phe	F
Proline	Pro	P
Serine	Ser	S
Threonine	Thr	T
Tryptophan	Trp	W
Tyrosine	Tyr	Y
Valine	Val	V

Oligonucleotides.

A, adenine; T, thymine; C, cytosine; G, guanine.

Mutations.

Amino acid mutations are represented as: code, number→code where the number indicates the position of the residue on the polypeptide chain. Mutant enzymes are referred to as in the following example:

Lys201→Glu would generate the mutant K201E.

Kinetic parameters.

K_m	Michaelis constant
k_{cat}	rate constant under saturating conditions
k_{et}	electron-transfer rate constant
k_2	second-order rate constant
t	time

Standard units.

m	metre	°C	degrees Celsius
g	gram	M	molar
s	second	V	volt
l	litre	Å	angstrom
Da	dalton units		

Textual abbreviations.

Abs	Absorbance
ATP	Adenosine-5′- triphosphate
bpy	2,2′-bipyridine
CD	circular dichroism
dipic	dipicolinato
DNA	deoxyribonucleic acid
dsDNA	double stranded DNA
E. coli	*Escherichia coli*
EDTA	ethylenediaminetetraacetate
FAD	flavin adenine dinucleotide
FDH	flavin binding domain (flavin dehydrogenase)
FDH_{wt}	flavin binding domain (wild type)
FMN	flavin mononucleotide
FUV	far ultraviolet
ΔG	free energy change
GdnHCl	guanidinium hydrochloride
GO	Spinach glycolate oxidase
I	ionic strength
im	imidazole
kb	kilobase
LB	luria broth
LMDH	L-mandelate dehydrogenase
M_r	molecular weight
NAD	nicotinamide adenine dinucleotide
NADP	nicotinamide adenine dinucleotide phosphate
NUV/Vis	near ultraviolet/visible
PAGE	polyacrylamide gel electrophoresis
PEG	polyethylene glycol
phen	1,10-phenanthroline
PMSF	phenylmethylsulphonyl fluoride
S. cerevisiae	*Saccharomyces cerevisiae*
SDS	sodium dodecyl sulphate
ssDNA	single stranded DNA
TB	terrific broth
Temed	N,N,N′,N′-tetramethylethylene diamine
TIM	triose phosphate isomerase
Tris	Tris(hydroxymethyl)aminomethane
UV	ultraviolet
Vis	visible

1. Introduction.

1.1. Biological electron transfer.

Redox chemistry is widespread throughout biology making electron transfer one of the most important processes in biological systems. Typical examples of such processes are: (i) The conversion of light energy to chemical energy in photosynthesis; and (ii) the production of ATP in mitochondria by oxidative phosphorylation, whereby electrons are transferred from NADH/$FADH_2$ to O_2. In both cases, and in the countless others that exist, electron transfer occurs between a number of redox centres *e.g.* haem, flavin, iron-sulphur and copper. These prosthetic groups are contained inside proteins which confer a certain degree of specificity and control over the otherwise indiscriminate redox centres. This prevents short-circuiting of the system which could lead to a decrease in its efficiency *e.g.* in the case of oxidative phosphorylation, failure to produce the optimum number of ATP molecules. It is the structure and properties of these proteins that allow them to exert control over the electron transfer process. Electron transfer between redox centres is often required to occur over long distances (>10Å) because of the surrounding protein matrix. Thus, the distance between redox centres can become a major factor in determining the rate of electron transfer. Other factors which have to be considered are the thermodynamic driving force between the redox centres, the intervening medium, *i.e.* the role played by the amino acids, and the degree of recognition which the proteins have for each other. This final point is the one which underpins this particular research project.

Much research has been undertaken into the factors controlling electron transfer and conflicting opinions have resulted, particularly regarding the route taken by electrons as they are transferred and the exact role played by the intervening medium. A number of reviews have been written on the subject of biological electron transfer (McLendon, 1988; McLendon, 1991; McLendon *et al.*, 1992; Moser *et al.*, 1992; Chapman *et al.*, 1995; Moser *et al.*, 1995; Larsson, 1998) and the following section attempts to introduce background theory and some of the ideas which have been proposed regarding the various regulating factors.

As stated previously there are a number of factors which must be considered when studying the phenomenon of protein mediated electron transfer and these can be discussed in two categories: (i) Thermodynamic factors; and (ii) physical factors. Both of these will be discussed and those points that remain the centre of debate will be highlighted.

1.1.1. Thermodynamic factors.

In order to fully understand the complexities of electron transfer in a redox protein system it is necessary to look at the basic theory as defined by Marcus (1956 & 1965). Equation.1 below describes the electron-transfer event when two bodies A^- and B react.

$$A^- - e^- \rightarrow A$$

$$B + e^- \rightarrow B^-$$

Equation .1. $$A^- + B \rightarrow A + B^-$$

There are two constraints on the reaction: (i) Energy is neither lost nor gained during the transfer process so that the total energy of the system must remain constant until electron-transfer is complete; (ii) according to the Franck-Condon principle an electron-transfer event is fast with respect to the time required for the reactants to change their nuclear configurations. Thus, the products formed must have the same nuclear configurations as the reactants. If this is not the case then a common isoenergetic configuration must be attained which is of higher energy than both the products and reactants. The energy required to reach this state will help determine the rate of electron-transfer *i.e.* the higher the energy the slower the transfer. Looking at Figure 1.1.1. the parabolas represent the combined change in energy of the reactants and the products as the combined nuclear configurations are altered *i.e.* the left hand bowl indicates that the reactants have an optimum combined nuclear configuration where the energy is lowest and that by agitating this configuration the energy of the reactants is increased to a less favourable state. Similarly for the right hand bowl

which represents the products. These have a different optimum nuclear configuration and thus the two are separated on the diagram.

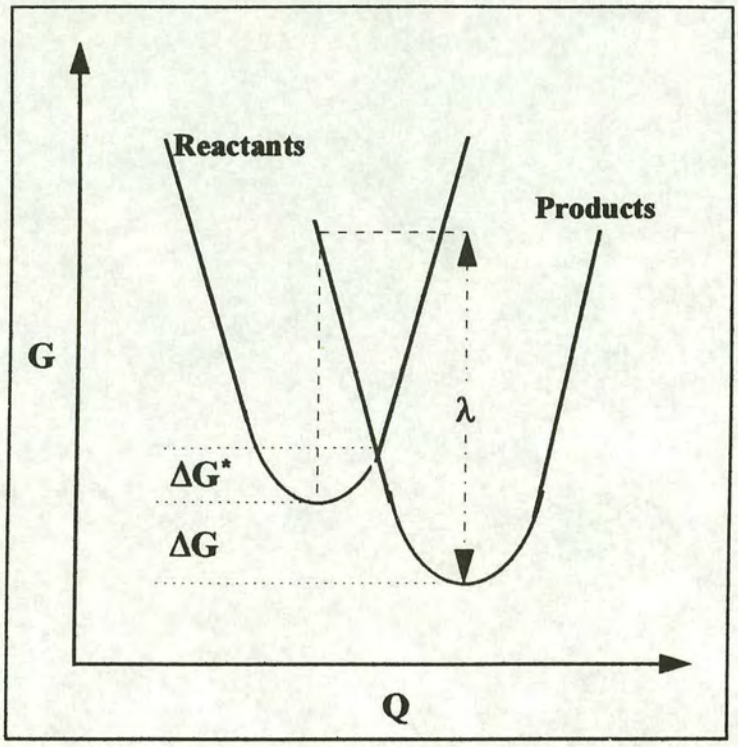

Figure 1.1.1. *Nuclear configuration (Q) vs energy (G) for an electron-transfer reaction.*

From this it can be seen that the rate of electron-transfer depends upon the difference in energy, ΔG, between the optimum nuclear configurations and the energy required to alter the nuclear configuration of the products to that of the reactants, λ. ΔG is referred to as the driving force and is proportional to the difference between the redox potentials of the two reactants, ΔE, (Equation .2).

Equation .2. $\Delta G = -nF\Delta E.$

The reorganisation energy (λ) is related with ΔG to the activation energy, ΔG^* (Equation .3).

Equation .3. $\Delta G^* = (\Delta G + \lambda)^2/4\lambda.$

The rate constant for electron-transfer is related to ΔG^* by Equation .4.

Equation .4. $$k' = k'_o \exp [-\Delta G^*/\kappa T].$$

where κ is the Boltzmann constant, k' is the observed rate of electron-transfer and k'_o is the rate of electron-transfer when ΔG^* is zero.

Since λ is always positive it can be seen that the $(\Delta G + \lambda)$ parameter will determine the rate of electron-transfer. The three possible situations which result are shown schematically in Figure 1.1.2.

- When $(\Delta G + \lambda)$ is greater than zero (normal mode). Here a decrease in ΔG increases the driving force making ΔG^* less positive so increasing the rate of electron-transfer (a).
- When $(\Delta G + \lambda)$ is equal to zero (activationless mode). In this case $\Delta G = -\lambda$, $\Delta G^* = 0$ and so the rate of electron-transfer has reached a maximum (b).
- When $(\Delta G + \lambda)$ is less than zero (inverted mode). Now ΔG becomes more negative therefore, ΔG^* becomes more positive and so the activation barrier increases and the rate slows (c).

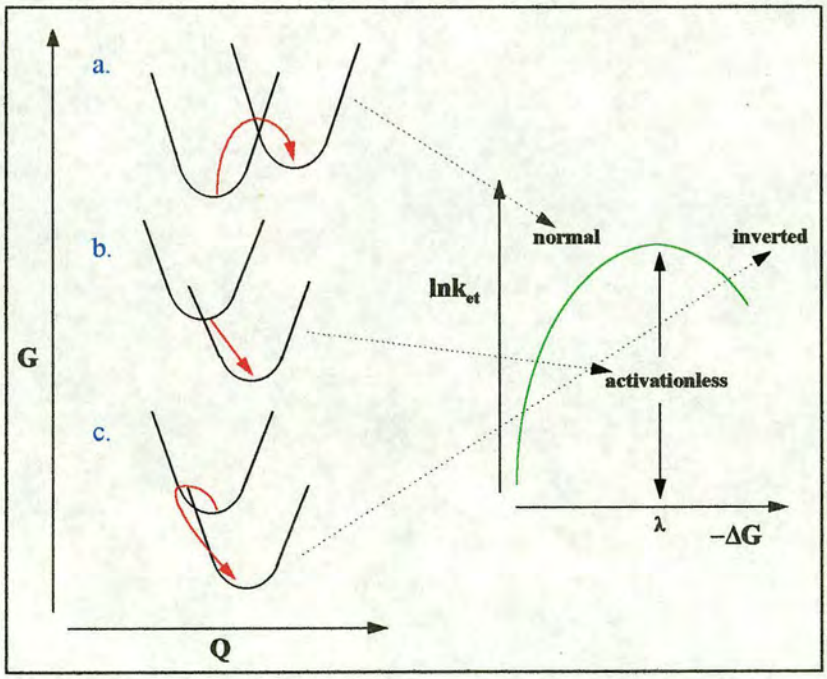

Figure 1.1.2. *(left) Typical energy diagrams for the (a) normal, (b) activationless and (c) inverted regions. The red arrows denote the reaction pathway. (right) The variation of the logarithm of the electron-transfer rate (k) with free energy difference between reactants and products (ΔG).*

Thus, thermodynamically the rate of electron-transfer would seem to be controlled by the activation energy which is dependent on the free energy (ΔG) and the reorganisation energy (λ) of the system in question. While the thermodynamics takes into account the driving force between the two proteins a number of other factors also play an important role.

1.1.2. Physical factors.

For efficient electron transfer to occur between two redox centres in two separate proteins we must see the electron move from its orbital on the donor to the vacant orbital on the acceptor and so the rate of this transfer will be dependent on the degree of overlap of the two electronic wavefunctions involved. This has been shown to decrease exponentially with increase in distance (Beratan *et al.*, 1990) and so the rate of electron-transfer is proportional to the distance between the centres and to the strength of the electronic coupling. The coupling strength is given by the tunnelling matrix element H_{AB}, (Equation .5).

Equation .5. $$H_{AB} = H^{o}_{AB} \exp [-1/2\beta(d-d^{o})].$$

where H^{o}_{AB} is the electronic coupling at close (Van der Waals) contact (d^{o}) and β is the rate of decay ($Å^{-1}$) of electronic coupling over distance d. Electron-transfer will not occur in a vacuum over long distances due to a β value of $2.8Å^{-1}$. Thus, the energy of the electron in the medium must be lowered and so the nature of the medium becomes very important. Research by Dutton and co-workers (Moser *et al.*, 1992) have produced values of β for a protein medium treating it as a homogeneous system and suggesting that it can be applied as such to inter- and intra-protein electron-transfer systems whereby the main factor determining the rate of electron transfer is the distance between the redox centres. By plotting log k′ vs distance, β is determined as the exponential decay coefficient of $1.4Å^{-1}$ and falls between that for a fully covalently bound system ($0.7Å^{-1}$) and that for a vacuum. This suggests that the protein medium is similar to that provided by a frozen organic solvent. If this is the

case then a 1.7Å variation in the distance between redox centres would lead to a 10-fold change in the rate of electron transfer.

Much of this research has been performed on the photosynthetic reaction system which is optimised for electron transfer. However, this value of β may not be so highly applicable to other redox protein pairs or intra-protein electron-transfers where the medium may be better thought of as heterogeneous. Thus an alternative view to the "direct through space" model has been proposed. The "tunnelling pathways" model devised by Beratan *et al* (1990) suggests that the pathway taken by an electron is not "as the crow flies" but is the most energetically convenient pathway utilising covalent bonds, hydrogen bonds and short through space hops. The same work has produced an algorithm which calculates the most efficient pathways from donor to acceptor atoms taking account of the bonding and non-bonding interactions between them. Initial research comparing this tunnelling model to Dutton's distance theory was performed on ruthenium modified cytochrome *c* and myoglobin (Sykes, 1988; Beratan *et al.,* 1990; Casimiro et al., 1993). Covalent attachment of ruthenium complexes to redox proteins, via surface histidines or lysines, creates a second redox-active centre. The ruthenium ion can be induced to donate or accept electrons by laser flash photolysis or pulse radiolysis. Thus, intra-protein electron transfer can be controlled over a fixed distance without interference from bimolecular association steps (Sykes, 1985). The distance between the two centres is easily measured from the X-ray crystal structure of the native protein. Both Ru^{II} and Ru^{III} states are relatively inert to substitution reactions and have low reorganisation energies making this couple ideal for electron-transfer studies. The reduction potential of the couple can also be optimised, over a range of approximately 1.5 eV, by altering the ligands of the complex (Bjerrum et al., 1995). This allows the driving force of the electron transfer to be altered. Commonly used complexes are $[Ru(bpy)_2(im)]^{2+}$ and $[Ru(NH_3)_5H_2O]^{2+}$. Kinetic data for intra-protein electron transfer in ruthenium modified cytochrome *c* and myoglobin have been analysed using both direct distance and tunnelling theories. Cytochrome *c* data fits well to the tunnelling theory of Beratan *et al* suggesting that distance alone is simply not enough to describe long

distance intra-protein electron transfer (Beratan *et al*, 1990; Winkler *et al*, 1992; Bjerrum *et al.*, 1995). The data for myoglobin fits poorly to both theories but it has been suggested that as it is an O_2 transport protein there is no single optimised pathway for electron transfer making it questionable as to how relevant the data is (Casimiro *et al.*, 1993). Similar experiments have been performed with azurin from *Pseudomonas aeruginosa*. This protein is made up predominantly from β-sheet which was suggested to be a better mediator of electron transfer than the α-helices of cytochrome *c* (Beratan *et al.*, 1991). Kinetic data confirm this theory with rate constants fitting well to the tunnelling theory with a β value of $1.1 Å^{-1}$, lower than that predicted by Dutton for a "homogeneous" protein medium (Winkler *et al.*, 1997). Thus, although Dutton's theory may well apply for an optimised electron-transfer system, much of the evidence suggests that the intervening medium must be considered when studying electron transfer in proteins. Furthermore the bonding and non-bonding interactions of the peptide medium cannot be generalised as "homogeneous" where clearly they affect electron transfer rates quite differently.

Another point which has caused controversy is where a prosthetic group ends and the protein medium begins. *e.g.* in the case of a haem centre does the electron get a "free ride" to the edge of the porphyrin ring. If so the only relevant distances are those between the edges of the prosthetic groups. Although distance and medium must play their part they are by no means sufficient to promote an efficient electron transfer. The amino-acid shell around the redox centre is there to prevent electron transfer to adventitious small molecules but also to confer upon the protein the ability to recognise its redox partner and ultimately bring them together in a configuration suitable for a successful electron transfer.

It has been shown by Tiede (1993), that electron transfer between c-type cytochromes and the photosynthetic reaction centre is drastically impaired if no significant binding affinity exists. This remains the case even when they exhibit high tunnelling density surfaces. This topic is discussed in more detail in Section 1.2.

1.2. Inter-protein recognition.

It has long been known that recognition between redox proteins is an important part of the biological electron-transfer process. However, much speculation has been made regarding the form this recognition takes. How specific is it from one redox protein to the next? Are the majority of redox proteins restricted to operating in only one system or are they less specific and able to operate in other electron transfer pathways? This section will describe some of the theories presently favoured using as examples some redox partnerships which have been studied in depth.

Until recently the most widely accepted method of recognition in redox protein partnerships was that of the "Lock and Key". As with Antibodies and Antigens it was assumed that a protein had one specific reaction site on its surface suitable only for its partner and thus was incapable of indiscriminate electron transfer and so short circuit of the pathway. This holds provided that each redox protein is required in only one pathway and so with a single donor and a single acceptor. However, it has become apparent that large numbers of redox proteins are physiologically active with numerous structurally dissimilar partners and indeed some show activity with non physiological partners *e.g.* the now classical pairing of cytochrome *c* and cytochrome b_5 (Mauk *et al.*, 1982; Wendoloski *et al.*, 1987; Mauk *et al.*, 1991) It has also been observed that the copper containing protein pseudoazurin from *Paracoccus denitrificans* can substitute for cytochrome c_{550} during nitrate reduction in a cytochrome c_{550} deletion mutant (Moir *et al.*, 1994). Multiple redox partners and mediation in an electron-transfer pathway by more than one protein cannot be easily explained by a specific-site theory. Electron-transfer proteins, it would seem, require a more subtle explanation for their often promiscuous behaviour. As this has become a fashionable topic of study there are, of course, numerous ideas.

Electrostatics have long been thought to play an important role in protein complexation and recognition but it has been difficult to apply classical electrostatic theory to macromolecules, like proteins, due to their large and complicated structures (Sharp *et al.*, 1990). McLendon (1991) proposed a "Velcro" motif whereby areas of

complementary charge on two interacting proteins act as hooks and loops on the protein surfaces (Figure 1.2.1.).

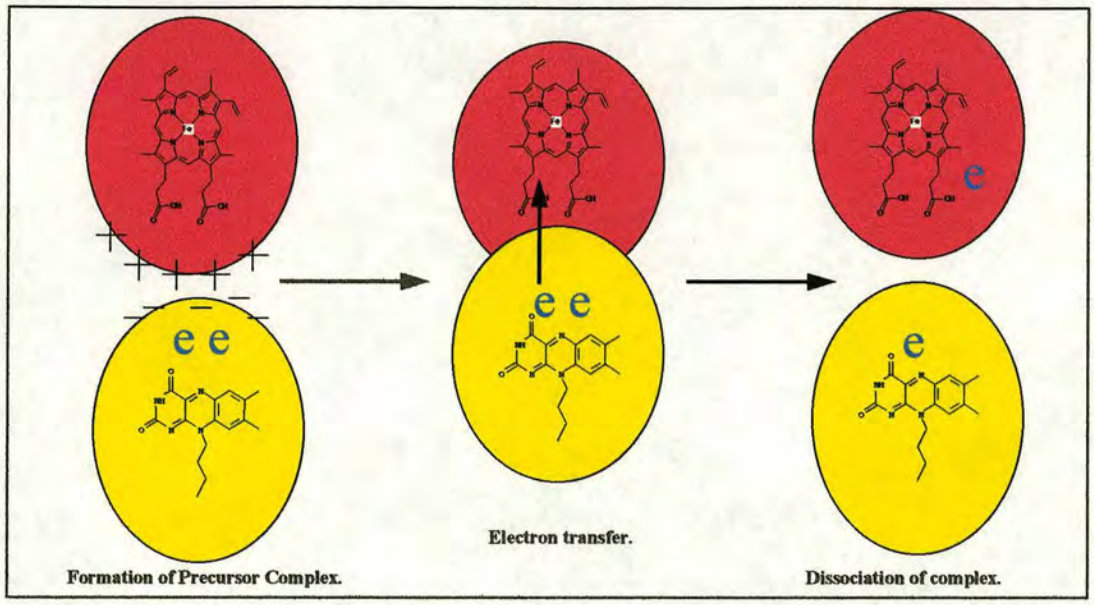

Figure 1.2.1. *A schematic diagram of the approach and binding of two redox proteins at complementary "velcro" sites, the formation of a precursor complex and the consequent electron transfer followed by dissociation. e = electrons.*

These charges bring the proteins together and allow them a certain amount of freedom when docking, enabling sampling of a number of sites until an electron-transfer complex is achieved. The two proteins could be envisaged coming together at a large docking patch around the prosthetic groups and then rolling to the position best suited to the structures involved. This more flexible approach has now been adopted by many studies and evolved into a "Pseudospecific docking theory". This is an adaptation of the complementary "velcro" patches but can more rigorously explain long-range attractions, high frequency and high efficiency collisions and multiple partners. "Pseudospecific docking" coined by Williams *et al* (1995) has been used to explain behaviour exhibited by the electron-transfer protein pseudoazurin from *Thiosphaera pantotropha*. Pseudoazurin is a 120 residue copper containing protein which shuttles electrons between various proteins in the bacterial periplasm. In this case its partners are nitrous oxide reductase and cytochrome cd_1 nitrite reductase. The crystal structure of pseudoazurin has been solved to 2.5Å (Williams *et al.*, 1995) and the surface residues of the protein studied for clues as to its binding

motif. Based on the knowledge that pseudoazurin has multiple partners and that one of these, cytochrome cd_1 nitrite reductase, can accept electrons from at least another two proteins (cytochrome c_{551} and cytochrome c_{550}) it was proposed that any binding between these could at best be only pseudospecific in nature. This binding would have to be between complementary patches. As hydrophobic areas will provide non-specific attractions the pseudoazurin surface was studied for such areas. Hydrophobic areas have been implicated in the interactions of a number of copper containing redox proteins including another pseudoazurin from the related species *Paracoccus denitrificans* (Moir *et al.*, 1993) and azurin from *Pseudomonas aeruginosa* (van de Kamp *et al.*, 1990 and Nar *et al.*, 1991). Such a patch does exist on the pseudoazurin surface around the metal site. It comprises 11 residues, nine of which are within 10Å of the metal ion. The majority of these residues are also conserved in a number of other pseudoazurins. As well as the hydrophobic patch a study of the electrostatic nature of the surface revealed that the protein has a highly asymmetric distribution of charge. There are 12 positive residues surrounding the hydrophobic patch (Figure 1.2.2.) and a large number of negative residues at the opposite side of the protein. Again these are heavily conserved in other pseudoazurins.

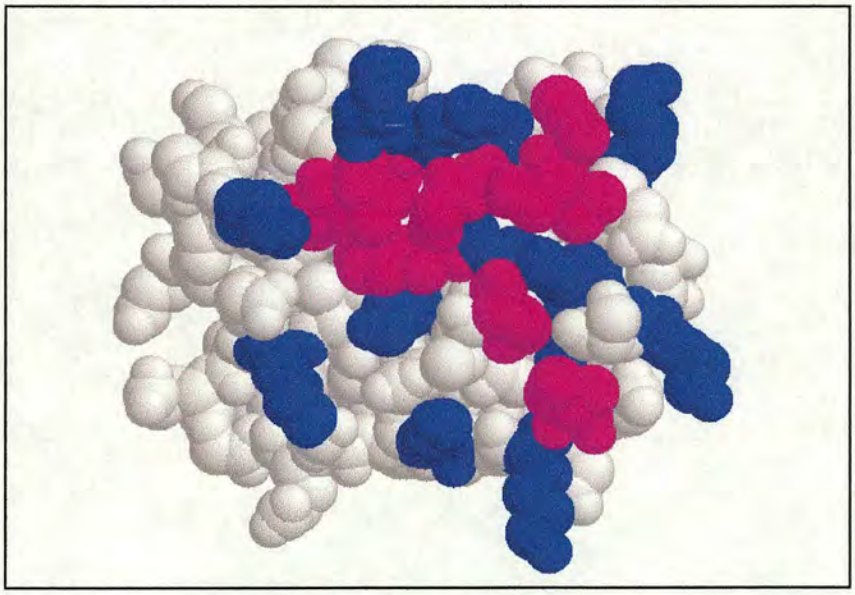

Figure 1.2.2. *The Hydrophobic patch on pseudoazurin from Thiosphaera pantotropha. Hydrophobic residues are shown in pink and basic (positively charged) residues are shown in blue.*

This bipolarity is likely to induce a dipole moment across the molecule similar to that observed with mitochondrial cytochrome *c* due again to a similar asymmetric distribution of charged residues (Koppenol *et al.*, 1982) (Figure 1.2.3.). Looking at the surface of cytochrome cd_1 nitrite reductase it transpires that it has a negatively charged hydrophobic patch complementary to pseudoazurin. It is probable that these two opposite dipoles act to steer the two proteins together from long range not only bringing them together but doing so in such a way that the prosthetic groups are at an optimum position for electron transfer with the hydrophobic patches holding the proteins together for the required time. This has been observed in many other systems including the non physiological partnership of vertebrate cytochrome *c* and bacterial flavodoxin (Matthew *et al.*, 1983). Again both proteins have asymmetrically distributed charge. Cytochrome *c* has a large positive area around the haem (Koppenol *et al.*, 1982) (Figure 1.2.3.) and flavodoxin has a complementary negative patch around the FMN.

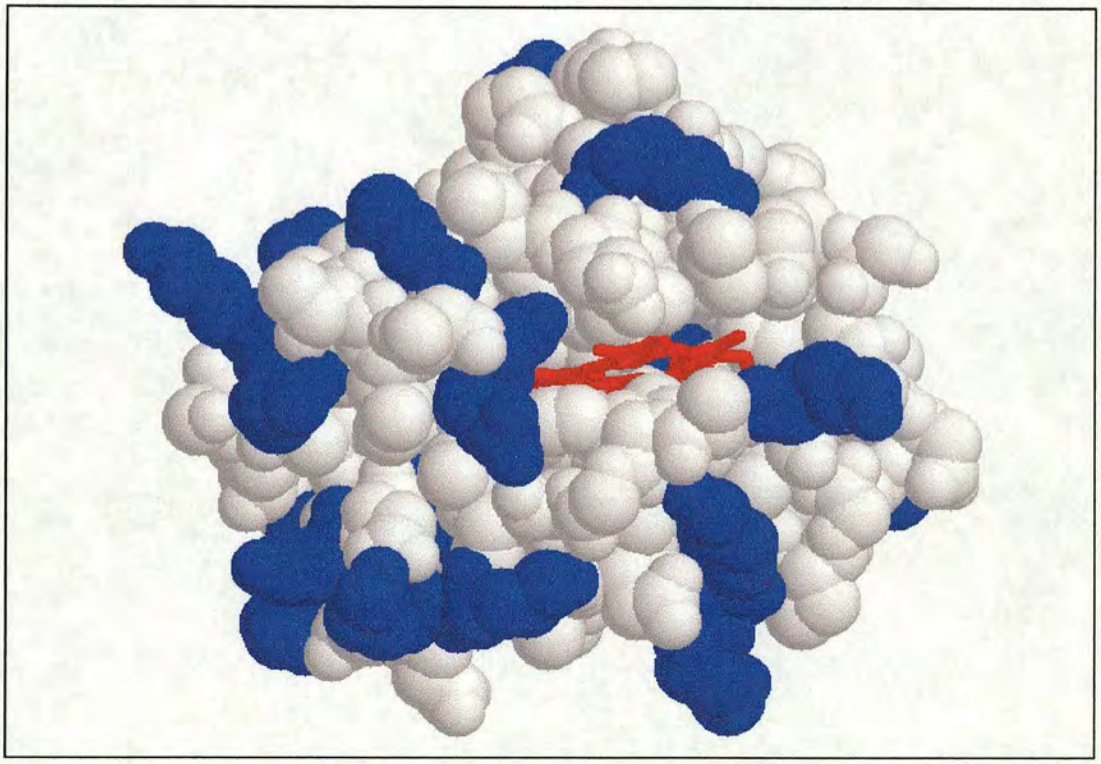

Figure 1.2.3. *Cytochrome c from Horse heart showing the haem molecule in red and the prominent basic (positively charged) residues distributed around it in blue.*

Here it was suggested that the role played by electrostatics was twofold. Initially they act to pre-orient the proteins along a connecting axis between the prosthetic groups. This restricts the number of degrees of freedom to a single rotational one about the axis allowing some sampling of the interface region prior to complexation (Figure 1.2.4.).

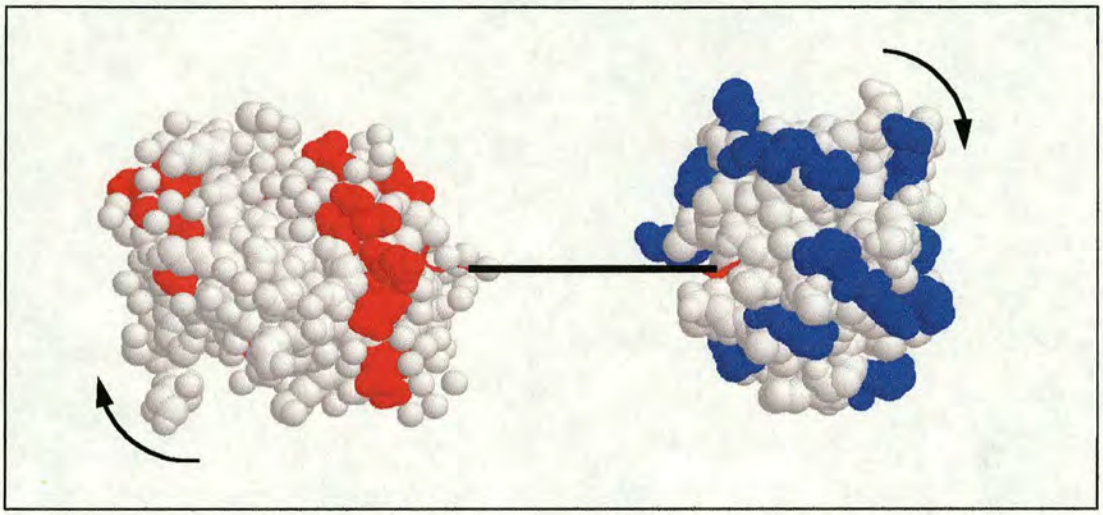

Figure 1.2.4. *A schematic diagram showing two electrostatically attracted proteins approaching along a single axis allowing limited rotational sampling of the complementary sites. Positively charged residues are highlighted in blue and negatively charged residues in red. Arrows denote rotation of the proteins about the axis.*

Secondly the charged fields can accelerate the association step during complexation in some cases forming salt bridges. This explains why ionic strength has such a marked effect on these interactions. Whether or not charged residues are incorporated in the binding, low ionic strengths will deshield the molecules making long distance attractions more effective. This behaviour is supported by kinetic studies of ionic strength effects on the amicyanin:methylamine dehydrogenase complex from *Paracoccus denitrificans* (Gray *et al.*, 1988). These implicate a hydrophobic:electrostatic patch in the complex binding. However, on closer inspection of the complex interface no electrostatic interactions were observed (Chen *et al.*, 1992). Of course this does not discount charged residues as a factor in bringing the two proteins together. Much of the data from the above examples suggests that the word "Collision", which infers a certain degree of randomness, is perhaps not the correct term for these circumstances as the proteins are under each

others influence long before physical contact is made. This was discussed by Janin (1997) with particular reference to the bacterial extracellular ribonuclease Barnase and its inhibitor Barstar (Figure 1.2.5.). The presence of Barnase, M_r 12 000, in a cell has been shown to be lethal necessitating its inhibitor Barstar, M_r 10 000, to have a femtomolar binding constant. Electrostatics play an important role in bringing the two together and again they both have complementary asymmetric charge distribution.

Figure 1.2.5. *The ribonuclease Barnase (green ribbon) and its inhibitor Barstar (black ribbon) showing the complementary asymmetric charge distribution which holds the two together (blue = positive, red = negative).*

Janin states that in the absence of long range electrostatic interactions an association of two proteins consists of two factors, (i) k_{coll}, the rate of random collision and (ii) p_r, the probability of the two colliding in an orientation that promotes a stable complex. This gives a bimolecular rate constant of $k_{coll}p_r$. Introducing coulombic interactions affects both these factors. The rate of collision increases by a factor of q_t and the probability that they are successful by a factor of q_r. These acceleration factors give a new bimolecular rate constant of $(k_{coll}q_t)(p_rq_r)$ making collisions much more frequent and pre-orienting proteins such that the collision is a successful one.

Similar to the work on cytochrome *c* and flavodoxin the approach of Barnase and Barstar is envisaged as along an axis (Figure 1.2.4.). The pre-orientation procedure is essential as the average lifetime of an encounter pair is fractions of a nanosecond allowing the two proteins no time to find the interaction sites but only to make fine adjustments to their pre-orientation. Much work has been done on mutation of residues to determine which are most important in the interaction (Jucovic *et al.*, 1996) and it has been shown that a single residue can perturb binding enough to make Barnase lethal to the cell in the presence of Barstar. This suggests that complex stabilisation has been affected rather than the mode of recognition. This has also been observed in the cytochrome *c*:cytochrome *c* peroxidase complex (Hake *et al.*, 1992). Mutations were made to residues on the negatively charged site of cytochrome *c* peroxidase with some having a greater effect on binding than others. This implies that as a whole the negative patch plays an important role in protein recognition but that to attain physical contact and complexation certain individual residues may play more important roles than others perhaps in *e.g.* the formation of salt bridges. A degree of flexibility in these residues then becomes more important in allowing them to accommodate their opposite number on the redox partner thus bringing us back to some of McLendon's ideas. Williams *et al* (1995) proposed this flexibility as a reason why in many cases the pseudospecific patches consist of mainly lysines (positively charged) and glutamates (negatively charged) in that the carbon chains of these are of sufficient length to allow a much larger area of interaction. The motion of these residues was studied using molecular dynamics simulations in the cytochrome *c*:cytochrome b_5 complex (Wendoloski *et al.*, 1987). These experiments suggested that the presence of electrostatic interactions at the interface promote much more flexible docking surfaces allowing the proteins to fine tune the interaction. A similar approach was adopted by Storch *et al* (1995) to study the flexibility of the entire cytochrome b_5 structure. These simulations suggest that in general the protein does not deviate dramatically from the crystal structure but that any perturbations which do occur correspond to those acidic residues around the haem purported to be involved in protein interactions.

In terms of stabilisation of these redox protein complexes to allow efficient electron transfer, a number of ideas provided by pseudospecific docking theory are very favourable (Matthew *et al.*, 1983). It is probable that proteins with asymmetric charge distributions and hydrophobic surface areas are more stable as complementary electrostatic complexes. Two factors will stabilise the complex: (i) The attraction of opposite charges; and (ii) the lowering of local dielectric constants due to the expulsion of solvent molecules as the hydrophobic surfaces come together. The principle contribution to the free-energy of complexation comes from the electrostatic interactions while the increase in entropy is due to solvent release which compensates for the entropy loss due to complexation of the two protein molecules. This is opposite to the conclusions of Mauk *et al* (1991) regarding the complex formed between microsomal cytochrome b_5 and horse heart cytochrome *c*. This has been shown to be a 1:1 complex the interaction of which is inhibited by high ionic strength (Mauk *et al.*, 1982). It has been proposed that the interaction is entropy driven by solvent exclusion and close packing of side chains at the interface whereas, the electrostatic interactions provide only the specificity to bring the two proteins close. This does not agree with much of the work which has been done on the electrostatics of this pairing. Theoretical modelling (Salemme *et al.*, 1976) indicated that lysine residues on cytochrome *c* and glutamate residues on cytochrome b_5 were very important in maintaining the complex. Mutations to some of the glutamate residues on cytochrome b_5 (Rodgers *et al.*, 1988) left the protein with a much decreased affinity for cytochrome *c* again implicating electrostatics at least in the recognition step. These experiments also explain the ionic strength effects previously mentioned. Finally and more generally it is also possible that the neutralisation of charges at the binding interface promotes electron transfer (Williams *et al.*, 1995) in the same manner as the decrease in local dielectric constants.

Clearly it is possible to destroy the electrostatic binding of two proteins but can the opposite be performed? It should be feasible using all the information gleaned from above to take two redox proteins where no apparent interaction exists and build in recognition:binding sites such that an electron-transfer reaction is enhanced

provided of course that the two are thermodynamically suitable. This proposal forms the basis of the work in this thesis and will be elaborated on in Chapters 3. & 4.

1.3. Haemoproteins.

There are an enormous number of haem containing proteins throughout biology which display a wealth of different functions. These functions include O_2 activation and reduction, O_2 transport and storage, electron-transfer mediation, and peroxide reduction. This functionality can be increased by coupling haem proteins with other prosthetic groups such as FMN, FAD and Cu centres. Such groupings allow haem proteins to participate in dehydrogenation and reduction of small molecules. It is this diversity of function which makes haem proteins so interesting and has given them the arguable title of "the most versatile redox centre in biology" (Chapman *et al.*, 1997). This versatility is provided by the different types of haem and by the protein framework surrounding them. There are four common haem types (Figure 1.3.1.). The most familiar are *b*-type haems (protohaem IX). These are found in the O_2 transport proteins, haemoglobin and myoglobin, *b*-type cytochromes, cytochromes P-450 and most peroxidases. The haem is bound to the protein non-covalently being held in place by the axial ligands of the Fe. In most cases these are two histidine side chains, bis-His. The propionate side-chains of the haem molecule may also be involved in forming salt-bridges to the protein structure (Mathews., 1985). Cytochromes *c* differ in their binding to the protein, being covalently attached via two thioether links between the vinyl groups at positions 2 and 4 of the porphyrin and the thiol groups of two cysteine residues on the protein. These cysteine residues exist as a common binding motif in the majority of eukaryotic *c*-type cytochromes (Cys-x-y-Cys-His). The Fe is hexadentate with either 2 histidines or a histidine and a methionine as axial ligands. The most obvious difference between the *a*-type haems and those above are a hydroxyethylfarnesyl group and a formyl group at positions 2 and 8 of the porphyrin respectively. Haem *a* is a prosthetic group in cytochrome aa_3 which is one component of the cytochrome oxidase system. Cytochrome cd_1 nitrite reductase contains a d-type haem. Unlike the previous haems the porphyrin of a

d-type cytochrome has saturated bonds and 4 carboxylic acid groups making it very hydrophilic.

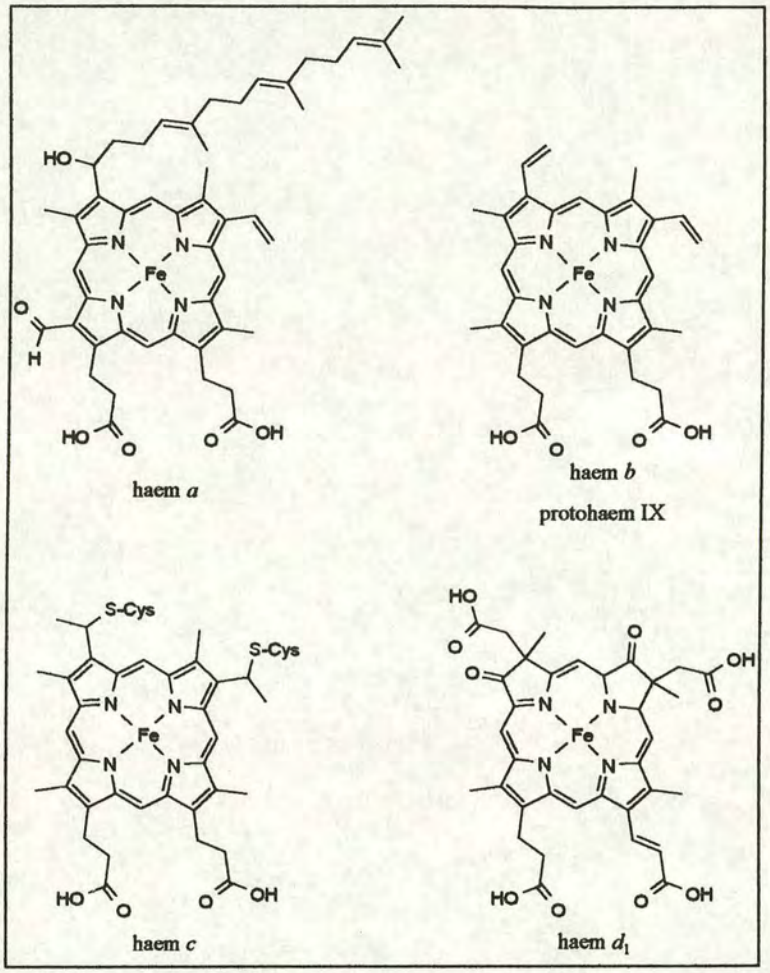

Figure 1.3.1. *The four common haem types found in biological systems.*

Electron-transfer haemoproteins can be split into 2 general groups: (i) Those which mediate simple electron transfer *e.g.* mitochondrial cytochrome *c* and (ii) those which are part of multi component systems coupling electron transfer to other enzymatic processes *e.g.* flavocytochrome b_2. Cytochromes *c* are probably the best understood of the cytochromes having been the focus of much research. They mediate single electron-transfers in a number of systems. To enable the *c*-type haem to do this between a variety of partners, its redox potential can be modulated over a range of ~700 mV by the surrounding protein matrix and the Fe axial ligands. For efficient electron transfer, as well as a suitable driving force, the reorganisation energy of the mediator protein should be low and the distance between prosthetic groups as short

as possible (Section 1.1.). Cytochromes *c* achieve the former by having a hexadentate haem which is low spin (S=1/2) when both oxidised and reduced. Thus, during electron transfer there is very little reorganisation as the Fe moves from the ferric to the ferrous states or *vice versa*. In membrane bound enzymes, such as cytochrome *c* oxidase (Malatesta *et al.*, 1995) distance between the many prosthetic groups is minimised by holding them close together within the relatively rigid protein framework. Soluble electron-transfer mediators like cytochrome *c*, on the other hand, rely on protein recognition to bring the prosthetic groups close together. This involves complementary electrostatic sites pre-orienting the interacting proteins (Section 1.2.). The electrostatic interactions can help bind the proteins together but this is often performed by hydrophobic interactions as with the cytochrome *c*:cytochrome *c* peroxidase complex (Pelletier *et al.*, 1992), and cytochrome *c*:cytochrome b_5 complex (Mauk *et al.*, 1982; 1991). Cytochrome *c* has an asymmetric charge distribution such that the area around the exposed haem edge is very positively charged (Koppenol *et al.*, 1982). It is this surface which is involved in electrostatic interactions in both systems mentioned above (Section 1.2.).

Haem groups also mediate electron transfer in some "coupled" systems whereby they donate to, or accept from, catalytic sites in systems such as flavocytochrome b_2, and cytochrome *c* oxidase. In flavocytochrome b_2 the *b*-type haem shuttles electrons from the dehydrogenase domain (which catalyses the oxidation of L-lactate to pyruvate) to cytochrome *c*. This system is described in more detail in Section 1.5. Similarly in cytochrome *c* oxidase one of the *a*-type haems acts purely as an electron transfer mediator between cytochrome *c* and the catalytic site of O_2 reduction. The cytochrome *c* oxidase system is described later in this section.

As well as simple electron-transfer roles haems can perform a wide range of catalytic reactions with O_2. Although a powerful oxidising agent, O_2 does not readily undergo reactions with organic compounds. It does however, bind and react with transition metals such as Fe. Thus, haems are present in a number of enzymes which catalyse the reduction or activation of O_2. Mammalian cytochrome *c* oxidase (M_r 200 kDa) is a complex, 13 subunit, enzyme often referred to as a "redox linked proton

pump". Spanning the mitochondrial inner membrane, it couples the reduction of O_2 to H_2O with the pumping of protons into the intermembrane space. The translocation of protons sets up a proton-motive force used to synthesise ATP from ADP. It has 2 *a*-type haems, 2 Cu centres, a Mg site and a Zn site. Haem *a* and Cu_A mediate electron transfer from the physiological donor, cytochrome *c*, into the active site. Haem *a* has a hexadentate Fe which is low spin. The second haem, a_3, is present at the site of O_2 reduction and is coupled with Cu_B. The presence of so many prosthetic groups has made the mechanism difficult to determine although much work has been done to determine the rates of intra-protein electron transfer (Winkler *et al.*, 1995). However, the overall reaction catalysed by the enzyme is shown in equation 1.3.1.

Equation 1.3.1. $4Cytc^{II} + O_2 + 8H^+_{out} \rightarrow 4Cytc^{III} + 2H_2O + 4H^+_{in}$.

(Where out = protons pumped from the matrix and in = protons pumped to the intermembrane space.)

One of the most interesting properties of haem is its ability under certain conditions to activate O_2. This ability manifests itself in the cytochromes P-450 (Munro *et al.*, 1996) which can insert 1 atom of oxygen into organic substrates (monooxygenase). These substrates come from a wide range of physiological and non-physiological compounds. The ability of P-450s to breakdown unusual and often toxic compounds allows many organisms to utilise them as a defence against xenobiotics. In some cases catabolism leads to the assimilation of energy from unusual carbon sources. Oxygen binding and activation occurs at a *b*-type haem site. There are two broad classes of cytochrome P-450. Class I are the terminal oxidases of a 3-component electron transfer chain including all but one of the bacterial forms. The P-450 is reduced by an FeS (ferredoxin) protein which in turn is reduced by an NAD(P)H dependent FAD-containing ferredoxin reductase. Class II systems consist of eukaryotic and mammalian hepatic drug metabolising forms. They are membrane bound being reduced by a single FAD- and FMN-containing protein (NADPH-cytochrome P-450 reductase). The only class II bacterial P-450 is P-450 BM3 from *Bacillus megaterium* ATCC 14581. It is a single peptide having two domains. The P-450 domain is reduced by a NAD(P)H cytochrome P-450 reductase

domain which, like eukaryotic systems, contains both FAD and FMN. The catalytic cycle of the P-450's is as follows. On binding of the substrate H_2O is displaced and Fe becomes high spin (S=5/2). The spin state shift is accompanied by an increase in the redox potential allowing reduction by the reductase domain. The ferrous Fe can now bind O_2. A further 1-electron reduction yields the short-lived active-oxygen species. The result of this is an extremely rapid monoxygenation for which the mechanism remains unclear but results in the loss of one atom of O_2 as H_2O and insertion of the other into the substrate.

Catalases and peroxidases perform very similar chemistry to the P-450s with all three utilising oxo-iron(IV) intermediates in their catalytic cycles. However, because they do not have large hydrophobic substrate binding pockets they do not catalyse the insertion of oxygen atoms into organic molecules. Instead they promote the decomposition of hydrogen peroxide as H_2O and O_2 or the breakdown of alkylhydroperoxides into H_2O and alcohol as shown in equations 1.3.2. and 1.3.3.

Equation 1.3.2. Catalases: $2H_2O_2 \rightarrow O_2 + 2H_2O$.

Equation 1.3.3. Peroxidases: $ROOH + XH_2 \rightarrow ROH + H_2O + X$.

(Where XH_2 represents reducing substrates such as amines, phenols, hydroquinones and cytochromes and R = hydrogen or an alkyl group).

These enzymes in general contain *b*-type haem prosthetic groups. Like the P-450s these haems are pentacoordinate with the sixth position free for substrate binding. The mechanism for peroxide reduction is complex but key intermediates are an oxo-iron(IV) haem and a radical cation on either an active site amino acid or the porphyrin ring.

Not only are there a number of different haem types but each type, under the influence of its protein framework and axial ligands, has the potential for an overwhelming diversity of function. The above examples are only a few of the many roles played by haem in a vast number of biological systems.

1.4. Flavins & flavoproteins.

1.4.1. Introduction.

The chemistry of flavins is one of the most diverse and widely observed in Biology. Based on the structure of Riboflavin (vitamin B_2), a 7,8-dimethylisoazoxalline ring, and its ribose side chain there are two redox active flavin molecules which act as enzyme cofactors or substrates (Figure 1.4.1.).

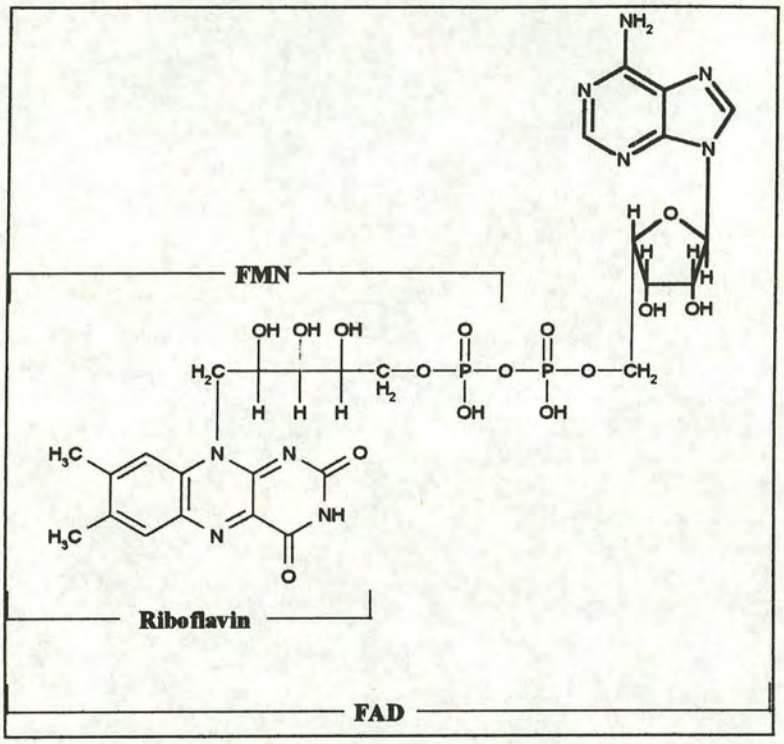

Figure 1.4.1. *The structures of riboflavin, flavin mononucleotide (FMN) and flavin adenine dinucleotide (FAD).*

Flavin mononucleotide (FMN) is produced by phosphorylation of riboflavin. If this is phosphorylated further and then adenylated the resulting molecule is Flavin adenine dinucleotide (FAD). The flavins get their name from the Latin word for yellow and indeed in the oxidised form are bright yellow in colour due to their strong absorbance in the 350-450 nm region of the spectrum. This can be seen for FMN in Figure 1.4.2. along with the resulting spectrum when FMN is reduced by dithionite producing a colourless molecule.

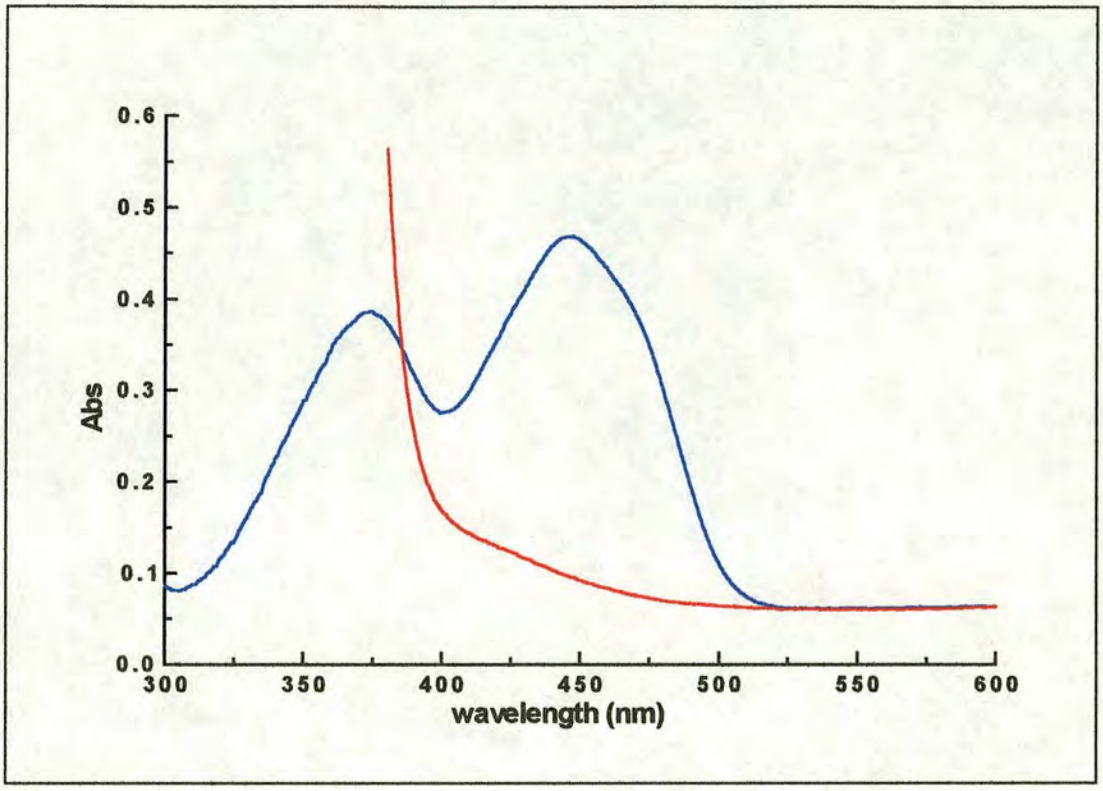

Figure 1.4.2. *The UV/Vis absorbance spectra for FMN in the oxidised (blue) and reduced (red) states. ~50μM FMN, Tris.HCl pH7.5, I = 0.1M. Reduced with sodium dithionite.*

The chemistry catalysed by flavin molecules usually involves oxidation and reduction of organic substrates and is focused around the isoalloxazine ring. Side-chains such as adenosine play no part other than to anchor the molecule to its host protein (Ghisla *et al*, 1989). The pryimidine nucleus of the isoalloxazine ring is an electron deficient group acting as an electron sink during the oxidation of substrates. These electrons are then delocalised on what can be thought of as a (4,5-diamino)-uracil group (Ghisla *et al*, 1989). In biology, flavins and nicotinamides are the primary electron acceptors from functional groups undergoing oxidation. These are strict two electron oxidations so that, stoichiometrically at least, either acceptor can be utilised. However, flavins have two distinct advantages over nicotinamides: (i) They are tremendously flexible in that they undergo facile 1-or 2-electron transfers where the nicotinamides are constrained to only 2-electron transfers; (ii) flavins can activate molecular oxygen as a redox partner whereas nicotinamides are inert. Thus flavins and flavoproteins have become known as biological transformers linking obligate 2-electron donors like L-lactate to strict 1-electron acceptors like cytochromes

(Walsh, 1980). It is these two abilities which allow flavoproteins to play important roles in such a diverse array of reactions from dehydrogenation and electron transfer to bioluminescence (Fisher *et al*, 1995). The prosthetic groups in the many hundreds of flavoproteins are essentially the same so that it is the protein structure in each case which must play the vital role of governing the reaction. The active-site residues determine which substrates are allowed to bind and in what orientation (Ghisla *et al*, 1986). More intriguingly perhaps this fine-tuning of the flavin molecule also determines whether or not it will be allowed to activate O_2. The reaction with oxygen has become one of the more fascinating parts of flavochemistry as well as forming the basis of a classification of the families of flavoproteins. Taking a look at the classification scheme below it can be seen that the majority of the proteins are dehydrogenases and that it is the manner of re-oxidation of the flavin that differentiates one class from another. As previously mentioned the ribose side-chain is used to anchor the molecule to the active site. In most cases the flavin:protein partnership exists as a tightly bound but non-covalent complex (Walsh, 1980). However, there are a small number of enzymes where the flavin is covalently attached (Mewies *et al*, 1997) or acts only as a substrate (Fisher *et al*, 1995)

Class 1. Transhydrogenases. These enzymes dehydrogenate saturated bonds of the type C-C, C-S, C-N & N-N provided that an activating group e.g. a carbonyl, lies adjacent to the αβ bond. This oxidation is linked to an electron-transfer protein. (Massey *et al*, 1980). These will react very slowly with molecular oxygen (O_2) producing superoxide (O_2^-) but do not exhibit sulphite (SO_3^{2-}) binding and have a very unstable blue semiquinone.

Class 2. Dehydrogenases/oxidases. After the initial dehydrogenation event these enzymes react with O_2 to give hydrogen peroxide (H_2O_2) as the only discernible product. They have also been classified by their ability to bind SO_3^{2-} very tightly (Massey *et al*, 1969) and stabilise a red semiquinone species (Massey *et al*, 1966).

$$FlH_2 + O_2 \longrightarrow H_2O_2 + Fl$$

(Fl = Flavoprotein)

Class 3. Dehydrogenases/oxygenases. Again the dehydrogenation of substrate is the first step here but the reaction with O_2 is different. Mono-oxygenases will split O_2 placing one atom into a substrate and the other into H_2O (Massey, 1994). Dioxygenases will place both atoms from O_2 into the substrate. These flavoproteins, as a general rule, do not bind SO_3^{2-} and tend to stabilise neither of the radical semiquinones (Massey *et al*, 1980).

$$FlH_2 + O_2 + RCHO \longrightarrow Fl + RCOOH + H_2O$$

Class 4. Dehydrogenases/electron transferases. This particular group have all but dispensed with the need for O_2. Any that do react, do so very slowly producing mainly H_2O_2 . These enzymes have adapted to utilise a number of other electron acceptors such as cytochromes and FeS clusters. They play important roles in substrate conversion and electron-transport chains. In general they are not bleached by SO_3^{2-} (Massey *et al*, 1969) and stabilise a blue semiquinone species (Massey *et al*, 1966). However, there is an exception in flavocytochrome b_2 from *Saccharomyces cerevisiae* which like the oxidases is bleached by SO_3^{2-} and has a stabilised red semiquinone (Lederer, 1978).

Class 5. Pure electron transferases. These do not catalyse dehydrogenation reactions but take part only in electron-transfer processes. These electron transfers may occur from other flavoproteins with 1 or 2 electrons to a number of other acceptors. They will not bind SO_3^{2-} and again stabilise the blue semiquinone. They will also react fairly rapidly with O_2 to produce at least in the first instance $O_2^{\cdot-}$ and the neutral blue semiquinone (Massey, 1994).

1.4.2. Flavin dependent dehydrogenases and oxidases.

One particular family of flavoproteins which has been studied thoroughly is that of the flavin dependent dehydrogenases and oxidases. Operating on various substrates, these proteins are related by structure or function utilising either FMN or FAD as the substrate-oxidising catalytic centre. The differences are observed in the physiological electron acceptor which is used. The dehydrogenases utilise a wide range of molecules such as haems, NADH and FeS clusters whereas the oxidases use only O_2.

Spinach Glycolate oxidase (Lindqvist *et al.*, 1989); Old Yellow Enzyme, *S. Carlbergensis* (Fox *et al.*, 1993); Trimethylamine dehydrogenase, bacterium W_3A_1 (Lim *et al.*, 1986); and flavocytochrome b_2, *S. Cerevisiae* (Xia *et al.*, 1990) are members of this group which have been structurally characterised by X-ray crystallography. The catalytic domain in each of these is an α8β8-barrel (Figure 1.4.3.). This structure occurs in about 10% of all known protein structures. It is an energetically highly favourable fold. The barrel consists of 8 parallel β strands surrounded by 8 α helices.

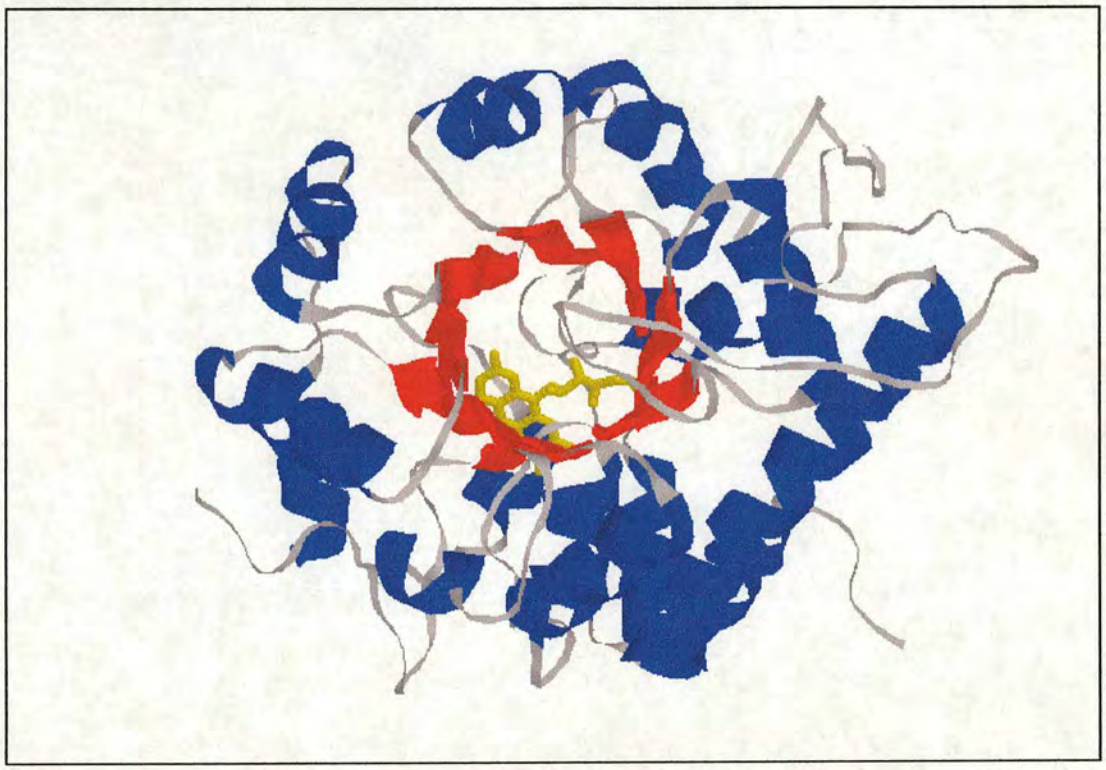

Figure 1.4.3. *The crystal structure of Spinach glycolate oxidase showing the α8β8-barrel structure. α-helices (blue), β-sheets (red) and the FMN (yellow) are highlighted.*

Each of the inner β-strands is attached to an α-helix by a peptide loop. In all the above examples of this family the prosthetic group for this domain is an FMN bound at the C terminal end of the β sheets (Figure 1.4.4.).

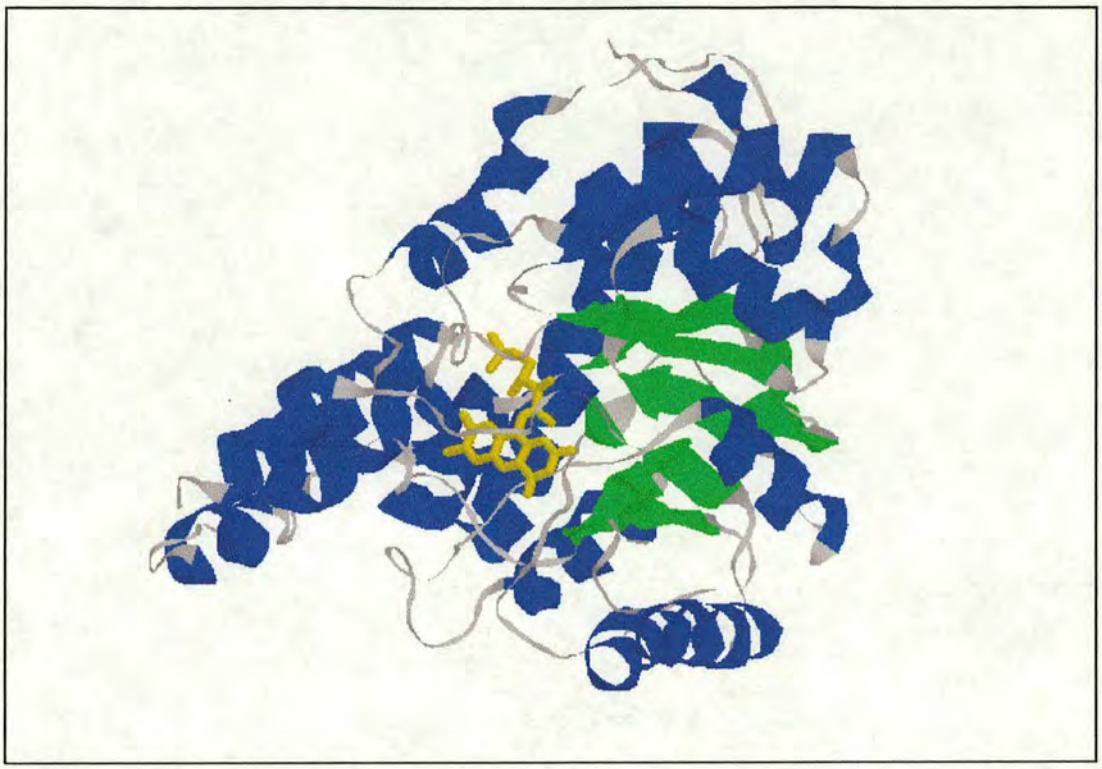

Figure 1.4.4. *The α8β8 barrel structure of the flavin binding domain from Saccharomyces cerevisiae flavocytochrome b_2 showing the binding of the FMN prosthetic group (yellow) at the C-terminal end of the barrel. α-helices (blue) and β-sheets (green) are highlighted.*

Although the overall structures of these proteins have been shown to be the same, in some cases there is little or no sequence similarity and this factor has made it difficult to determine whether these have evolved convergently to a favourably folded structure or divergently from an αβ-barrel to perform their various roles throughout biology (Scrutton, 1994). For example the two α–hydroxy acid oxidases Glycolate oxidase (GO) and the flavin binding domain of flavocytochrome b_2 (FDH) have 39% sequence identity. However, there is little identity between these and Trimethylamine dehydrogenase. FDH and GO are structurally almost identical with external loops and helices being observed in both indicating that they probably evolved divergently from a common ancestor. These regions are not observed in trimethylamine dehydrogenase but all three do share a common FMN binding motif probably induced by the barrel structure rather than due to individual residues involved in its binding. Although they are structurally very similar their catalytic properties are quite different. GO oxidises glycolate to glyoxylate and then reduces O_2 to H_2O_2. It operates by a "ping pong"

mechanism whereby the product glyoxylate leaves the active site before any reaction with O_2 can occur (Macheroux *et al.*, 1991). Flavocytochrome b_2 however, oxidises L-lactate to pyruvate reducing its own cytochrome domain and transferring electrons to cytochrome *c* having no intrinsic activity with O_2 at all. *S.cerevisiae* flavocytochrome b_2 and *R. graminis* L-mandelate dehydrogenase (L-MDH), another α–hydroxy acid oxidase, have been compared. It transpires that L-MDH is also a flavocytochrome b_2 being a homotetramer, having a similar molecular weight to flavocytochrome b_2 and utilising FMN in its active site (Yasin *et al*, 1993). Much of the kinetic data obtained suggest that the catalytic mechanisms of the two are similar with the only major difference being the mutually exclusive substrates that they utilise (Smékal *et al*, 1993). Although the crystal structure for L-MDH has not yet been solved all the evidence indicates that the flavin binding domain is also an αβ-barrel. Both have a cytochrome domain spliced onto the N terminus of the flavin binding domain acting in both cases as an electron transferase from the flavin to the acceptor thus providing further evidence for divergent evolution from the barrel structure flavoproteins. Because the majority of members of the group are single domain proteins using only FMN it has been suggested that a fairly late fusion event between the gene for FDH or L-MDH flavin domain and that for a cytochrome took place producing these two flavocytochromes (Scrutton, 1994).

1.5. Flavocytochrome b_2 (*Saccharomyces cerevisiae*)

1.5.1. Location and physiological role.

Flavocytochrome b_2 is a soluble, L-lacate:cytochrome *c* oxidoreductase. Found in the inter-membrane space of yeast mitochondria its main physiological role is to provide pyruvate for the Krebs cycle during aerobic respiration on L-lactate (Figure 1.5.1.). However, it also plays a vital role in a short electron-transfer chain allowing the cell to respire on L-lacate as its sole carbon source and so giving yeast an advantage over other species when growing on such a source.

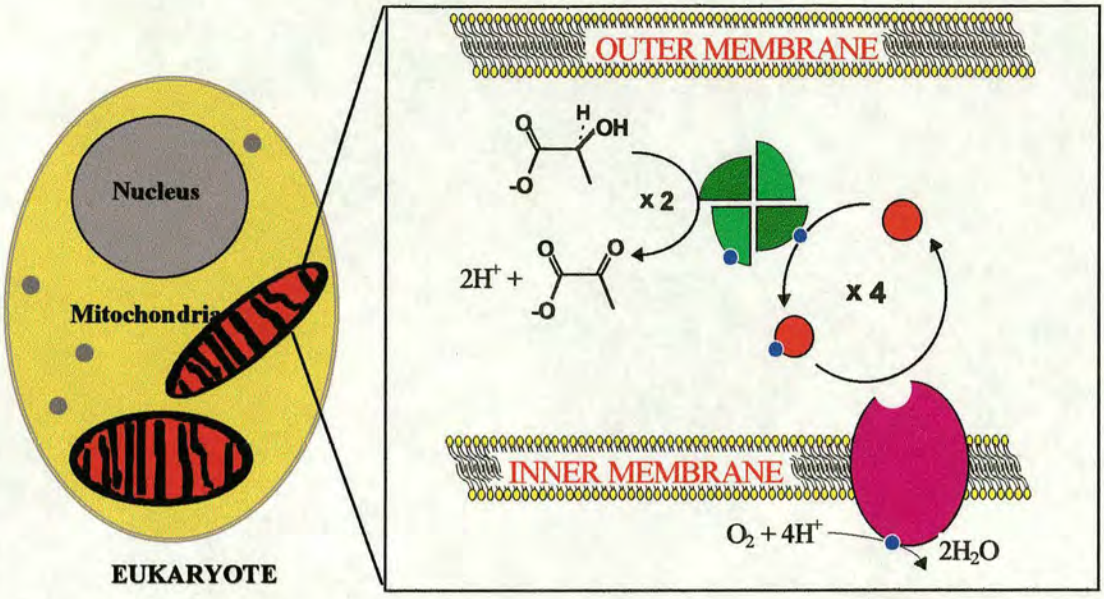

Figure 1.5.1. *A schematic diagram showing the intermembrane space of yeast mitochondria and the components which allow yeast to respire on L-lactate alone.*

Flavocytochrome b_2 oxidises L-lactate to pyruvate taking the 2 electrons to form a hydroquinone on the flavin mononucleotide (FMN) prosthetic group. It passes these one at a time to the haem group. They are then moved on to the physiological electron-transfer partner cytochrome *c*. Cytochrome *c* completes the pathway by transferring the electrons to cytochrome *c* oxidase where they are used to reduce O_2 to water.

1.5.2. The structure of flavocytochrome b_2.

The crystal structure of flavocytochrome b_2 has been solved to 2.4Å resolution (Xia and Mathews, 1990) showing that the enzyme is a homotetramer with each subunit consisting of two structurally and functionally distinct domains (Figure 1.5.2.). Each subunit is approximately M_r 57 500 making the entire tetramer M_r 230 000. Each subunit comprises 511 amino acids. The *N*-terminal cytochrome domain (M_r10 500, residues 1-100) covalently binds a protohaem IX prosthetic group. The haem is bis-His ligated in a typical *b*-type cytochrome manner through Histidines 43 and 66 producing a low spin Fe centre in both the oxidised and reduced states. The haem domain is attached to the main bulk of the enzyme by a short stretch of peptide, (residues 89-103) known as the "hinge".

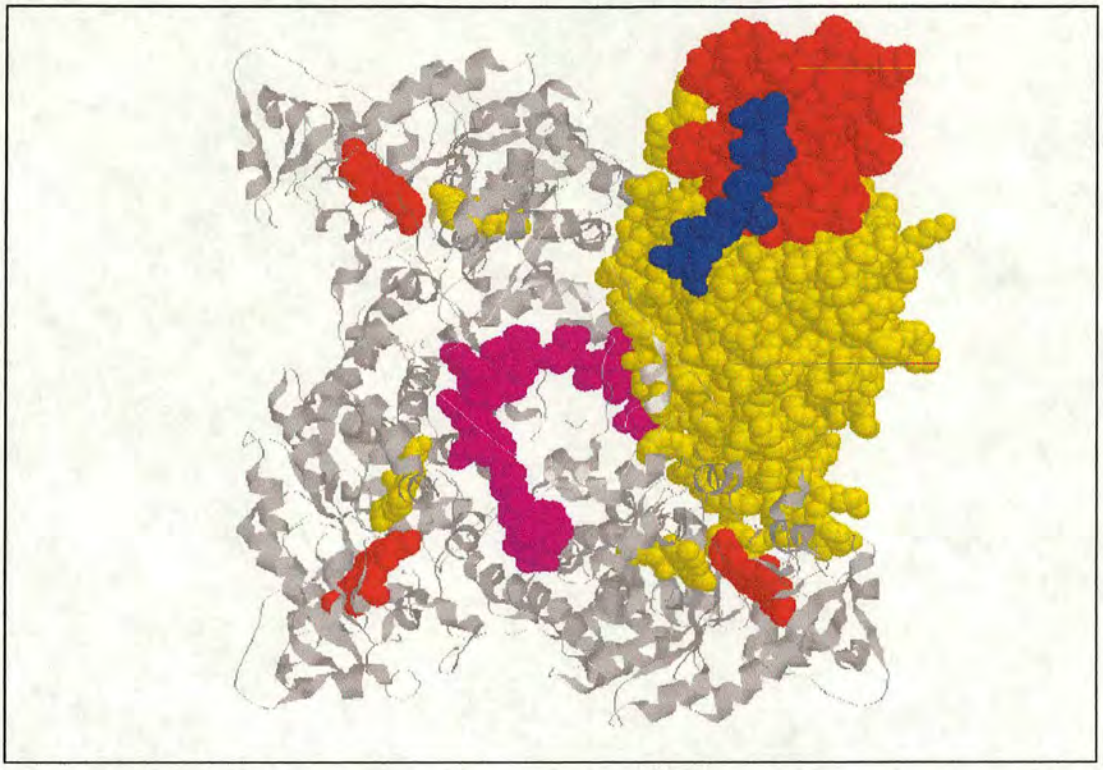

Figure 1.5.2. *The crystal structure of the flavocytochrome b_2 tetramer. One subunit is represented in spacefill while the remaining three are in ribbon. The FDH domain and FMN groups (yellow), the haem domain and haem groups (red), the hinge (blue) and the C-terminal tail (magenta) are highlighted.*

In the cyrstal structure only two of the haem domains show electron density with the remaining two being highly disordered and so crystallographically invisible. This along with NMR studies by Labeyrie *et al* (1988) suggested a large degree of movement by the cytochrome domain relative to the larger flavin binding domain (FDH). However, it is now believed that the hinge acts merely as a tether between the two domains allowing enough movement for efficient electron transfer (Bell *et al.*, 1996). Experiments by Sharp *et al* (1996) provide evidence that the hinge is at the optimum length for rapid intra-protein electron transfer. FDH contains a non-covalently bound FMN group around which are positioned the active site residues. The domain has M_r 47 000 comprising 388 amino acids in the common α8β8-TIM barrel structure. The *C*-terminal tail runs from residues 488-511. The crystal structure indicates that the tail forms a number of contacts with the other three subunits in the tetramer perhaps playing a role in holding the subunits in the tetrameric configuration. However, on

studying a tail-deleted mutant White *et al* (1989) discovered that these subunits retained their tetrameric structure. Their studies indicated that the mutant had a very high degree of FMN loss during turnover hinting at another structural role for the tail, that of retaining the structural integrity of the active site. The final important structural feature of flavocytochrome b_2 is a stretch of 17 or so residues halfway along the FDH sequence (298-315). This is a loop region which has been shown to be proteolytically sensitive causing problems in the attempts to isolate FDH by proteolysis (Section 1.5.4). It is known to be highly flexible and so is crystallographically invisible. One of the purposes of solving the FDH crystal structure is to determine the loop's position relative to the active site and the solvent exposed regions of the FMN.

1.5.3. Mechanisms of electron transfer and catalysis.

The mechanism and electron-transfer rates for L-lactate oxidation and cytochrome *c* reduction by flavocytochrome b_2 have been the focus of much research and some controversy over recent years (Chapman *et al.*, 1991; Lederer, 1991). This research has provided rate-constants for each step in the catalytic cycle. The cycle consists of five electron-transfer events (Figure 1.5.3.) and has been shown to proceed at ~$100s^{-1}$ per molecule of L-lactate per mole of enzyme (~$200s^{-1}$ per mole of cytochrome *c* reduced) (Miles *et al.*, 1992).

Step 1 is the oxidation of L-lactate to pyruvate with the reduction of FMN to flavin hydroquinone. The mechanism of this step has proved difficult to determine. Two proposals have been made and these are discussed later in the section. However, the rate constant for this step has been determined by stopped-flow kinetics to be 604 ± $60s^{-1}$ (Miles *et al.*, 1992).

Steps 2 and 4 are the intra-molecular reduction of b_2-haem by flavin hydroquinone and semiquinone respectively. The rate constant for step 2, flavin hydroquinone to b_2-haem, was also measured by Miles *et al* (1992) and found to be 445 ± $50s^{-1}$.

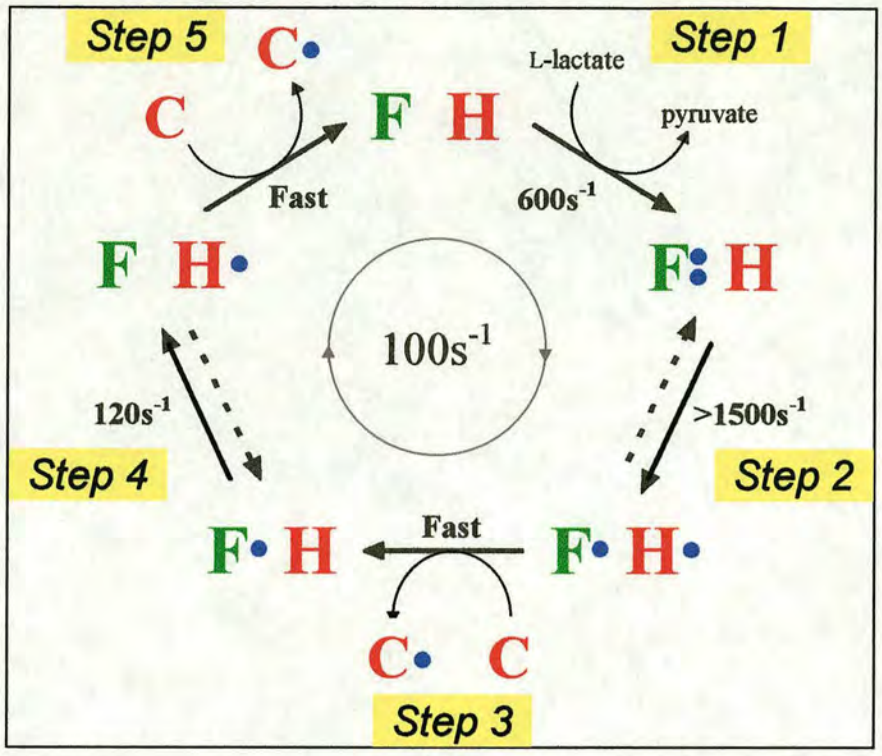

Figure 1.5.3. *Model proposed to explain the electron transfer events which make up the catalytic cycle of flavocytochrome b_2 in saturating amounts of L-lactate and cytochrome c. F = FMN, H = b_2 haem, C = cytochrome c, • = electron.*

However, this is only an approximation as haem reduction shows a definite lag behind FMN reduction and 3 steps have been shown to be involved in the reduction of FMN and haem (Chapman *et al.*, 1994). Taking account of these two factors the rate constant for electron transfer from flavin hydroquinone to haem has been estimated at ~1500s^{-1} (Chapman *et al.*, 1994). In the absence of an electron acceptor, each subunit of flavocytochrome b_2 can accommodate 3 electrons. Electron rearrangement between the flavin semiquinones produces 2 flavin hydroquinones and 2 oxidised flavins. Thus oxidation of two further molecules of L-lactate per flavocytochrome b_2 tetramer is possible (Capeillère-Blandin, 1975; Pompon, 1980; Labeyrie, 1982). During turnover, where this process is not observed, the enzyme acts as a 2-electron transferase. Thus step 4, the second intra-molecular electron transfer, is observed between flavin semiquinone and b_2-haem. Recently the rate constant for this step was shown to be 120s^{-1} and so is the rate-limiting step of the catalytic cycle (Daff *et al.*, 1996a). This is believed to be because the flavin semiquinone molecule exhibits an increase in redox potential of ~100 mV in the presence of the reaction product

pyruvate (Tegoni *et al.*, 1984; Hazzard *et al.*, 1994) and so is more stable than flavin hydroquinone or oxidised flavin under these conditions.

Steps 3 and 5 are cytochrome *c* reduction by b_2-haem. It has been proposed that the reduction of cytochrome *c* follows a two step process: (i) a reversible association of the proteins which rate-limits the cycle and (ii) an irreversible electron-transfer step. Kinetic data from stopped-flow traces of cytochrome *c* reduction fit well to single exponentials indicating that the reaction is limited by a single rate-determining step (Daff *et al.*, 1996b). The irreversible electron-transfer results from the large difference in reduction potentials of the two haems involved. The rate of electron transfer in the pre-formed complex has been estimated at $\geq 1000 s^{-1}$ (Daff *et al.*, 1996b). The second-order rate constant, which is a measure of the rate of association of the two proteins, was also recorded by Daff *et al* (1996b) and found to be $34.8 \pm 0.9 \mu M^{-1}s^{-1}$.

The active-site residues of flavocytochrome b_2 have been studied in great detail using site-directed mutagenesis (Chapman *et al.*, 1991; Lederer, 1991; Lederer *et al.*, 1996). The residues which are believed to play important roles in catalysis are shown in Figure 1.5.4. From the crystal structure of flavocytochrome b_2 it has been proposed that the reaction product, pyruvate, is bound in the active site by hydrogen bonds from 3 residues. The product carboxylate interacts with both R376 and Y143 while Y254 bonds to the carbonyl group (Xia *et al.*, 1990). Mutation of either R376 or Y254 causes a dramatic decrease in enzyme activity suggesting that both are indeed crucial to efficient catalysis (Reid *et al.*, 1988). Similarly Y143 has been shown to be very important and although it probably plays a role in binding and orientation of the substrate it is also believed to be essential to intra-molecular electron transfer (Miles *et al.*, 1992). The anionic flavin hydroquinone is thought to be stabilised by K349. The fact that a K349R mutant exhibits no dehydrogenase activity supports this proposal (Reid et al., 1988). The active-site base is H373 which participates in hydrogen abstraction from L-lactate. It is believed that D282 helps to stabilise the protonation of this histidine (Gondry *et al.*, 1996).

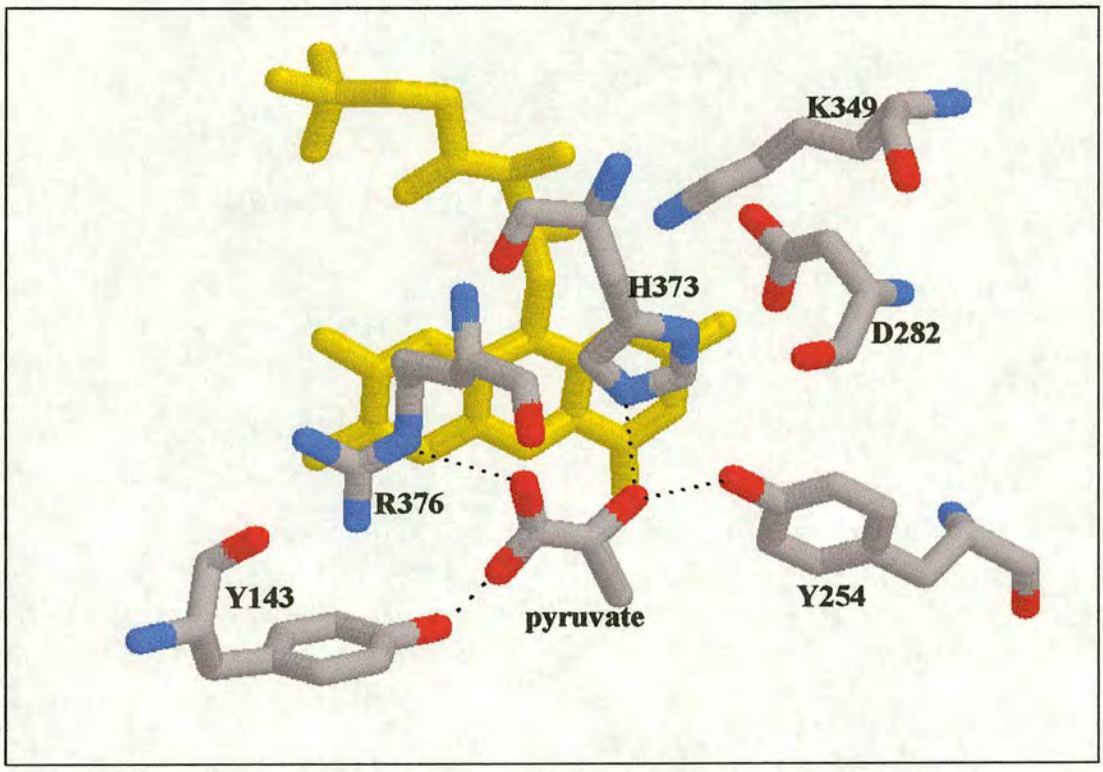

Figure 1.5.4. *The active site residues of flavocytochrome b_2 surrounding the FMN (yellow) and the reaction product pyruvate.*

There has been much debate over the nature of this hydrogen abstraction. Two possible mechanisms have been proposed: (i) abstraction as a proton leaving a carbanion intermediate or (ii) abstraction as a hydride (Chapman et al., 1991; Lederer, 1991). The two mechanisms are shown in Figure 1.5.5. The argument for the carbanion mechanism comes from Urban & Lederer (1985) but the evidence is not conclusive. The proposed mechanism requires the pK_a of H373 to be 15 in order to abstract the α proton from L-lactate. This means that the protein structure must enforce an increase in the pK_a of H373 of 8 pH units. It remains unclear as to how this would be accomplished. By the hydride mechanism H373 removes the more easily abstractable hydroxyl proton. This allows a concerted mechanism to proceed resulting in direct hydride transfer to the flavin N5. Although the hydride mechanism sounds more plausible there is no evidence to conclusively prove it.

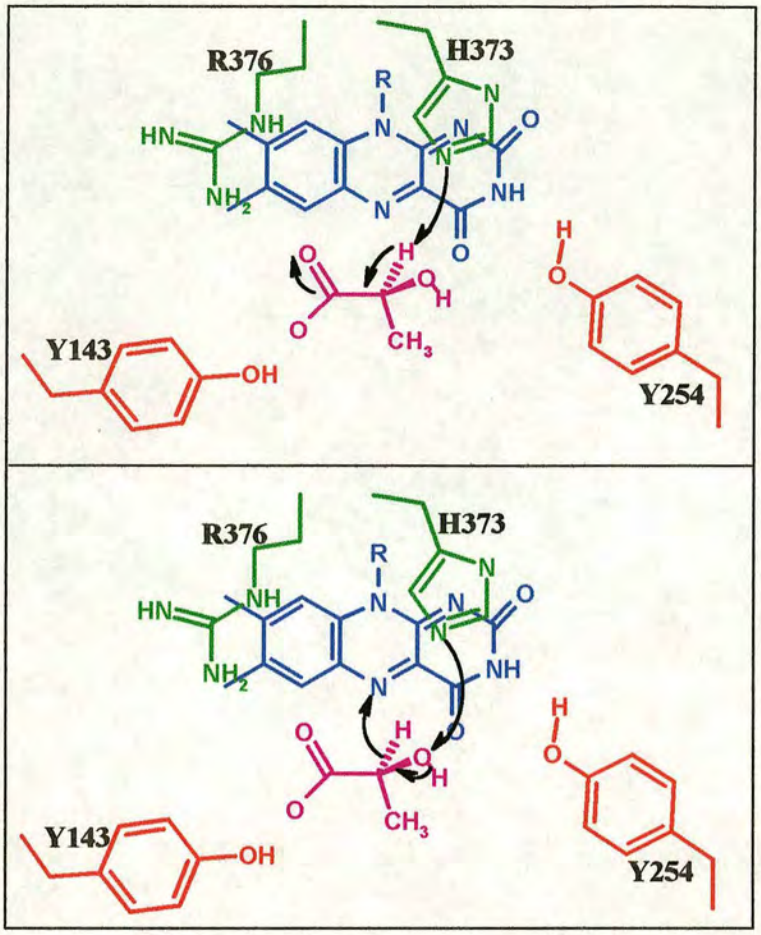

Figure 1.5.5. *The proposed mechanisms of L-lactate dehydrogenation by flavocytochrome b_2. Top; the carbanion mechanism resulting in a covalent bond to the flavin N5. Bottom; the hydride mechanism which involves a direct hydride transfer to the flavin N5.*

1.5.4. The Flavodehydrogenase domain (FDH).

The massive absorbance of the haem domain over the FMN group has made spectroscopic study of FDH very difficult. Thus, isolation of FDH became a priority in the bid to fully understand all the steps in both the catalytic and electron-transfer mechanisms of flavocytochrome b_2. Many attempts have been made to cut the two domains apart using proteolysis and chemical denaturation (Mevel Ninio *et al.*, 1977). However, due to the presence of the proteolytically sensitive loop, these procedures succeeded in producing two chains one of which was the haem binding domain plus ~200 residues from FDH with the other comprising the remaining FDH residues. Due to this severe disruption of FDH its correct size and structure could not be determined. Iwatsubo *et al* (1977), adopting more subtle tactics, were able to produce

an apoprotein by incubation of flavocytochrome b_2 in 6M Guanidinium hydrochloride (GdnHCl). This removed FMN and the tightly bound haem. By dialysing out the GdnHCl from the apoprotein in a 10-fold excess of FMN the flavoprotein was reconstituted successfully. The ensuing kinetic analysis of this species suggested that, in terms of lactate oxidase activity the haem-free enzyme was essentially unhindered. However, cytochrome *c* reductase activity had been eliminated. This agreed with the previous work of Forestier *et al* (1971) which had already proposed that the cytochrome domain of flavocytochrome b_2 was essential if the enzyme was to exhibit cytochrome *c* reductase activity. Much of the uncertainty surrounding the operation of FDH has been cleared up by the independent expression of the domain in *E. coli* (Balme *et al*, 1995). This allowed FDH to be expressed in large amounts (~10 mg/l) and studied without the uncertainty introduced by proteolysis and denaturation. This expression has been taken a step further by the recent work of Østergaard (1997) who engineered FDH into a significantly improved expression system allowing production to approach ~50 mg/l. The kinetic studies enabled by such over-expression have shown the true properties of the domain and how it functions. It now transpires (Balme *et al*, 1995), as suggested many times previously, that FDH is a very good L-lactate dehydrogenase and, when utilising the artificial electron acceptor $[Fe(CN)_6]^{3-}$, has a k_{cat} of $273s^{-1}$ which is about 70% that of intact flavocytochrome b_2 ($400s^{-1}$). However, although incredibly slow, FDH does show detectable cytochrome *c* reductase activity with a rate of $0.02s^{-1}$. It would seem then that the haem domain is essential for efficient inter-protein electron transfer from FMN to cytochrome *c*.

Although the crystal structure of independently expressed FDH has never been solved it has been assumed that in general it will have the energetically favourable $\alpha 8\beta 8$ folding motif which has become synonymous with the flavin oxidase/dehydrogenase family (Section 1.4.2.). Since the haem domain appears to have no contacts involved in keeping the tetrameric structure, it was likely that FDH would also be a tetramer and this is indeed the case. Although FDH seems to exist in the same conformation as it does in the intact enzyme there are some areas which cause concern. The main one is the proteolytically sensitive loop (298-315) which is

highly disordered in the intact flavocytochrome b_2 crystal structure making its position in relation to the barrel unknown. The loop appears in a number of related proteins, notably GO. Experiments have been performed to swap the loops of GO and FDH in an attempt to determine their properties (Østergaard *et al*, 1997). The mutations caused large decreases in k_{cat} and in some cases massive increases in K_m suggesting a role in substrate specificity. However, it should be remembered that in flavocytochrome b_2 the loop is pinned back by the haem domain with no influence on the active site and so any effects observed in independently expressed FDH are unlikely in the intact enzyme.

Thus, speculation on the evolution of these and the other family members can be made. Has flavocytochrome b_2 evolved in a divergent manner from a group of αβ-barrel flavoproteins acquiring its cytochrome domain by an act of gene fusion and loosing the need for this loop? Does the loop in GO still provide a function? Some of the evolutionary aspects are discussed in Section 1.4. One of the main aims of attaining the structure of FDH is to determine a function for this loop. The possibility in independently expressed FDH is that removal of the cytochrome domain allows the loop to fold over on top of the exposed FMN molecule. This action by a sizeable stretch of peptide would undoubtedly cause steric problems for an approaching electron acceptor providing a possible explanation for the total lack of electron transferase activity with its own independently expressed cytochrome domain and the dramatic (10 000-fold) decrease in cytochrome *c* reductase activity. This particular subject will be discussed in greater detail in Chapter 5.

2. Materials and Methods.

General Laboratory chemicals, where unspecified, were obtained from the Sigma Chemical Company.

2.1. Molecular biology techniques.

2.1.1. Site-directed mutagenesis.

Site-directed mutants of the flavin binding domain (FDH) of flavocytochrome b_2 were generated using the Kunkel method (Kunkel, 1985). This method incorporates a selection system for mutated DNA which utilises the tolerance of *E. coli* strain BW313 (*duf ung*$^-$) towards the nucleoside uracil.

Template DNA for mutagenesis reactions was from the plasmid encoding FDH_{wt} (pGR401) or from the plasmid encoding mutant proteins (pRC23) (section 7.5. for plasmid details). Uracil containing, single-stranded DNA (ssUDNA) is required as a template and was generated by transforming the plasmid into the strain BW313. This strain is deficient in the enzymes dUTPase and uracil glycosylase, the products of the *dut* and *ung* genes receptively. Thus, deoxyuridine 5′-triphosphate (dUTP) can compete with deoxythymidine 5′-triphosphate (dATP) for incorporation into ssDNA. Once incorporated the nucleotide is not removed. ssDNA containing 20-30 uracil-containing residues per genome is produced from BW313 using the helper phage M13K07. Isolation of the ssDNA is described in 2.1.3.1. The mutagenesis reaction then takes place in three steps.

- **Phosphorylation reaction.**

To allow DNA ligase to join the two ends of the new DNA strand, *i.e.* to extend the primer, the oligonucleotide must be phosphorylated.

5µl 5x phosphorylation buffer 1 M TrisHCl pH 8.0
0.3 M $MgCl_2$
0.1 M DTT
20 mM ATP

5 units T4 polynucleotide kinase (0.5 µl 10 units/µl)

15-20 µl oligonucleotide (4 pmol/µl)

5-10 µl dH_2O to a total volume of 30 µl

The mixture was incubated at 37°C for 40 mins, then heated to 70°C for 10 mins. This inactivates the polynucleotide kinase and stops the phosphorylation reaction. The oligonucleotide was used in mutagenesis immediately but can be stored at -20°C and used later.

- **Annealing reaction.**

This reaction anneals the phosphorylated oligonucleotide (Table 2.1.) to the template DNA. The mixture was incubated at 70°C for 5 mins, then cooled to 35°C over ~30 mins.

0.05 pmol ssUDNA template

0.5 µl phosphorylated oligonucleotide (1.25 pmol)

2 µl 10x annealing buffer (0.2 M TrisHCl pH 7.5)

dH_2O to a total volume of 20 µl

- **Synthesis reaction.**

3.3 µl T4 DNA polymerase (3 units/µl = 10 units)

0.7 µl T4 DNA Ligase (3 units/µl = 2 units)

6 µl 5x synthesis buffer

The synthesis reaction produces double stranded DNA (dsDNA) based on the ssDNA template by extending the oligunucleotide which codes for the desired mutation(s). The mixture was incubated at room temperature for 5 mins, at 37°C for 90 mins and was then transformed immediately into *E. coli* strain TG1 (*dut*$^+$, *ung*$^+$) or stored at -20°C until required. As this strain is intolerant of uracil, the template DNA containing uracil is destroyed leaving only the synthesised mutant DNA to replicate giving a high yield of mutated DNA.

Name	Sequence	Mutation
Wild Type	GCT/ACA/GCT/TTG/TGT/AAA/CTG/GGA/AAC/C	-
SLR001	GCT/ACA/GCT/GAG/TGT/AAA/CTG/G	L199E
SLR002	GCT/TTG/TGT/GAA/CTG/GGA/AAC/C	K201E
SLR003	GCT/ACA/GCT/GAG/TGT/GAA/CTG/GGA/AAC/C	L199E/K201E
LEN001	G/TTA/TCA/AAG/GAA/ATT/GAC/CC	F325E
M7348	TG/AAG/CTG/GAA/TTT/TCC/AAT	K296E
SLFW011	GCG/TTA/TCA/GCG/GAA/ATT/GAC/CCC	K324A/F325E

Table 2.1. *Oligonucleotides used for site-directed mutagenesis experiments. Letters highlighted in red indicate the codon altered from the wild type sequence. Supplied by PE-Applied Biosystems UK, Kelvin Close, Birchwood Science Park North, Warrington, Cheshire, WA3 7PB.*

2.1.2. Transformations.

The plasmid encoding FDH can be moved easily between various strains of *E. coli* allowing expression of protein (TG1 or pop2136) and production of ssDNA for either mutagenesis (BW313) or for sequencing purposes (TG1).

2-4 µl plasmid DNA
dH_2O to 10 µl total volume (DNA + H_2O)
100 µl competent cells

The mixture was incubated on ice for 20 mins allowing the DNA to adhere to the cell walls. It was then subjected to thermal shock by rapid transfer to a water bath at 42°C for 30 s and then allowed to cool again for 5 mins in an ice/water bath. This process causes the cell wall to undergo a pulse-opening allowing the plasmid to enter. SOC medium was added (800 µl) and incubated at 37°C for 45 mins. This allows phenotypic selection of the selectable marker *i.e.* ampicillin resistance. The cells were then spun out of the solution, resuspended in a small volume of residual medium and spread on agar/ampicillin plates (section 2.1.9.). The plates were incubated overnight at 37°C.

The efficiency of the transformation was monitored using the following simple control experiments.

- competent cells with no plasmid have no ampicillin resistance and therefore produce no colonies.
- competent cells transformed with the plasmid pTZ19R produce very large numbers of colonies.

Competent cells were produced using the $CaCl_2$ method (Sambrook *et al.*, 1989). These were found to be most efficient when used immediately but could be stored at -80°C.

2.1.3. DNA isolation.

2.1.3.1. Single stranded DNA (ssDNA).

Generation of ssDNA for sequencing and mutagenesis was by the same technique. The relevant dsDNA was transformed into the host strain. A single colony was used to inoculate 5 ml of LB and incubated at 37°C for 4-5 hrs until mid-log phase. 2 ml of this was transferred to a fresh bijou, inoculated with 1.3 µl of the helper phage M13K07 (2×10^7 pfu) and incubated for 2 hrs. 400µl of this was used to sub-culture a further 10 ml of LB containing 70 µg/µl kanamycin and 50 µg/µl ampicillin. This was incubated in a shaker incubator, at 37°C overnight. Taking 1.5 ml of the culture in an Eppendorf the cells were spun out by brief centrifugation. From the supernatant the DNA can be precipitated by adding 300µl 20% PEG/2.5 M NaCl. This was collected as a pellet, resuspended in 200 µl H_2O and subjected to successive cleaning with 400 µl phenol:chloroform (50:50) to remove lipids and protein. The Eppendorf was centrifuged at 13000 min^{-1} for 5 mins. At the interface of the two solutions impurities were seen to precipitate. The aqueous phase was removed carefully for the next step with cleaning being repeated until no further impurities were extruded. To the clean DNA solution, 40 µl of 3M Na Acetate pH 5.2 was added along with 1 ml 95% ethanol. Precipitation of DNA was induced by incubation at -20°C for at least 1 hr. The DNA was pelleted, washed carefully with 70% ethanol and dried. The resulting translucent pellet was resuspended in 50µl of dH_2O and stored at -20°C.

2.1.3.2. Plasmid DNA.

Plasmid DNA was isolated from *E. coli* using 50 ml Alkaline lysis plasmid preps or Plasmid mini preps. A single colony was used to inoculate 5 ml LB, 50 µg/µl ampicillin. This was incubated at 37°C until mid-log phase and used to inoculate 45 ml LB in a 250 ml flask, 50 µg/µl ampicillin. This was incubated overnight at 37°C. The cells were spun down at 4000 min^{-1} for 10 mins in silinated Corex tubes. The pellets were resuspended in 2 ml of TEG/lysozyme, mixed by inversion and left on ice for 15 to 30 mins. This degrades the cell wall. The glucose solution acts as an isotonic preventing "wall free" spheroplasts from degrading. To this is added 4 ml 0.2M NaOH/1 % SDS. The SDS dissolves cell membranes. The addition of NaOH promotes DNA strand separation (chromosomal and plasmid). The solution was mixed by inversion and left on ice for 5 mins. Na Acetate pH 5.2 was added (3 ml, 3 M) again mixing by inversion and leaving on ice for 20 mins. The pH drop allows DNA strand reannealment to occur. However, chromosomal DNA is very big and on strand separation aggregates into insoluble masses. Plasmid DNA, being circular and small remains soluble and can reanneal The solution was spun at 10000 min^{-1} for 10 mins to remove the chromosomal DNA. The supernatant was ethanol precipitated by adding 16 ml ethanol and incubating on ice for 15 mins. The plasmid DNA was then pelletted by spinning at 10000 min^{-1} for 10 mins. The pellet was resuspended in 2 ml of solution B and cleaned using 2 ml of phenol:chloroform (50:50). Removing the aqueous phase to a clean tube, the organic phase was back extracted with another 2 ml of solution B. This can be repeated if required. The aqueous phases were combined, mixed with 8 ml ethanol, incubated on ice for 15 mins and spun at 10000 min^{-1} for 10 mins. The pellet was resuspended in 400 µl TE buffer, transferred to an Eppendorf and incubated with 20 µl boiled RNaseA for 1 hr at 37°C. 20 µl of 4 M NaCl was added and the aqueous phase extracted twice with equal volumes of phenol:chloroform (50:50) and once with chloroform. The aqueous phase was incubated on ice for 10 mins with 800 µl ethanol. Spinning for 5 mins in a microfuge produced a plasmid DNA pellet which was resuspended in 200 µl dH_2O and stored at -20°C.

The Alkaline lysis mini prep allows a much smaller scale version of the above plasmid prep using only a 5 ml culture split into 1.5 ml Eppendorfs. The only difference is in the cleaning of the plasmid DNA where, rather than back extracting the organic phase with H_2O, successive volumes of organic phase are used on the aqueous phase. The plasmid DNA is ethanol precipitated, washed with 70% ethanol, resuspended in 20 µl dH_2O and stored with 1µl RNaseA at -20°C.

2.1.3.3. Solutions.

TEG/Lysozyme

25 mM TrisHCl pH 8.0

10 mM EDTA

50 mM glucose

Solution B

40 mM TrisHCl pH 8.0

1 mM EDTA

0.1 M Na Acetate

0.1% SDS

2.1.4. DNA digestion.

Restriction enzymes were used to cut the FDH_{wt} and mutant DNA from plasmids. Fragments could then be ligated into expression plasmids. The host plasmid pGR401, used for DNA manipulation, was digested using the enzymes *Xba*I and *Hind*III in the following manner.

1-2 µl plasmid DNA

1.5 µl Multicore buffer (Promega)

7.5-8.5 µl dH_2O

2 µl *Xba*I

2 µl *Hind*III

The solution was incubated overnight at 37°C. To determine the efficiency of the digest and to isolate the FDH DNA fragment the digest mix was run on a 0.8% agarose gel. Using a 1 kb DNA ladder, Gibco BRL, the fragment was shown to run at about 1.4 kb. The DNA was then purified from the gel material (Section 2.1.6.). The DNA can be used immediately or stored at -20°C until required. The procedure was repeated with the over-expression plasmids pJF118 and pRC23. This generates cohesive ends on the new plasmid for the mutant FDH fragment to be ligated into.

2.1.5. DNA ligation.

The FDH DNA fragment and the digested plasmid were ligated together to give the completed expression system.

1 µl vector DNA

1-6 µl insert DNA (wide range to encompass the concentration for maximum efficiency).

1.5 µl $[Co(NH_3)_6]Cl_3$

3.5-6 µl dH_2O

3 µl ligation buffer (NEB buffer2 + 100 µg/ml Bovine serum albumin)

1 µl Ligase (NEB), 20 units/µl diluted 5-fold for use.

Total volume = 15 µl

Control experiments were performed with insert only and vector only. These produced no colonies on transformation provided that the digests and ligations were complete. The mixture was incubated at 18°C overnight. This was then diluted 2-fold with half being used immediately for transformation into the expression strain TG1 and the remainder being stored at -20°C for future use.

2.1.6. DNA purification from agarose.

- **Gel Mix.**

  0.17 g Agarose, high purity

  25 ml diluted TAE buffer, heated to dissolve the agarose.

  2 µl of 10 mg/ml ethidium bromide, acts as a DNA marker

- **Markers.**

  5 µl H_2O

  5 µl marker mix, (1 kb ladder, Gibco BRL)

  5 µl loading buffer

- **Samples.**

For purifying digest mixes, 3 15 µl lanes were combined allowing 4 digest mixes to be pooled and run as one 60 µl sample. To each 15 µl mix, 5 µl of loading buffer was added. Gels were run at 38 mA for about 1 hr to resolve the fragment DNA from the plasmid. The required piece of DNA was removed from the gel with a sharp blade. To purify the DNA from the agarose slice, the Geneclean III kit and procedure was used (Bio-Rad). This utilises a silica matrix EZ-GLASSMILK™ to bind DNA thus removing it from solution. DNA was eluted from the matrix using a wash solution.

2.1.7. DNA sequencing.

All mutated DNA was sequenced using the SEQUENASE™ kit and protocol from United States Biochemical.

- **Annealing reaction.**

The primer 295A was selected to sequence the region of DNA immediately around the area where the mutations were being directed. Having the sequence GTG/GGC/CTT/CTA/TTC/CT it was designed to mutate tryptophan 143 to a phenylalanine. The primer was annealed to the ssDNA as follows.

7 µl DNA

2 µl sequencing buffer

1 µl primer

The mixture was heated at 65°C for 2 mins and then cooled slowly to < 35°C.

- **Labelling reaction.**

To the annealed DNA the following was added.

1 µl DTT (0.1 M)

2 µl labelling mix, diluted

0.5 µl [α-^{35}S]-dATP (1000-1500 Ci/mmol)

2 µl diluted Sequenase, to side of tube. When microfuged all reactions begin together.

The mixture was incubated at room temperature for 5 mins.

- **Termination reaction.**

The termination mixes were incubated at 37°C prior to use in the reaction. To these 3.5 µl labelling mix was added and incubated for a further 5 mins. The termination reactions were stopped by adding 4 µl of stop solution. Prior to loading on a sequencing gel the samples were heated to 75°C for at least 2 mins, ensuring that the DNA was fully denatured.

- **Sequencing gel recipe.**

  25.2 g Urea

  12 ml Acrylamide solution (30 % Acrylamide, 0.8 % Bisacrylamide, w/v)

  6.5 ml 10x TBE buffer

  65 ml H_2O

The polymerisation agents used were (i) 65-70 µl Temed and (ii) 110 µl 25% Ammonium persulphate (freshly prepared).

Sequencing gels were run at 65 mA for ~40 min to pre-heat prior to loading the samples. Samples were heated and loaded in two batches to prevent cooling during the loading process. A running time of 1.5-2 hrs was used. Gels were then removed to blotting paper and soaked in fixing solution (5% acetone and 15% methanol) for 15 mins, dried and contact exposed to film overnight.

2.1.8. Maintenance and growth of stocks.

Expression system stocks were stored in two ways. Single colonies were picked from original transformants and streaked onto agar/ampicillin plates. These were stored at 4°C and remained usable for 3 weeks to 1 month at which time they were restreaked onto fresh plates. Single colonies were also used to inoculate 5 ml starter cultures. These were incubated at the appropriate temperature until mid-log phase then stored with glycerol (50 % v/v) in liquid nitrogen or at -80°C. When thawed these could be streaked onto agar plates or used directly as inoculant for 5 ml starter cultures. The two expression systems used operated under different promoter systems (section 7.5.) and so required different growth conditions.

- **pJF118/TG1**. (section 7.5.) 5 ml starter cultures were used to inoculate 500 ml of terrific broth in a 2 L flask, 50 μg/ml of ampicillin. Flasks were incubated and shaken at 37°C and 200 rpm until mid-log phase was reached, O.D. = 0.5 at 600 nm, generally taking about 5-6 hrs. Cultures were then induced with 0.5 mM IPTG (isopropyl-β-D-1-thiogalactopyranoside) and left at 37°C overnight. Wet cell weight produced by this system was generally 8-10 g/L. Typically only 3 L cultures were required per protein preparation.

- **pRC23/pop2136.** (section 7.5.) 5 ml starter cultures were used to inoculate 500 ml Luria broth in a 1 L flask, 100 μg/ml carbenicillin. These cultures were incubated at 30°C shaking at 200 rpm until mid-log phase was reached again taking approximately 5-6 hrs. Protein over-expression was induced by increasing the growth temperature to 42°C. Cultures were incubated at 42°C overnight. Wet cell mass produced by this system was generally 4 g/L. Typically 6-7 L was required per protein preparation.

2.1.9. Culture media.

Luria Broth.

10 g/l Difco Bacto Tryptone.

5 g/l Difco Bacto Yeast Extract

5 g/l NaCl

dH_2O

Terrific Broth.

12 g/l Difco Bacto Tryptone.

24 g/l Difco Bacto Yeast Extract

4 ml/l glycerol

12.54 g/l K_2HPO_4

2.31 g/l KH_2PO_4

dH_2O

SOC Medium.

2 % Difco Bacto Tryptone

0.5 % Difco Bacto Yeast Extract

10 mM NaCl

2.5 mM KCl

10 mM $MgSO_4$

20 mM glucose

dH_2O

All media was autoclaved after production. Antibiotic was dissolved in dH_2O and sterilised by filtration before adding to the cooled media as required.

Agar/ampicillin plates.

The required volume of LB was prepared, agar was then added to 1.5 % (1.5g per 100 ml), mixed thoroughly and autoclaved. Ampicillin was added (50 μg/ml) when the media had cooled. The Agar was poured just prior to setting.

2.2. Protein isolation and purification.

2.2.1. Cell harvest.

Cultures were centrifuged at 5000 min^{-1} for 15 mins using a Sorvall RC 5B centrifuge and GSA head with 6 x 500 ml fixed angle pots. The temperature was controlled at 5°C. The cell mass was pooled and stored at -20°C until required for protein extraction.

2.2.2. Protein extraction.

A typical preparation used 30-40 g of wet cell mass. The cells were partially thawed then snap frozen in liquid nitrogen for 5 mins. The cells were thawed and resuspended in 100 ml of lysis buffer. This solution was stirred gently for 1.5-2 hrs at 4°C. The cells were then burst open using sonication to ensure maximum release of protein. A Hert Systems Ultrasonic Processor XL was used at a power setting of 30 % and an intensity of 8 for 3-4 mins (20 s bursts). The cells were kept on ice to prevent the solution warming up during the sonication process. The cell debris was centrifuged out of the solution at 15000 min^{-1} for 15 mins at 4°C. The protein solution was assayed for L-lactate/ferricyanide oxidoreductase activity. The specific activity of the protein was monitored throughout the purification, allowing comparisons to be made with the amount of protein recovered from each step (Table 2.2., section 2.2.6.). The lysed solution was diluted approximately 4-fold with dH_2O and made 10 % glycerol by weight. This brings the solution to the correct ionic strength for column chromatography and the glycerol mimics the conditions of the cell interior helping to prevent FMN loss from the active site.

2.2.3. Column preparation and solutions.

The purification of FDH from *E. coli* involves only two columns utilising anion exchange and gel filtration chromatography.

2.2.3.1. Column preparation.

- **Anion Exchange.**

A column approximately 10 cm long and 2 cm in diameter containing Diethylaminoethyl, DE-52 material (Whatman) was prepared. The material was batch equilibrated twice with fresh 100 mM phosphate buffer pH 7.0. After allowing the material to settle, buffer and fine particles were decanted off. The material was then resuspended in 10 mM phosphate buffer pH 7.0. The slurry was poured into the column ensuring that a flat and even bed was achieved. The column was then washed with at least two column volumes of 10 mM phosphate buffer pH 7.0.

- **Gel filtration.**

A column approximately 30 cm x 0.5-1 cm containing Sephadex G25 or G50 (Sigma) was used. The material was batch washed twice in volumes of Tris.HCl pH 7.5 I = 0.1 M. Again buffer and fine particles were decanted off between washes. The material was resuspended in the same buffer and poured, again ensuring an even and flat surface. This column could be used for many purifications provided it was not allowed to dry out and was washed thoroughly between preps.

2.2.3.2. Purification solutions.

- **Phosphate buffer pH 7.0**

  500 mM, 2-3 L volumes for dilution as required.

  305 mM dibasic sodium phosphate, Na_2HPO_4.

  195 mM monobasic sodium phosphate , NaH_2PO_4.

  made to final volume with dH_2O.

- **Tris.HCl pH 7.5, I = 0.1 M.**

  500 ml dH_2O

  10 ml 1 M standard HCl

5.265 g NaCl, concentration can be varied to alter the ionic strength of the solution.

Adjusted to pH 7.5 using a saturated solution of Trizma™ base.

Made up to 1 L with dH_2O.

- **Lysis Buffer.**

100 ml, 100 mM phosphate buffer pH 7.0.

10 mM L-lactate.

10 mM EDTA.

Immediately prior to resuspending cells add,

1 mM PMSF.

0.2 mg/ml egg white lysozyme.

- **L-lactate/Ferricyanide activity assay solution.**

10 mM L-lactate lithium salt.

2 mM potassium ferricyanide.

Tris.HCl pH 7.5, I = 0.1 M.

Active FDH is reduced by L-lactate and oxidised by ferricyanide. On reduction of ferricyanide its bright yellow colour is lost. This can be observed at 420 nm on a spectrophotometer.

2.2.4. Anion exchange chromatography.

The diluted supernatant was loaded directly onto the DE-52 column. FDH binds fairly diffusely, but in the top half of the column allowing much of the remaining cell debris and protein to elute as a murky brown solution. The eluate was tested for L-lactate/ferricyanide ($[Fe(CN)_6]^{3-}$) oxidoreductase activity to ensure that FDH was binding to the material. The column was washed with 10 mM Phosphate buffer, pH 7.0. The murky brown colour of the column material was washed away revealing bound FDH as a broad, bright yellow band. This band often covered half of the column due the diffuse binding and very high levels of expression in the pJF118/TG1 system. While washing with 10 mM Phosphate buffer, pH 7.0, the UV absorbance at 270 nm was observed until reaching a minimum. The concentration of phosphate was

increased slowly from 10 mM to remove as much of the contaminating protein as possible. However, FDH begins to elute with 20 mM Phosphate buffer. Thus, washing was more effective if large volumes of low concentration buffer were used. To elute FDH in a tight band, ≥ 60 mM Phosphate buffer, (pH 7.0) is required, depending on the protein and the charges which have been introduced *e.g.* FDH_{wt} elutes at 50 mM Phosphate buffer whereas the quadruple mutant L199E/K201E/K324A/F325E, where three negative residues have been introduced, requires 100 mM Phosphate buffer. Thorough washing of the DE-52 column ensures maximum purity of the protein. The bright yellow eluate was precipitated with ammonium sulphate, to concentrate the enzyme, and gel filtered to remove the salt and exchange the buffer.

2.2.5. Ammonium sulphate precipitation and gel filtration.

To precipitate FDH from the solution, the eluate was made 80 % (561 g/L) in ammonium sulphate. The solution was stirred at 4°C until the ammonium sulphate was fully dissolved. The solution was spun at 15000 min^{-1} for 15-20 mins producing a bright yellow pellet. The pellet was then dissolved in the minimum volume of buffer. Generally, Tris.HCl pH 7.5, I = 0.1 M was used for assays and so was the buffer of choice for storage. The maximum volume required for dissolution was 2-3 ml. This solution was applied directly to the gel filtration column. The column beads are full of pores designed to exclude large molecules, like proteins, allowing them to flow down the column unhindered. The pores are big enough to admit small molecules causing equilibria to be set up as the small buffer and salt molecules pass in and out of the pores. Thus, these travel down the column much more slowly than the protein and so resolution is achieved. The principle is the same when trying to separate different sized proteins. The protein solution was collected in fractions and its purity determined by comparing the ratio of absorbance at 270 nm with that at 452 nm. If Abs at 270 nm/Abs at 452 nm was ≤ 8 then the protein was acceptably pure for most kinetic experiments, giving one major band and only two or three faint contaminant bands on an overloaded SDS gel (Figure 2.1.). The concentration of the protein was determined using previously published extinction coefficients (Iwatsubo *et al.*, 1977)

at 452 nm for the FMN. A 3 L culture of pJF118/TG1 produced up to 100 mg of pure FDH. Suitable fractions were stored in aliquots of 200 µl-1 ml in liquid nitrogen.

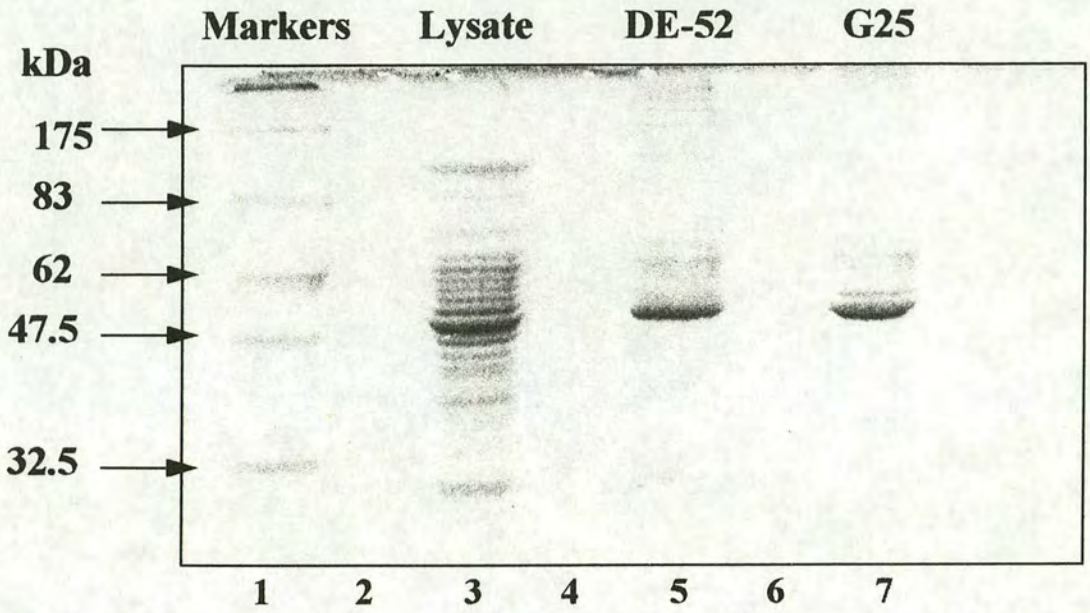

Figure 2.1. *A 12 % SDS polyacrylamide gel of the purification of FDH_{wt} which can be seen at M_r = 47000 in lanes 3(lysate), 5(DE-52) & 7(G-25). The protein weight markers in lane 1 are broad range pre-stained markers (175-6.5 kDa) supplied by NEB. Gels were run using the Mini-PROTEAN® II electrophoresis cell kit from BIO-RAD.*

2.2.6. Specific activity measurements during purification.

	Vol ml	ΔA/Δt	Moles $[Fe(CN)_6]^{3-}$ reduced s^{-1}.
Lysate	70	0.191	0.138
DE-52	38	0.531	0.06
G 25	3.75	0.35	0.038

Table 2.2. *Specific activities during purification of L199E/K296E. This indicates a return of 27 % of the activity detected in the initial lysate solution.*

Specific activity was calculated using the following equation.

$$(\Delta A/\Delta t \times 60) \times ((\text{assay vol}/\varepsilon \times y) \times \text{total volume})$$

Where $\Delta A/\Delta t$ = rate of change of absorbance at 420 nm.

assay volume = 1 ml

y = volume of protein solution used in the assay = 20 µl

ε = extinction coefficient for $[Fe(CN)_6]^{3-}$ at 420 nm = 1040 M^{-1} cm^{-1}

assay time = 120 s

$[Fe(CN)_6]^{3-}$ = 2 mM

[L-lactate] = 10 mM

All assays were performed in Tris.HCl pH 7.5, I = 0.1 M buffer.

2.3. Steady-state kinetic analysis.

To determine the effect of substrate concentration on reaction rate the FDH_{wt} and mutant proteins were studied under steady-state conditions. Data were analysed using Michaelis-Menten kinetics (Appendix 1.). All experiments were performed on a Shimadzu 2101 UV/vis spectrophotometer at 25°C. The buffer used in each case was Tris.HCl pH 7.5, I = 0.1 M, except for the ionic strength experiments where I was varied from 0.05 M to 0.5 M by addition of the appropriate amount of NaCl. Protein solution, previously stored under liquid nitrogen, was kept on ice during the experiment until required and in most cases was fully active for up to 2 hrs. At this point protein activity began to deteriorate significantly. Assay solutions were made up in the spectrophotometric cuvettes without the protein and incubated in a water bath at 25°C for 5-10 mins prior to measurement. Each assay solution consisted of the substrate, L-lactate, the acceptor, $[Fe(CN)_6]^{3-}$ or cytochrome *c*, in the appropriate concentrations and were made up to the final volume with buffer excluding the volume of protein. The protein was injected into the cuvette to begin the reaction. The assay solution was mixed gently by inversion to prevent bubbles forming and placed in the spectrophotometer. For each enzyme, Michealis-Menten curves were determined using the substrate L-lactate and the electron acceptor $[Fe(CN)_6]^{3-}$. This allowed comparisons of activity to be made between the mutants and FDH_{wt}. Experiments were performed in duplicate and in random order to prevent sequential error. The rate of change of absorbance of the acceptor ($\Delta A/\Delta t$) was followed spectrophotometrically over 2 mins. The gradient of the straightest and most consistent part of this trace was used in each case. Using this value for $\Delta A/\Delta t$, k_{obs}

was calculated from the equation shown below and then plotted against the concentration of the substrate being varied to generate a Michaelis-Menten curve, allowing calculation of the kinetic parameters k_{cat} and K_m.

k_{obs} (s^{-1}) = $\Delta A/\Delta t$ (min^{-1}) x assay vol (l) / ε x 60(s) x p.l.(cm) x protein vol (l) x [protein] (M)

where k_{obs} = the observed reaction rate.

ε = The extinction coefficient of cytochrome *c* or $[Fe(CN)_6]^{3-}$.

p.l. = the pathlength of the cuvette.

2.3.1. $[Fe(CN)_6^{3-}]$ dependence.

The concentration of $[Fe(CN)_6]^{3-}$ was varied to determine its effect on the rate of turnover while the concentration of L-lactate was kept constant and saturating.

[L-lactate] = 10 x K_m or ~70 mM to ensure saturation.

$[Fe(CN)_6^{3-}]$ = 0.05-50 mM.

[FDH] = ~2 x 10^{-7} M.

Fresh stocks of L-lactate (500 mM) and $[Fe(CN)_6]^{3-}$ (100 mM) were made in assay buffer and stored at 4°C when not in use.

p.l. = 2-5 mm to keep absorbance as low as possible at high concentrations of $[Fe(CN)_6]^{3-}$.

Assays were followed at 420 nm (ε = 1040 M^{-1} cm^{-1}) or 450 nm (ε = 268 M^{-1} cm^{-1}) again to ensure that the absorbance at high concentrations of $[Fe(CN)_6]^{3-}$ was as low as possible. The gradient of the negative slope $\Delta A/\Delta t$ produced by the loss of absorbance of $[Fe(CN)_6]^{3-}$ as it is reduced by FDH was used as shown above to give an observed rate constant k_{obs}.

2.3.2. [L-lactate] dependence.

The concentration of L-lactate was varied to determine its effect on the rate of turnover while the concentration of $[Fe(CN)_6]^{3-}$ was kept constant and saturating.

[L-lactate] = 0.05-500 mM.

$[Fe(CN)_6]^{3-}$ = 10 x K_m or 5-10 mM to ensure saturation, but to keep the absorbance as low as possible. Short p.l. cuvettes (2-5 mm) were used.

[FDH] = ~2 x 10^{-7} M.

The same stock solutions were used and assays were followed as in the $[Fe(CN)_6^{3-}]$ dependence experiment.

2.3.3. [Cytochrome *c*] dependence.

The [cytochrome *c*] was varied to determine its effect on the rate of turnover while the concentration of L-lactate was kept constant and saturating.

[L-lactate] = 10 x K_m or 70 mM.

[Cytochrome *c*] = 0.1 - 100 μM.

[FDH] = 2 x 10^{-7} M.

A fresh stock of ~500 μM horse heart cytochrome *c* (Sigma) was made by dissolving ~12 mg in 2 ml of assay buffer. This was kept on ice and diluted as required. Assays were followed at 550 nm (ε = 22640 M^{-1} cm^{-1}) using cuvettes of pathlength 1 cm to 2 mm ensuring that, at high concentrations of cytochrome *c*, the absorbance was kept as low as possible. The reduction of cytochrome *c*, observed at 550 nm, produced a positive slope with gradient $\Delta A/\Delta t$. This was used as shown above to give values of k_{obs}. The rate of reduction of cytochrome *c* by FDH is very slow, about 0.02 s^{-1}. Thus, it was often observed that the traces were curved slightly possibly due to the re-oxidation of cytochrome *c* by O_2. In fact allowing an experiment to run for up to 30 mins would show cytochrome *c* becoming almost fully oxidised again.

The [cytochrome *c*] dependence was determined at a number of ionic strengths. This provides information on the nature of the interaction between cytochrome *c* and FDH_{wt}. Experiments were performed as described previously, using buffers made up to the appropriate ionic strength with NaCl. To do this, two stocks of Tris.HCl were made with ionic strengths of 1 M and 0.01 M. These were then mixed to give buffers with ionic strengths in the range 0.05 M-0.5 M. A similar procedure was used to give L-lactate and cytochrome *c* solutions in the same range. To convert the FDH_{wt} solution from I = 0.1 M to the desired ionic strength, it was mixed with either 0.01 M

or 1 M buffer. The following equation was used to determine the correct volume of buffer.

e.g. converting 0.1 M FDH_{wt} to 0.5 M FDH_{wt}

$$(1 \text{ ml } FDH_{wt} \times 0.1 \text{ M}/1 \text{ ml} + y) + (y \times 1/1 \text{ ml} + y) = 0.5 \text{ M}$$

where y = the volume of 1 M buffer required to convert 1 ml of FDH from 0.1 M I to 0.5 M I.

Values of k_{obs} were plotted directly against the ionic strength (I) of the solution. According to Debye-Hückel theory (section 7.3.) they were divided by their concentration to give a second-order rate constant (k_2). The $\log k_2$ was plotted against $\sqrt{I}$ to give an ionic strength plot. The gradient of the line obtained indicates the charges involved at the interaction between the two species (z_+z_-). However, the theory is meant for point charges and, as it is difficult to determine exact charge contributions from each protein, the data obtained are merely qualitative. The nature of the interaction can be determined as the interaction of opposite charges (-ve/+ve) or like charges (-ve/-ve or +ve/+ve).

2.4. Stopped-flow kinetic analysis.

2.4.1. Introduction.

Stopped-flow experiments were performed to study the effects of the mutations on binding of both inorganic complexes and cytochrome *c* to FDH. The fast pre-steady state rates of oxidation of fully reduced FMN were observed. Stopped-flow involves the rapid mixing of 2 equal volumes of solution into a spectrophotometric cell of fixed pathlength. On mixing, the instrument is triggered recording the absorbance of the reacting solution and generating a trace with a specified time base (Figure 2.2.). The instrument's resolution is limited by its dead time (dt). This value is derived by calculating the time difference between the point at which the reaction can be traced back to (t = 0) and the point at which the absorbance is actually recorded (t = dt). The dead-time can be measured by recording any single exponential reaction over which the total absorbance change is known. The dt for an Applied Photophysic's

instruments is estimated at 0.9 to 1.1 ms. However, the resolution is also impaired by the mixing time. This value is more difficult to quantify. Measurement begins as soon as the two solutions are injected into the cell, but the reaction will not be at full speed until the two have mixed completely, causing a lag phase to be observed. Due to these factors, reactions which occur faster than 1000 s^{-1} will be impossible to resolve and much of the absorbance change will be lost. Since all reactions in this report occurred at a rate of 500 s^{-1} or less this was not a problem.

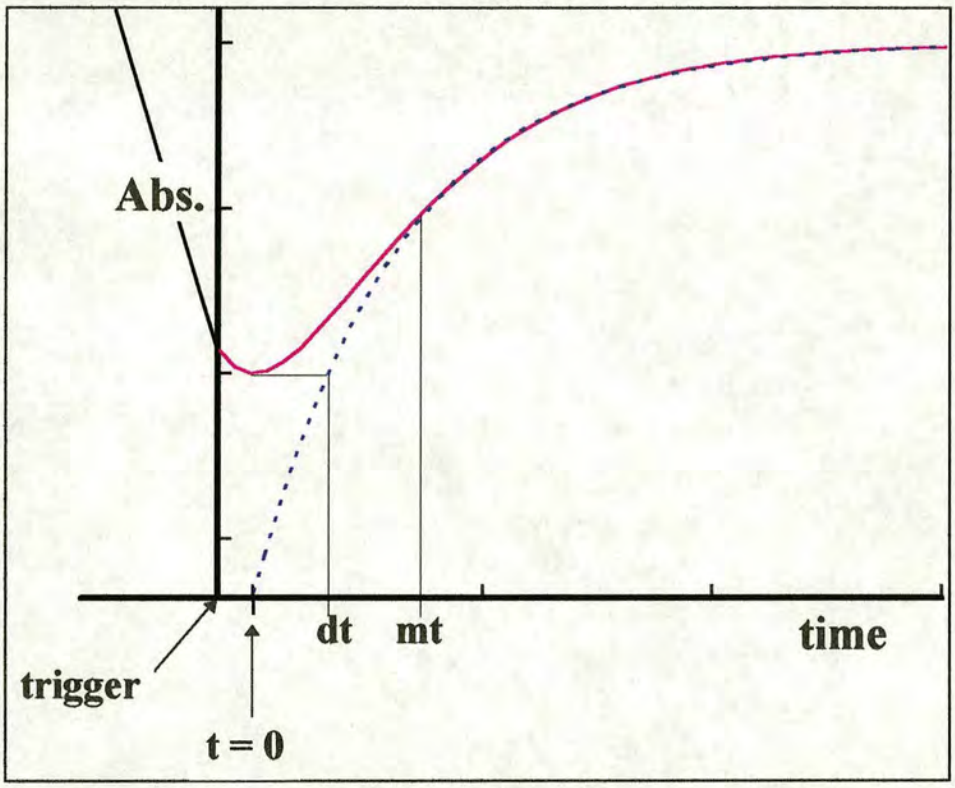

Figure 2.2. *A schematic diagram of a stopped-flow trace (absorbance vs time), fitted to a single exponential function (blue dashed line) showing the parameters dead time (dt), mixing time (mt), zero time (t = 0) and the trigger point where observation begins.*

2.4.2. Procedure.

All experiments were performed on an Applied Photophysics SF.17 Micro volume stopped flow spectrofluorimeter at 25°C, in Tris.HCl pH 7.5, I = 0.1 M buffer. An FDH stock solution of 4 μM was made in Tris.HCl pH 7.5, I = 0.1 M. This was kept on ice for the duration of the experiment. 4 μM FDH gave a concentration of 2 μM when shot into the apparatus and mixed with the acceptor. Glycolate was used as the substrate at approximately 50 mM from a stock of 500 mM. This was made with

glycolic acid dissolved in Tris.HCl buffer and titrated with NaOH solution back to pH 7.5. Flavocytochrome b_2 has a higher K_m for glycolate than L-lactate, but still utilises it as a fairly efficient substrate. This allows it to be used where rapid re-reduction of the enzyme by the substrate would hinder observation of the oxidation of the enzyme.

Electron acceptors were also made up in fresh stock solutions of Tris.HCl pH 7.5, I = 0.1 M. Cytochrome *c* 2 mM, $Fe(CN)_6^{3-}$ 100 mM, $Co(phen)_3^{3+}$ 4 mM, $Co(dipic)_2^{1-}$ 5 mM. Concentrations of cobalt complexes were determined spectrophotometrically using the following extinction coefficients: $Co(phen)_3^{3+}$ at 330nm ε = 4660 M^{-1} cm^{-1}, at 350 nm ε = 3620 M^{-1} cm^{-1} (Chapman *et al.*, 1983a); $Co(dipic)_2^{1-}$ at 510 nm ε = 630 M^{-1} cm^{-1} (Mauk *et al.*, 1979). The electron acceptor concentration was varied from 10 μM to 2 mM. All assays were monitored at the same wavelength, 450 nm, except assays of cytochrome *c* reduction, which were performed at one of its own isosbestic points, 432.7 nm, to prevent interference from its own intense absorbance. For each experiment at least five traces were taken over a timescale ranging from 10-500 ms. These were overlaid to give an average. The average was then fitted to a single exponential from which an observed rate of FMN oxidation was determined. Plotting k_{obs} against the [acceptor] gave a straight line through the origin. The gradient of this line represented a second-order rate constant, the bimolecular rate of the reaction. Solutions of varying ionic strength were made in the same manner as those for the steady-state assays. Otherwise the experiments were performed in the same way as the other stopped-flow experiments. For each acceptor, one concentration was chosen where an increase or decrease in rate due to ionic strength changes would be most clearly observed. Similar numbers of traces were taken at each ionic strength and averaged as before. Again, a single exponential fit was used to determine the rate of oxidation of FMN. The values for k_{obs} are divided by [acceptor] and treated as for the steady-state data, producing an ionic strength plot. In the case of inorganic complexes, where a definite charge is known, the plot gave a good indication of the site on FDH being utilised by the electron acceptor and the charges on FDH involved at that site.

2.5. Redox potentiometry.

The method described by Dutton (1978) coupled with spectrophotometry was used to measure the FMN mid-point potential of the FDH triple mutant K201E/K324A/F325E. The measurements were carried out using a calomel electrode under anaerobic conditions.

2.5.1. Preparation of redox standard solutions.

- Fe (III)/EDTA solution: EDTA was dissolved in 10 ml of 0.1 M acetate buffer to 10 mM concentration and the pH adjusted to 5.0. Fe(III)sulphate was dissolved in this solution to 0.5 mM.
- Fe (II) solution: Fe (II) ammonium sulphate was dissolved in 10 ml of degassed dH_2O to 100 mM.
- Ferricyanide solution: 30 mg of potassium ferricyanide was dissolved in 5 ml of degassed 0.1 M phosphate buffer.
- L-lactate solution: 10 mg of L-lactate lithium salt, were dissolved in 5 ml of degassed 0.1 M phosphate buffer.

2.5.2. Redox mediators.

The FMN redox centre of FDH is shielded by the protein framework from the surrounding solvent, preventing effective contact between it and the surface of the measuring electrode. To allow free transfer of electrons in the solution, a series of mediators are introduced to the solution to act as fluxes between the redox couple and the electrode. These mediators did not react chemically with the FMN group and had mid-point potentials covering the entire range of the redox couple being measured.

Mediator:	**E_m(mV)**
2-hydroxy-1,4-naphthoquinone	-140
Anthraquinone-2-sulphonic acid	-225
Benzyl Viologen	-300

5 ml, 10 mM stock solutions of each mediator were made up in degassed 100 mM phosphate buffer. These were wrapped in tin foil to prevent light-induced decomposition.

2.5.3. Procedure.

All experiments were performed at 25°C under anaerobic conditions. Spectra were recorded using a Shimadzu UV1201 UV/Vis spectrophotometer. 2 ml of a 200 μM stock solution of K201E/K324A/F325E were run down a G75 gel filtration column (5 cm x 2.5 cm), equilibrated with 100 mM phosphate buffer pH 7.0. This equilibrates the protein in the required buffer and helps to de-oxygenate the protein. The protein was eluted in about 8 ml to give an absorbance at 452 nm of about 0.25 Abs units. 10 μl of each mediator was added to the solution to give a final mediator concentration of ~10 μM. The solution was stirred steadily throughout the experiment with a magnetic flea. $[Fe(CN)_6]^{3-}$ was added in 5 μl volumes to ensure that the protein was fully oxidised. When this was achieved, the starting potential was taken and a UV/Vis spectrum from 700 to 250 nm collected at a scan speed of 2 nms^{-1}. Aliquots of L-lactate solution were then added to reduce the protein in ~5 mV steps with spectra taken at each potential. When the protein was fully reduced the process was reversed this time adding $[Fe(CN)_6]^{3-}$ until the protein was fully oxidised. The potentials were corrected relative to the standard hydrogen electrode (SHE) by $E_h = E + 244$ mV. To analyse the data, the percentage oxidised protein was plotted against its corresponding redox potential. This gave a sigmoidal curve which could be fitted to the single electron Nernst equation, allowing calculation of the mid-point potential E_h in mV. The slope, if the system was in equilibrium, was 29.5 ± 5 indicating a 2 electron transfer process.

The Nernst Equation for the redox couple $ox + ne^- = red$

$$\mathbf{E = E_h + RT / nF \ln [ox]/[red]}$$

Where E is the measured potential (mV), E_h is the mid-point potential (mV), R is the molar gas constant (J mol^{-1} K^{-1}), T is the absolute temperature (K), F is the Faraday constant (C mol^{-1}), n is the number of electrons, [ox] is the concentration of the oxidised species and [red] is the concentration of the reduced species.

2.5.4. Calibration of the electrode.

The calibration solution used was 10 ml of 0.5 mM Fe(III), 10 mM EDTA and 0.1 M acetate buffer pH 5.0. The solution was thoroughly degassed. Aliquots (10 µl) of Fe(II) sulphate were titrated into the Fe(III) solution and the potential recorded after each addition. These potentials were corrected relative to the standard hydrogen electrode as before and plotted against $\log_{10}([ox]/[red])$. This gives a straight line with a slope of ~59 mV and an intercept of ~130 mV (Figure 2.3.).

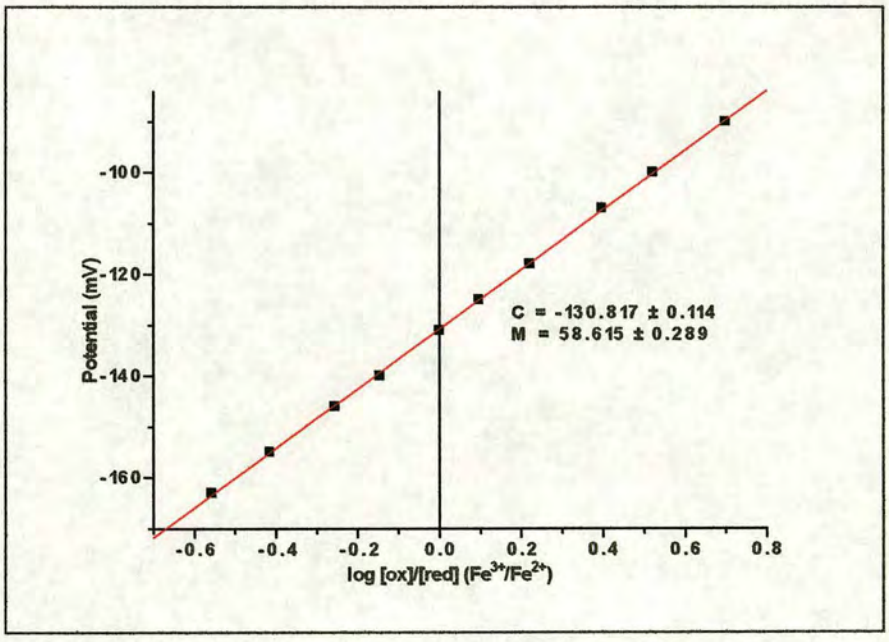

Figure 2.3. *A plot of potential (mV) vs log ([ox]/[red]) for the calibration of the calomel electrode using Fe(III)/EDTA and Fe(II) ammonium sulphate.*

2.6. Crystallography.

At present there is no crystal structure for independently expressed FDH. The crystal structure for the intact enzyme has been utilised where necessary for the purposes of molecular modelling studies and selection of target residues for site-directed mutagenesis. It has been assumed that FDH remains relatively unperturbed by the removal of the cytochrome domain. It is of course unlikely that FDH is completely unaltered making it preferable to have a structure for independently expressed FDH. The work of growing crystals for this purpose has been undertaken.

2.6.1. Crystal growth of FDH_{wt}.

The "art" of protein crystal growth is looked upon as a vital area of modern enzymology but continues to prove itself impossible to predict. With this in mind a number of screens were used to provide preliminary crystallisation conditions or, at least, solubility data. Three screens, supplied by Hampton Research, California, USA, were used to cover wide ranges and combinations of possible precipitants, salts and buffers relatively quickly. Crystal Screen™ is a preliminary screen of 50 formulations based on a number of the most widely used and effective buffers, salts and organic solvents. Crystal Screen II™ extends the range covered by the original Crystal Screen utilising some lesser known chemicals. MembFac™ is aimed at crystallising membrane bound proteins but in this case was used as an extra screen because protein was available in large quantities. The hanging drop method of crystallisation was adopted. FDH_{wt} purified as previously described was used at a concentration of 8.9 mg/ml. Screen solutions in 500 µl volumes were used as the mother liquor in each well. The mother liquor (2 µl) was then mixed with the protein (2 µl) to give a 4 µl hanging drop. The trays were sealed and left at 20°C overnight. Reasonable crystals were attained from the following conditions in the MembFac tray:

12 % PEG 4K, 0.1 M Na Citrate pH 5.6 and 0.1 M Lithium Sulphate.

Based on this formulation the conditions were varied including % PEG, Buffer, pH of buffer, concentration of salt, concentration of protein and temperature. The best conditions were found to be:

175 mM Na Citrate buffer pH 4.9, 17-18.25 % PEG 4K and 8.86 mg/ml FDH_{wt}.

The trays were set up at room temperature but allowed to incubate for 1 hr at 4°C. Protein (3 µl) and mother liquor (3 µl) were mixed to give a 6 µl hanging drop. The tray was kept at 4°C and remained undisturbed for 36 hrs. Approximately 20 crystals could be grown reproducibly under these conditions, with the largest and best looking being approximately 0.1 x 0.3 mm. The crystals were yellow in colour and cuboid in shape. On removal from 4°C to room temperature they were visibly stable for only 1 hr before showing signs of deterioration, making it necessary to freeze them in liquid nitrogen prior to X-ray diffraction.

2.6.2. X-ray crystallography.

To date the crystals of FDH_{wt} have produced a diffraction pattern to 2.75 Å resolution from a synchrotron source, which should allow the structure to be determined by molecular replacement with the intact flavocytochrome b_2 structure. Refinements are ongoing.

2.7. Fluorimetry.

2.7.1. Introduction.

Fluorescence is a spontaneous emission of energy by an excited molecule which ceases immediately on removal of the excitation source. This contrasts with phosphorescence which continues to emit sometimes hours after the excitation source has been removed. This indicates that fluorescence is an immediate conversion of absorbed light into re-emitted energy. The fluorescence process begins with the absorbance of energy from the source beam by the molecule in question generating an excited singlet electronic state. The molecule can then collide with its neighbouring molecules allowing it to loose some energy and step down the vibrational levels towards its ground state. However, it may be that these neighbouring molecules are unable to deal with the large energy changes required to get the excited molecule to ground. This allows the excited state to survive long enough to emit spontaneously the remaining excess energy as radiation. The fluorescence occurs at a lower

frequency than the incident because it occurs after some of the vibrational energy has been lost to the surroundings. Thus fluorescent green and blue dyes absorb in the UV and blue but emit in the visible. Hence FMN is excited at 450 nm while fluorescing at 520 nm. The intensity of fluorescence depends on the ability of the solvent molecules to accept the excess quanta of energy. Water with very widely spread vibrational bands may accept large quanta of electronic energy and so quench fluorescence.

2.7.2 GdnHCl-induced unfolding.

With a view to comparing the stability of mutant FDH proteins with that of FDH_{wt} and flavocytochrome b_2 (intact and core), studies of the fluorescence of FMN and aromatic amino acids were carried out during guanidinium hydrochloride (GdnHCl) denaturation. Flavin fluorescence is quenched by protein contact such that when flavin is bound in a protein the quantum yield (E_{in}/E_{out}) is low. As the protein unfolds and flavin is released the fluorescence becomes more intense and the quantum yield increases. All experiments were performed using a Shimadzu RF-5301PC Spectrofluorophotometer at room temperature in Tris.HCl pH 7.5, I = 0.1 M buffer. A Tris.HCl baseline gave a low background fluorescence which was subtracted from subsequent experiments. A 1 cm pathlength, 3 ml volume, quartz fluorimetry cuvette was used. As the intensity of fluorescence as a function of FMN concentration is known to be linear in the concentration range 0.1 mM-10 μM (Iwatsubo *et al.*, 1965), the concentration of protein was kept at ~1 μM. For FMN fluorescence the excitation wavelength was 450 nm and the emission wavelength 520 nm (detecting over the range 500-600 nm). Aromatic residues were excited at 290 nm and emitted at 350 nm (detecting over the range 300-400 nm). The instrument was set for a fast scan with high sensitivity. Excitation and emission slit widths were varied between 3 and 5 nm to give a strong signal. Protein solutions were made up and incubated with GdnHCl for 10 mins prior to measurement. The shutter was set to automatic to prevent photobleaching of the fluorophore by the beam while measurements were not being made. The fluorescence of each sample was given in counts s^{-1} against the wavelength (nm). The fluorescence of FMN was found to be quenched at concentrations of GdnHCl greater than 1 M making it impossible to follow accurately after this point.

2.8. Circular dichroism.

2.8.1. Introduction.

The effect of circular dichroism (CD) is produced by the differential absorption of left handed and right handed light from a plane polarised source. This can occur when the absorbing chromophore is intrinsically chiral or has become chiral as a result of covalent binding to a chiral centre. In the apparatus the source of plane polarised light is a Xenon lamp. This beam is split into the two constituent parts by passing through a modulator *e.g.* an electro-optic crystal such as ammonium dihydrogen phosphate (Fig 2.4A).

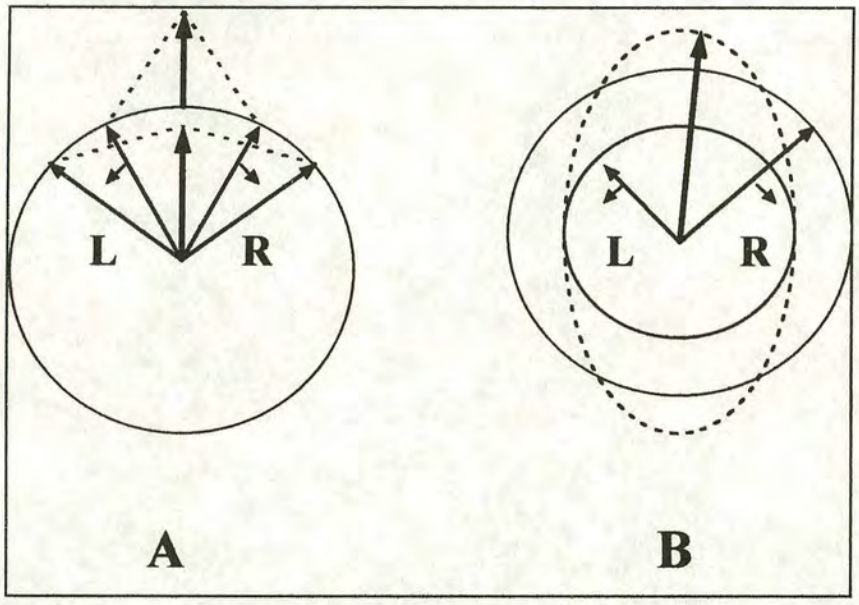

Figure 2.4. (A) on the left shows the constituent parts of a plane polarised source of light. (B) on the right shows the resultant ellipsoid when left handed light is absorbed more by the sample.

The modulator transmits the two parts in turn and if they remain unaffected by the sample they are recombined as the original plane polarised beam. If however, one type of light is affected by the sample more than the other then the resultant beam is an ellipsoid (Fig 2.4B). The instrument measures the extent of dichroism either as ΔA which is the difference between the absorbance of the two components A_L-A_R or as the ellipticity in degrees (θ) $\theta = \tan^{-1}$ (b/a) where b and a are the minor and major axes of the ellipse. θ can be related to ΔA by the following;

$$\theta = 32.98\ \Delta A$$

Biological work tends to give dichroism in the order of 10 mdeg which corresponds to a change in absorbance of 3 x 10^{-4} absorbance units. Such a small change requires close monitoring to ensure that useful results are obtained. The structural information which can be obtained from this technique is shown in Table 2.3. Although not able to resolve in atomic detail like NMR and X-ray diffraction, CD has been widely adopted as an easily accessible technique for preliminary structural studies requiring relatively little sample compared to the other methods. It has proven useful in providing overall indications of a protein's secondary and tertiary structures, its stability in conjunction with denaturing agents, such as GdnHCl, and binding of proteins to each other and to other ligands.

Wavelength nm	Structure
≤190-240	Protein secondary structure, α–helices, β–sheets, amide peptide bonds
250-290	Aromatic amino acids. Phenylalanine 270 nm, Tryptophan 290 nm, Histidine and Tyrosine 280 nm.
260-300	Protein tertiary structure, overall folding of protein. "fingerprint region"
300-600	Non protein chromophores e.g FMN, FAD, Haem.

Table 2.3. *Residues and structural features visible to the CD technique across the FarUV - Visible range.*

2.8.2 GdnHCl-induced unfolding.

Only one of the mutations, K201E, was less stable than FDH_{wt} in terms of FMN loss during either purification or analysis. Thus stability studies were undertaken with K201E and FDH_{wt} utilising CD and GdnHCl-induced unfolding techniques. All experiments were performed on a JASCO J600 CD Spectropolarimeter at room temperature in Tris.HCl pH 7.5, I = 0.1 M. CD spectra in the Far UV (FUV) (190-260 nm) and Near UV/Visible (NUV/Vis) (260-600 nm) regions were collected for each protein over a range of [GdnHCl] from 0-6M. For the FUV spectra 500 µl protein at 5.05 µM was incubated in 0-6.0 M GdnHCl from a 7 M stock (99% pure,

Aldrich) made in Tris.HCl pH 7.5, I = 0.1 M. A CD spectrum was collected for each after 10 mins in a cell of pathlength 0.02 cm at scan rate 10 nm min^{-1}. The same procedure was used for the NUV/Vis spectra using 1 ml protein at 15 μM and a 0.5 cm pathlength cell at a scan rate of 20 nm min^{-1}. An incubation time of 10 mins was allowed prior to the collection of each spectrum. Spectra were given in millidegrees against wavelength and were compared with each other by overlaying.

2.8.3. FDH:Cytochrome *c* interaction.

To determine if mutations to FDH had enhanced interactions between the enzyme (K201E and L199E/K201E/K324A/F325E) and the physiological partner cytochrome *c*, CD spectra were taken of mixtures of each mutant with cytochrome *c*. Binding interactions would be manifest as structural changes observed in the spectra. Similar experiments were performed between b_2-haem domain and cytochrome *c* with FDH_{wt} to act as controls and to investigate the interactions in the wild type system where electron transfer from FDH_{wt} to either cytochrome *c* or b_2-haem has been shown to be negligible (Brunt *et al.*, 1990; Balme *et al.*, 1995). All experiments were performed on a JASCO J600 CD Spectropolarimeter at room temperature in Tris.HCl pH 7.5, I = 0.01 M. Spectra of individual proteins were taken in the FUV and NUV/Vis regions at the concentrations shown in Table 2.4.

	Concentration NUV/Vis (μM)	**Concentration FUV (μM)**
b_2 core	21.05	5.2
FDHwt	21.05	5.2
cytochrome *c*	21.05	33
K201E	10.5	0.88
L199E/K201E/K324A/F325E	21.05	2.52

Table 2.4. *The concentration of protein used for each individual CD experiment over both FUV and NUV/Vis ranges.*

The pathlength used was 0.5 cm and the cell volume 1 ml for NUV/Vis spectra. For FUV spectra the pathlength was 0.02 cm with a cell volume of 300 μl. Algebraic

(predicted) mixes can be calculated from the combination of these spectra. These predicted spectra assume that no gross structural changes have taken place between the mixed proteins. If the physical mixes of these are markedly different from the predictions then it may be that there are interactions between the proteins leading to structural alterations. Physical mixes of the following were obtained at the concentrations shown in Table 2.5.

Mix	Concentration FUV (μM)	Concentration NUV/Vis (μM)
b_2-haem:FDH	10.05 (both)	2.6 (both)
cytochrome *c*:FDH	11.0 (both)	2.6 FDH, 16.5 cyt *c*
QUAD:cytochrome *c*	11.0 (both)	1.3 quad, 16.5 cyt *c*
K201E:cytochrome *c*	0.875 (both)	5.25 (both)

Table 2.5. *The protein concentration for physical mix CD experiments in both the FUV and NUV/Vis ranges.*

The predicted and physical mix spectra were given in mdeg vs wavelength (nm) and were compared by overlaying and looking for alterations.

2.9. Isothermal titrations.

By monitoring the energy required to keep a cell at constant temperature it is possible to determine the energy involved during a chemical reaction in that cell. Having one reactant in the cell and titrating exact, small amounts of the other allows the reaction to be controlled and the cell to be kept at the experimental temperature. In this case it was hoped that any enhanced interaction between FDH mutants and cytochrome *c* would be observed. All experiments were performed on either a Microcal Omega Isothermal Titration Microcalorimeter or a Microcal MCS ITC System (both from Microcal Inc, 22 Industrial Drive East, Northampton, MA 01060.2327, USA) at 25°C in Tris.HCl pH 7.5, I = 0.1 M. All solutions were thoroughly degassed on a vacuum pump prior to use and were at room temperature before being introduced to the apparatus. FDH enzyme (2 ml) was injected into the cell ensuring no air bubbles were introduced to the system. The concentrations of protein used are shown in the

Table 2.6. Cytochrome *c* (1.05 mM) was then titrated in 10 µl aliquots into the FDH solution and the heat of the reaction studied. A robotic arm was used to ensure that each aliquot was exactly 10 µl and injected every 3 mins.

FDH	Concentration (µM)
Wild Type	30
K201E	60
L199E/K201E	50
K201E/K324A/F325E	50
L199E/K201E/K324A/F325E	85

Table 2.6. *The protein concentrations used in each isothermal titration.*

Control experiments were performed to ensure that dilution effects were not responsible for any observations. Cytochrome *c* (3 mM) was titrated into 2 ml Tris.HCl pH 7.5, I = 0.1 M producing a standard endothermic dilution trace. Tris buffer was titrated into the cytochrome *c*:FDH mixture. Again this produced a standard dilution trace.

2.10. Molecular modelling.

2.10.1. Introduction.

In the absence of a crystal structure for the independently expressed FDH, molecular modelling studies were undertaken with a number of specific aims.

- To suggest a structure for the proteolytically sensitive loop (N299-N311) which is highly mobile and invisible in the crystal structure of intact flavocytochrome b_2.
- To investigate the binding of cytochrome *c* to FDH_{wt} to explain the very slow rate of electron transfer between the two.
- To perform a feasibility study on replacement of the loop by shorter stretches of peptide with the aim of negating any steric problems caused by the loop during interaction with electron acceptors.
- To visually explore the binding of artificial electron acceptors and correlate this with kinetic data.

2.10.2. Visualisation.

The program Sybyl, by Tripos, was used for all visualisation, energy minimisation and docking procedures. Crystal structures of flavocytochrome b_2 and cytochrome *c* were obtained from the Brookhaven Data Bank. Structures of $Fe(CN)_6^{3-}$ and $Co(phen)_3^{3+}$ were obtained from the Cambridge Crystallographic Database. Files were saved as either mol2 or pdb files.

2.10.3. Docking.

Docking was done either manually or using the Sybyl Docking program. The docking program calculates the energy of the steric and electrostatic interactions between the ligand and the site molecule. However, because of the intensive nature of these calculations the atoms of the ligand molecule are placed on a grid. For a large ligand, in order that calculations fit the memory, the grid spacing has to be widened. Thus, the position of a small ligand can be determined more precisely and so the values for energies obtained by this method are more likely to be accurate for small ligands than for large ones. Manual docking was performed by manipulating the molecules and checking by eye for any steric collisions. Use of auto-monitoring to highlight close and colliding atoms was attempted, but caused slowing of the computer to such an extent that it was counter-productive. However, it was useful for docking of small electron acceptor molecules such as $Fe(CN)_6^{3-}$. Creating Connolly surfaces helped in checking for steric collisions by assisting in the determination of the best initial orientation of the molecules.

2.10.4. Annealing and Energy minimisation.

Energy minimisation attempts to lower the energy of the whole molecule by testing the energy in nearby conformations for each atom within the molecule. When a lower energy conformation has been found the program tests nearby conformations from this point in search of another conformation of even lower energy. This iterative method does not necessarily find the lowest possible energy conformation of a protein, but only a local minimum. Minimisation in these experiments was performed using the Tripos force field for determining the energy of the atoms. This sums the

energy of the various interactions (bond stretching, bond angle bending, planar atom bending, bond twisting and Van der Waals non-bonded interactions) between the atoms to obtain an overall energy for the molecule. The Powell method was also utilised for determining the energy gradient.

Simulated annealing mimics the effects of raising the temperature of the molecule and cooling it slowly, thus enabling conformations to escape from the local energy minimum. Except where indicated, all experiments were performed with a starting temperature of 200 K, holding and cooling times of 1000 fs each and an exponential gradient. The experiment was repeated 10 times. A single molecule from the 10 was chosen based on low energy and sensible geometry with regard to ϕ/χ angles.

In most cases only part of the molecule needed to be energy minimised. It was necessary to ensure that the rest of the molecule was held in place such that the protein structure was not disrupted. This was done by creating aggregate sets containing all atoms except those involved in minimisation. This usually included anything which was not deemed as part of the loop or was not in its immediate vicinity. Any atom that is part of an aggregate is defined as being unable to move and is ignored by the program in its geometry optimisation. However, atoms within aggregates, but close to the minimisation area, will contribute Van der Waals interactions to the atoms, being minimised and so these atoms although remaining fixed in position, will be included in the energy calculations.

2.10.5. Charge computation.

Charges were computed using the Gasteiger-Hückel method. This uses the method described by Gasteiger and Marseili to calculate s-charges and the Hückel method to calculate p-charges with both components being summed to give the total atomic charge.

2.10.6. Creation of Connolly surfaces.

Connolly surfaces are created by simulating the rolling of a ball over the surface of the molecule. The surface is generated where the ball surface touches the outer edge of

the Van der Waals radii of the atoms. The detail of the surface thus depends on the radius of the probe ball. All Connolly surfaces were generated using a probe radius of 1.4 Å.

3. Altering the electron acceptor specificity of FDH.

3.1. Introduction and Aim.

In chapter 1. (Section 1.4.) the function, structure and location of flavocytochrome b_2 from *Saccharomyces cerevisiae* were discussed. Intact flavocytochrome b_2 has been extensively characterised (Chapman *et al.*, 1990) and become a valuable model system for research into both inter- and intra-protein electron transfer (Sharp *et al.*, 1994; Chapman *et al.*, 1996; Daff *et al.*, 1996). Recently the flavodehydrogenase domain, FDH, has been expressed independently of the cytochrome domain (Pallister *et al.*, 1990; Balme *et al.*, 1995) allowing experiments to be performed on FDH without the influence of the cytochrome domain or the strong spectral absorbance associated with its haem. Since then FDH has been fully characterised in terms of its catalytic behaviour with L-lactate, its physiological partner cytochrome *c* and the artificial electron acceptor ferricyanide, $[Fe(CN)_6]^{3-}$ (Balme *et al.*, 1995). This work has shown that although independently expressed FDH is an effective L-lactate dehydrogenase, its ability to reduce cytochrome *c* is negligible. The question of cytochrome *c* reductase activity will be discussed in detail in Chapter 4.

As discussed in Section 1.2. the process of inter-protein recognition is, in the majority of cases, based on pseudo-specific recognition between complementary surface sites. It was also stated that FDH reduces the artificial electron acceptor $[Fe(CN)_6]^{3-}$ very efficiently. Assuming that the pseudo-specific recognition theory can be applied to a protein:inorganic molecule complex, it is likely that positive residues near the active site of FDH provide a coulombic attraction for $[Fe(CN)_6]^{3-}$. By mutating these to negatively charged residues it should be possible to tune the electron acceptor specificity of FDH promoting its interaction with positively charged molecules and limiting that for negatively charged molecules. If so, this would demonstrate the power of protein engineering as a tool for manipulating enzyme-catalysed reactions and provide support for the idea that pseudo-specific recognition sites play an important role in electron transfer reactions.

The aim of the work described in this chapter was to design and build a new recognition site on the surface of FDH thus, altering its electron acceptor specificity. Allied with the ability to build synthetic redox proteins (Robertson *et al.*, 1994) and

manipulate substrate specificity (Daff *et al.*, 1994; Sinclair *et al.*, 1998) this would be a potent technique making it easier to envisage the "tailoring" or even the custom building of an enzyme for a specific task.

This chapter reports on, and discusses, a number of points: (i). The design of a negatively charged recognition site on FDH; (ii). The mutation of prominent hydrophobic and positively charged residues close to the active site of FDH; and (iii). The effects of these mutations on the properties of the enzyme, particularly the rates of electron transfer from FDH to a range of positively and negatively charged inorganic complexes.

3.2. Results and Discussion.

3.2.1 Selection of target residues.

The optimum face on FDH for efficient electron transfer is likely to be that which is obscured by the cytochrome domain in intact flavocytochrome b_2 *i.e.* where the FMN molecule is now partially exposed to solvent and the point at which electron acceptors can get closest to the FMN. To select suitable residues for mutation on FDH, which from now on will be referred to as FDH_{wt} (wild type), it was necessary to study the residues around the active site and close to the exposed edge of the FMN. This was done using the crystal structure of intact flavocytochrome b_2 and the molecular graphics software Rasmol. In the absence of a crystal structure for independently expressed FDH_{wt}, all structural studies were performed by removing the cytochrome domain co-ordinates from the original flavocytochrome b_2 structure and assuming that the structure of FDH was not seriously perturbed by this. Figure 3.1. shows the surface of FDH immediately surrounding the exposed FMN. A number of prominent residues which are likely to interact with approaching acceptors have been highlighted.

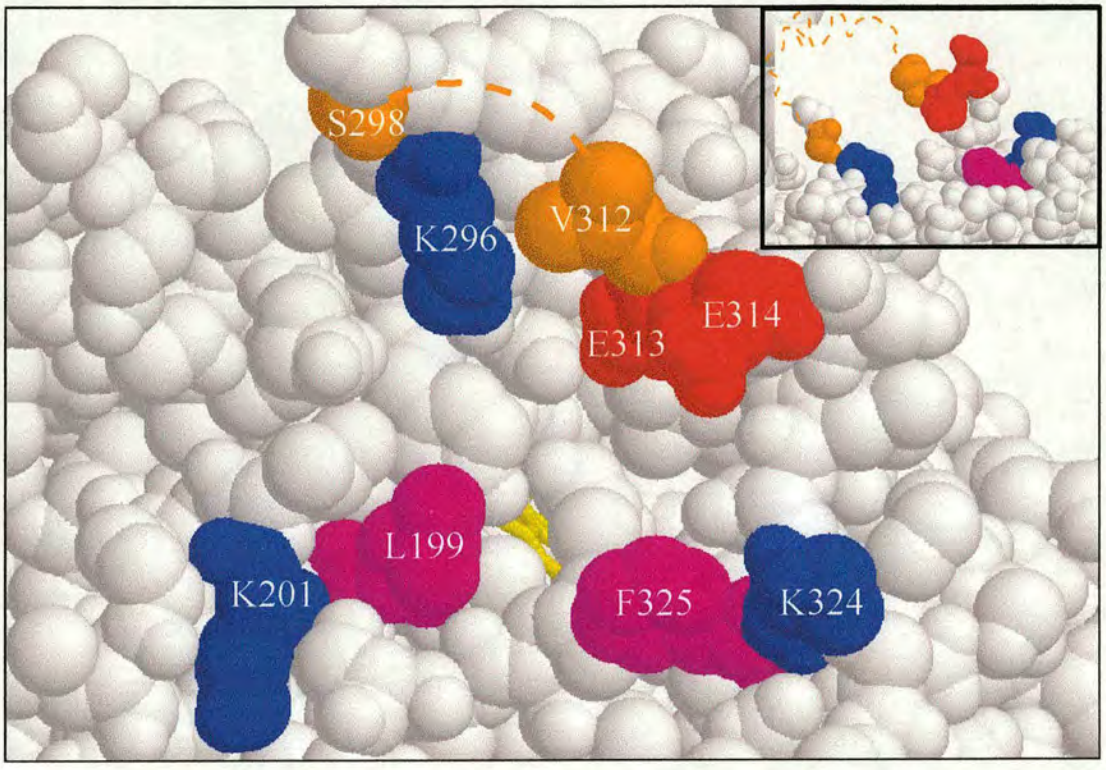

Figure 3.1. *A spacefill representation of the FDH surface area close to the exposed FMN. Highlighted regions are: The exposed edge of FMN (yellow); basic residues (blue); acidic residues (red) and hydrophobic residues (pink). The approximate position of the proteolytically sensitive loop, which is highly disordered and so invisible in the crystal structure, is indicated by a dashed line from Ser 298-Val 312 (orange). Insert; rotated by 90° the profile of FDH shows the protruding loop residues relative to those on the surface.*

The nature of this surface area is predominantly positively charged and hydrophobic. The three lysines (201, 296 and 324) form a triangle of positive charge around the FMN molecule. The region of negative charge closest to the FMN is provided by two glutamate residues, 313 and 314. However, this negative charge is likely to be masked by the basic residues already mentioned. In addition to the surface residues there are a further 4 positively charged lysine residues on the proteolytically sensitive loop (299-315). As described in Section 1.5.4. the loop is highly disordered and so not visible in the crystal structure. Thus, the influence which its basic residues exert on the surface of FDH remains undetermined. This face of FDH is, therefore, ideally suited for electron transfer to $[Fe(CN)_6]^{3-}$ but the exact opposite of that required for electron transfer to positively charged molecules. In order to encourage interaction with

positively charged molecules, and decrease the affinity for $[Fe(CN)_6]^{3-}$, mutants have been constructed (Section 2.1.1.) replacing these positive and hydrophobic residues with negatively charged glutamates and neutral alanines. Residues L199, K201 and F325 were mutated to glutamates and incorporated in single, double, triple and quadruple mutants. K296 and K324 were mutated to a glutamate and an alanine respectively and incorporated into the multiple mutants. By removing the positively charged lysines the affinity for $[Fe(CN)_6]^{3-}$ ought to be decreased and by introducing negatively charged glutamates positively charged acceptors attracted. As suggested in Section 1.2. the flexibility of the glutamate residue creates a much larger reaction surface than would be possible if the shorter aspartate residue was used. The mutant enzymes are shown in Table 3.1.

Mutations made to FDH_{wt}		**Charge introduced**
L199E	leucine 199 to glutamate.	**-1**
K201E	lysine 201 to glutamate.	**-1**
F325E	phenylalanine 325 to glutamate.	**-1**
L199E/K201E	leucine 199 & lysine 201 to glutamates.	**-2**
L199E/K296E	leucine 199 & lysine 296 to glutamates.	**-2**
K201E/K324A/F325E	lysine 201 & phenylalanine 325 to glutamates. lysine 324 to alanine.	**-2**
L199E/K201E/K324A/F325E	leucine 199, lysine 201 & phenylalanine 325 to glutamates. lysine 324 to alanine.	**-3**

Table 3.1. *Site-directed mutants of the flavin binding domain of flavocytochrome b_2. The left hand column gives the shorthand notation of each mutant. The centre column gives a written description of each mutant and the right hand column indicates the charge introduced by each mutant.*

3.2.2. Mutant protein isolation and purification.

Mutant protein was purified exactly as FDH_{wt} (Section 2.2.) except during elution from the anion exchange column. Here, the increased negative charge from the introduced glutamate residues caused tighter binding to the column, requiring higher concentrations of phosphate buffer for elution. The L-lactate:$[Fe(CN)_6]^{3-}$

oxidoreductase activity of each mutant was followed throughout the purification procedure, ensuring that the mutations had no adverse effects on expression or flavin incorporation. Only two of the seven mutants exhibited behaviour suggestive of seriously impaired catalysis. These were the double mutant L199E/K201E and the quadruple mutant L199E/K201E/K324A/F325E. The expression levels for these were poorer than the others and lower activity was detected at all stages of the purification. However, both mutants became fully reduced on addition of L-lactate, making it unlikely that the mutations have seriously perturbed substrate binding. Looking at the residues involved in each mutant it may be the combination of L199 & K201 which causes loss of activity. Individually none of the mutations had such severe effects. Similarly, the combination of K324A/F325E did not cause problems in other mutants. The surface of FDH_{wt} (Figure 3.1.) shows that L199 and K201 are very close indeed to the FMN and mutating both at the same time may have affected FMN incorporation.

3.2.3. Structural studies

3.2.3.1. Circular Dichroism.

To ensure that the mutations had no adverse effects on the structural integrity of FDH, circular dichroism was used to study the unfolding of each enzyme. Guanidine hydrochloride (GdnHCl) was used as a denaturant. The CD experiments were performed on FDH_{wt} and K201E, the mutant which had shown most inclination to lose FMN during turnover. The resulting spectra are shown in Figures 3.2a and 3.2b. Section 2.8. describes this technique and the analysis of spectra.

Figure 3.2c. shows an analysis of the CD spectra, comparing the loss of both FMN and protein structure by the two enzymes during GdnHCl unfolding. The loss of secondary structure by the enzymes *i.e.* the α-helices and β–sheets, can be observed by CD at 220 nm. The plot shows that unfolding of the helices and sheets, under denaturing conditions, is essentially the same for FDH_{wt} and K201E. Maximum unfolding occurs for both at ~4 M GdnHCl. The loss of tertiary structure by the enzymes is observed as the decrease of the very strong signal at 270 nm.

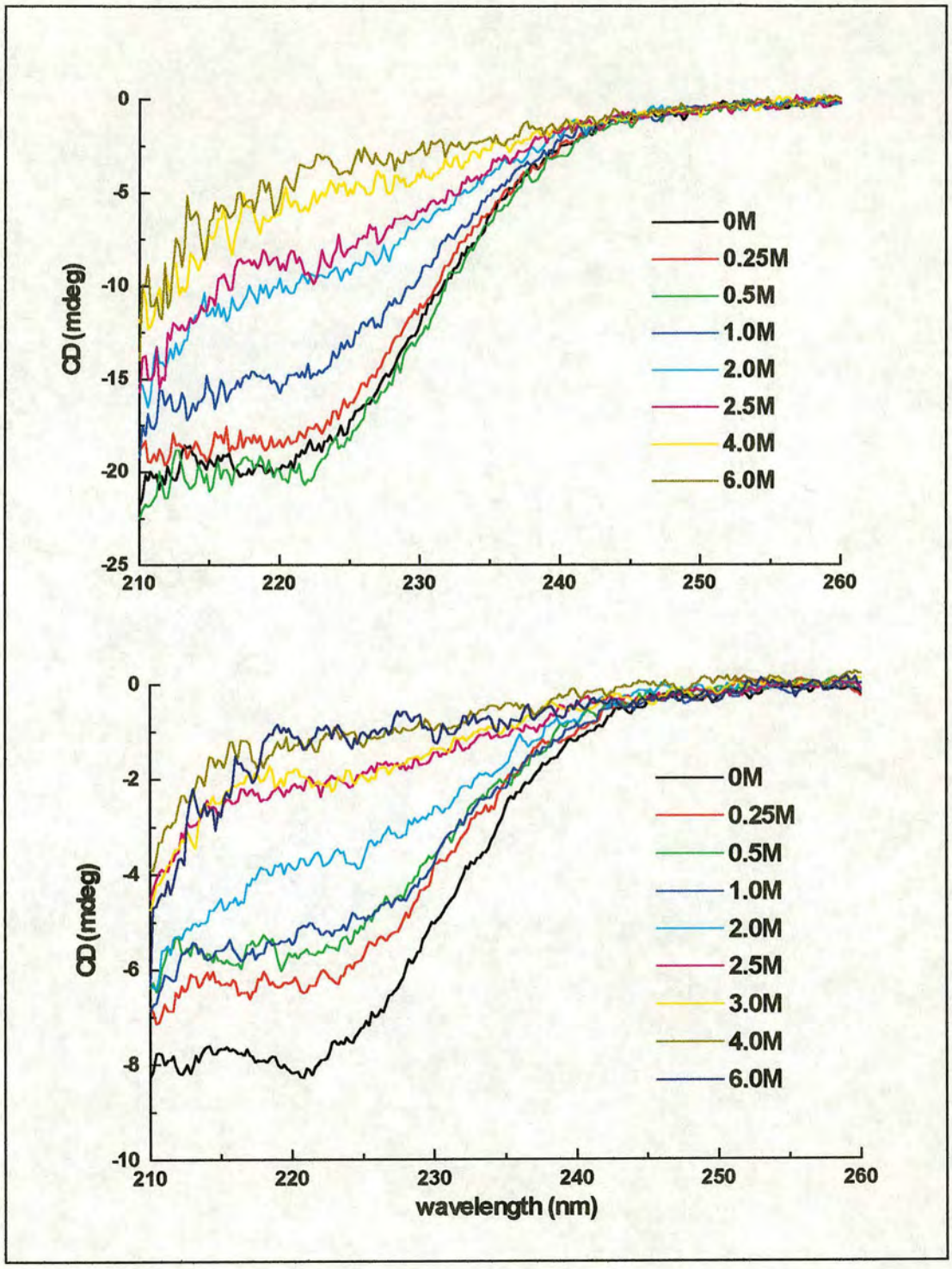

Figure 3.2a. *CD spectra in the FUV region for both FDH_{wt} (bottom) and K201E (top) showing the GdnHCl-induced unfolding of the proteins. All experiments were performed in Tris.HCl pH 7.5, I=0.1 M at 25°C. GdnHCl was of high purity analytical quality.*

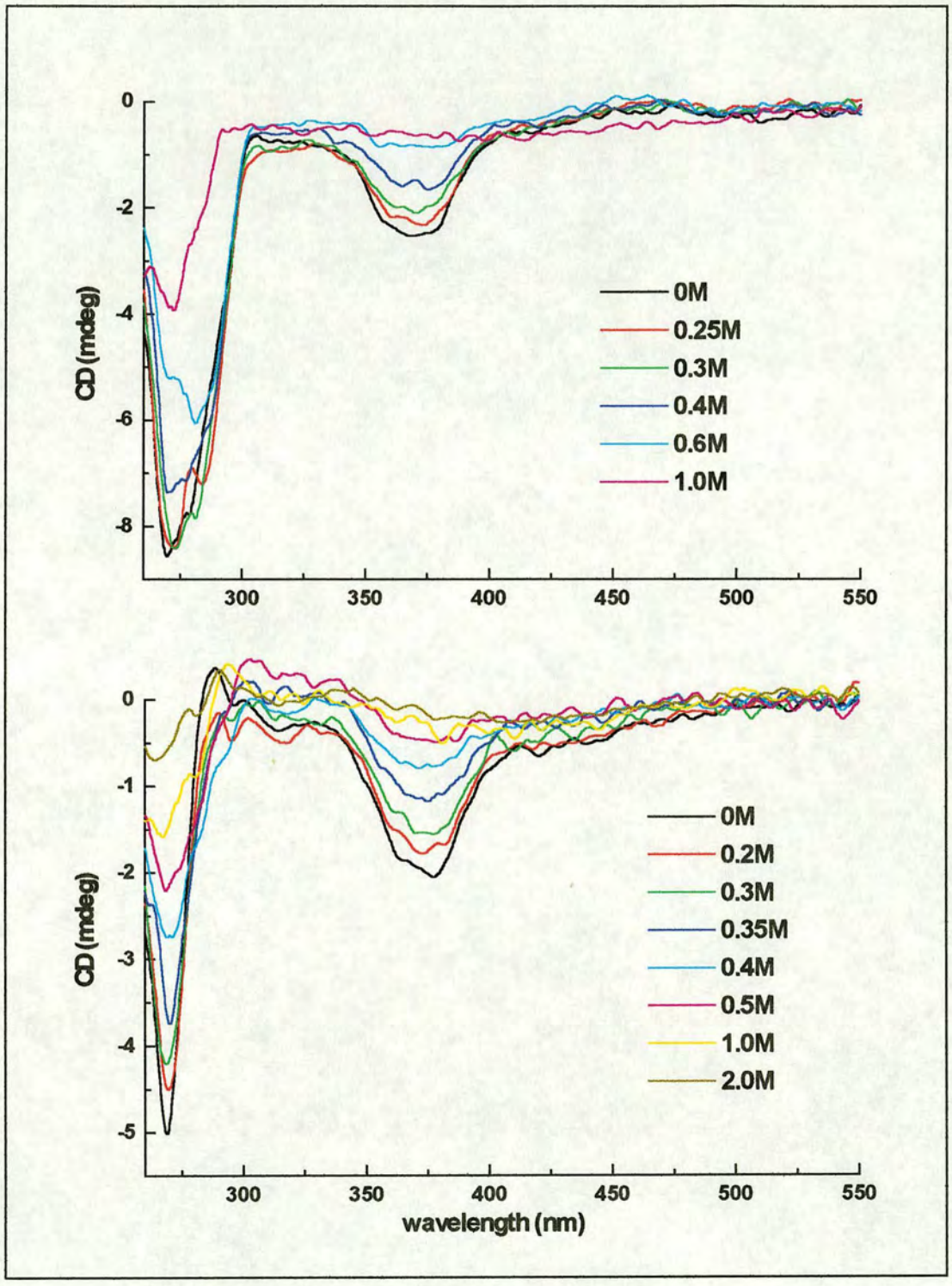

Figure 3.2b. *CD spectra in the NUV/Vis region for both FDH_{wt} (bottom) and K201E (top) showing the GdnHCl-induced unfolding of the proteins. All experiments were performed in Tris.HCl pH 7.5, I=0.1 M at 25°C. GdnHCl was of high purity analytical quality.*

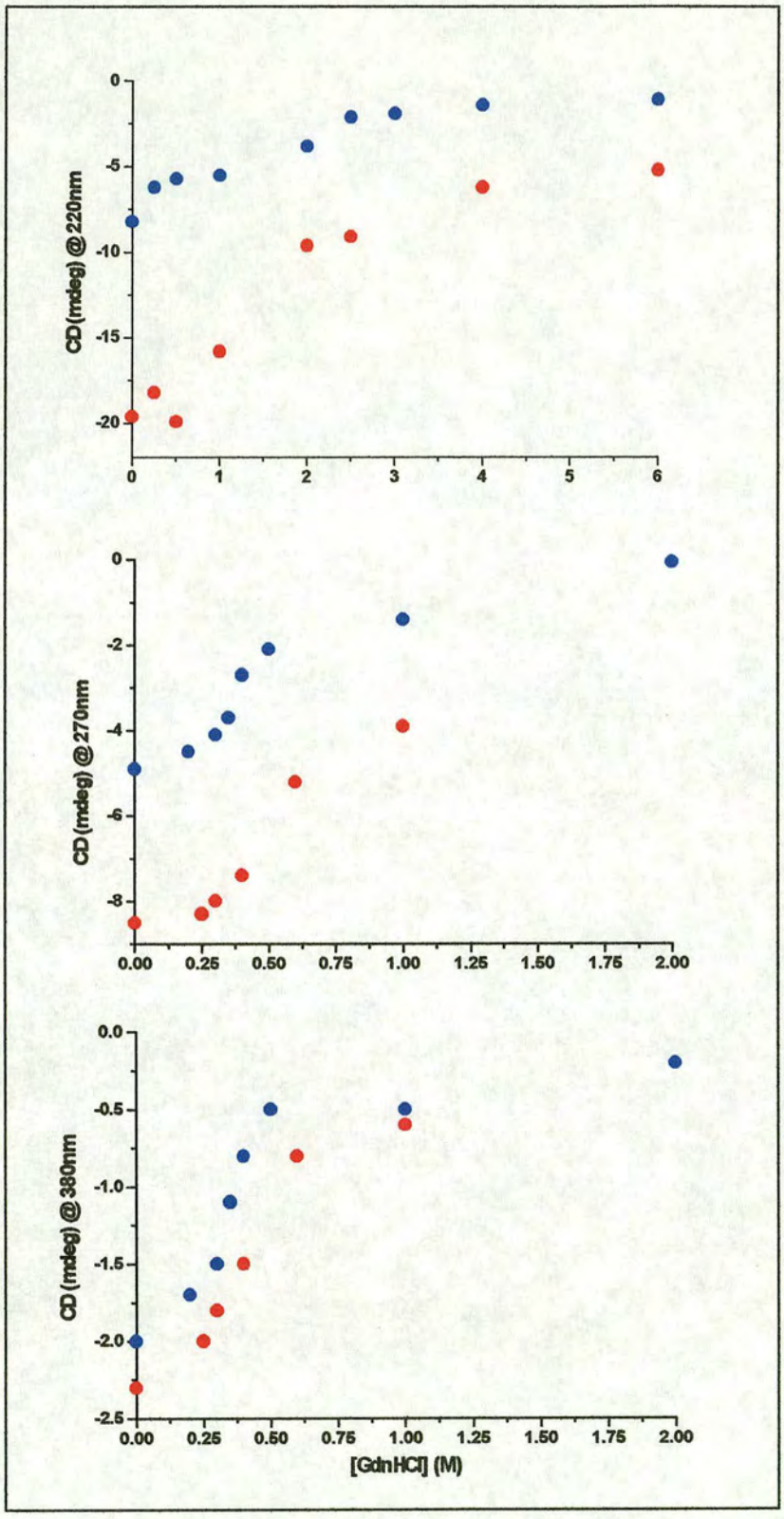

Figure 3.2c. *Plots of [GdnHCl] vs CD (mdeg) of FDH_{wt} (•) and K201E (•) showing loss of 2° structure at 220 nm (top), 3° structure at 270 nm (centre) and chirally bound FMN at 380 nm (bottom).*

This was also very similar for both enzymes with maximum unfolding occurring at ~1 M GdnHCl. The strong signal associated with the asymmetry of protein-bound FMN can be seen at 380 nm. Free FMN exhibits a very weak visible-CD spectrum. As FMN is released from the enzyme the signal strength diminishes gradually. Again there is no major difference between the two enzymes with maximum loss of FMN occurring in both by ~0.5 M GdnHCl. Thus, K201E, even though it exhibits increased FMN loss, would seem to be structurally as stable as FDH_{wt}.

3.2.3.2. Fluorescence spectroscopy.

The GdnHCl-induced unfolding of the mutants was also studied using fluorescence spectroscopy. Here both K201E and the quadruple mutant (L199E/K201E/K324A/F325E) were examined. The spectra obtained for FMN fluorescence from these and FDH_{wt} are shown in Figure 3.3. It is clear that all three exhibit maximum fluorescence at 0.8-1M GdnHCl. This corresponds to the results obtained from the CD experiments confirming maximum FMN loss at similar concentrations of denaturant (previous section). Experiments were performed to determine the effect of [GdnHCl] on the fluorescence of free FMN. It was discovered that $\geq$ 1 M GdnHCl severely quenched the fluorescence of free FMN. Thus data obtained at higher concentrations of GdnHCl was deemed unreliable. This quenching effect is shown in Figure 3.3. as the dotted spectra. A point to note concerning the FMN fluorescence is the much greater difference between maximum and minimum fluorescence for FDH_{wt} than for the mutant enzymes. The increase in intensity for FDH_{wt} between 0-1 M GdnHCl is close to 10-fold whereas for K201E and L199E/K201E/K324A/F325E it is only 3-fold and 2-fold respectively. For K201E this may be due to weaker FMN binding leading to FMN loss during purification and so low FMN content in the purified enzyme. This would explain the very much lower maximum fluorescence for K201E compared to FDH_{wt}. In the case of the quadruple mutant, although this experiment was more sensitive having wider slit widths, it would seem that there has been greater FMN loss prior to denaturation. This suggests

again that the FMN is not bound as tightly in the mutant as in FDH_{wt} and that on dilution in buffer FMN may be lost.

The fluorescence from aromatic residues was also studied during GdnHCl induced unfolding (Figure 3.4a.). This fluorescence is principally due to tryptophan residues which are much more fluorescent than either tyrosine or phenylalanine. The fluorescence of these residues, as in CD, allow investigation of the tertiary structure of the enzymes. The spectra in Figure 3.4a. show that superficially, at least, the tertiary structures of all three enzymes are similar. They all exhibit a change in emission wavelength, from ~330 nm to ~350 nm, between 1-2 M GdnHCl. This is reflective of the unfolding process of the enzymes. It should also be noted that the intensity of fluorescence decreases as the emission wavelength changes. This is probably due to quenching as was observed for FMN fluorescence. The emission wavelength change and the quenching effect can be seen more clearly in Figure 3.4b. This is a plot of aromatic fluorescence at 330 nm vs [GdnHCl] for all 3 enzymes. The plot suggests that FDH_{wt} is slightly more stable than the mutants with the change in emission wavelength occurring at a higher concentration of GdnHCl. However, it should be remembered that quenching occurs at $\geq$ 1 M GdnHCl making the fluorescence intensity decrease prior to the actual wavelength shift.

The implications from these studies are that the mutations have had very little effect on the secondary or tertiary structure of the enzyme. However, it is possible that they do affect the binding of FMN leaving the enzyme without the full complement of its prosthetic group. This may well explain some of the low activities which are observed particularly with the quadruple mutant (Section 3.2.4.).

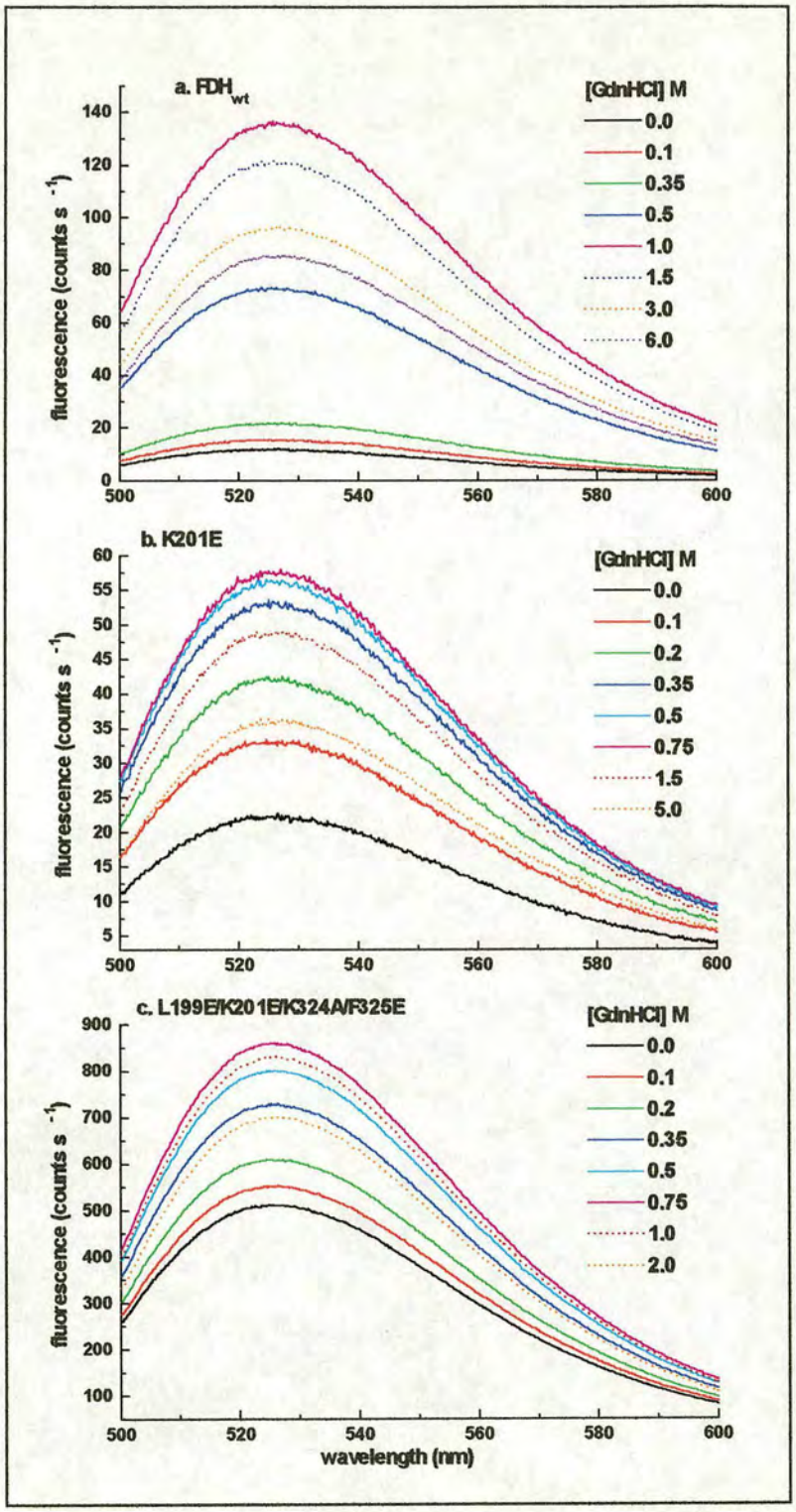

Figure 3.3. *FMN fluorescence spectra for GdnHCl-induced unfolding of (a) FDH_{wt} 1.5 μM (b) K201E 0.4 μM and (c) L199E/K201E/K324A/F325E, 0.9 μM. Excitation wavelength-450 nm. Slit widths nm, Excitation:Emission, were as follows (a) 3:3, (b) 3:3 and (c) 5:5. All experiments were performed in Tris.HCl pH7.5, I = 0.1M at room temperature in a 3ml, quartz fluorimetry cuvette (Sigma), p.l. = 1 cm.. GdnHCl was of high purity analytical quality.*

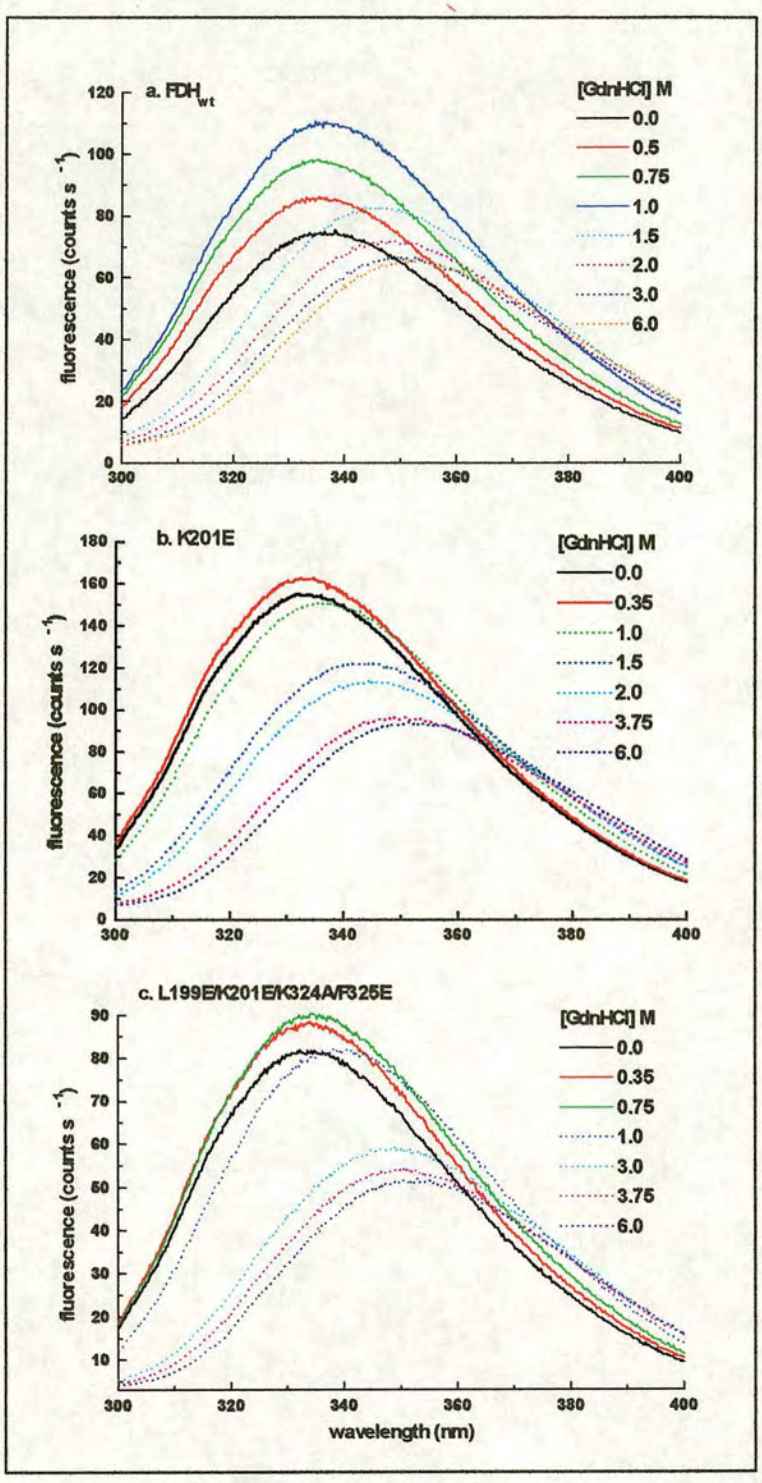

Figure 3.4a. *Aromatic residue fluorescence spectra for GdnHCl-induced unfolding of (a) FDH_{wb}, 1.5 μM (b) K201E, 0.4 μM and (c) L199E/K201E/K324A/F325E, 0.9 μM. Excitation wavelength-280 nm. Slit widths, Excitation:Emission, were as follows (a) 3:3, (b) 5:5 and (c) 5:5. All experiments were performed in Tris.HCl pH 7.5, I=0.1 M at room temperature in a 3ml, quartz fluorimetry cuvette (Sigma), p.l. = 1 cm. GdnHCl was of high purity analytical quality GdnHCl was of high purity analytical quality*

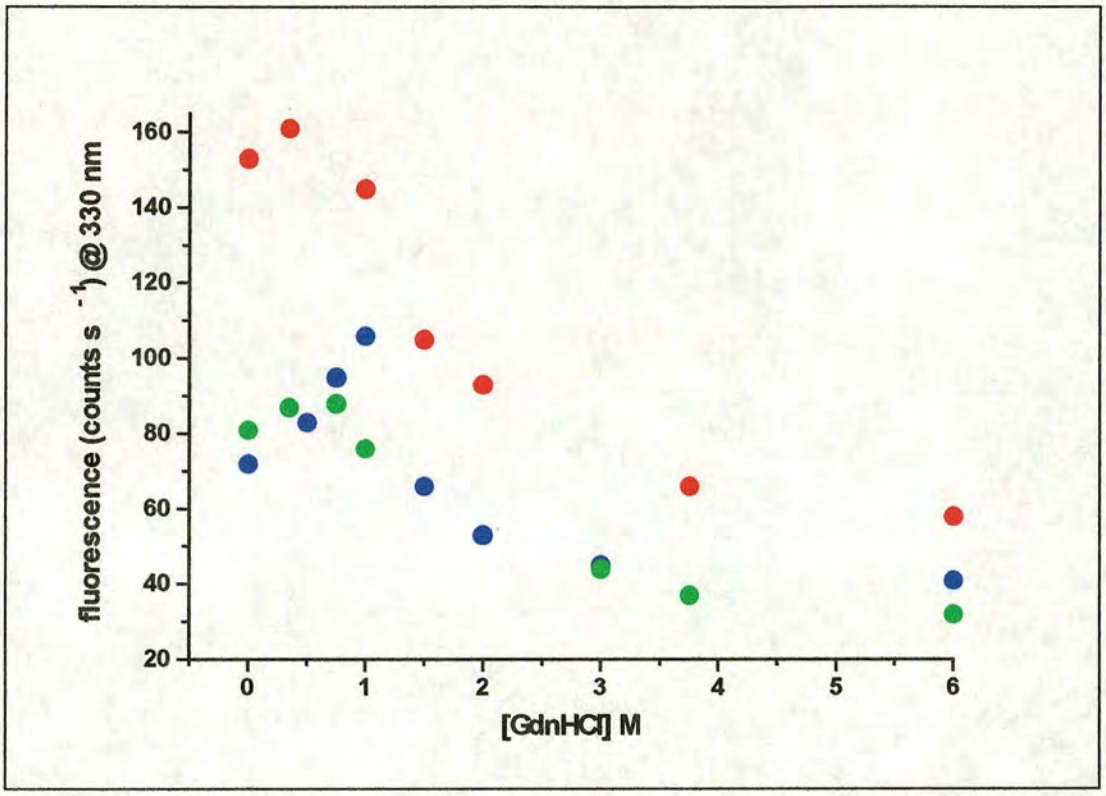

Figure 3.4b. *[GdnHCl] vs fluorescence at 330 nm for the GdnHCl-induced unfolding of* FDH_{wt} (•), *K201E* (•) *and L199E/K201E/K324A/F325E* (•).

3.2.4. Steady-state characterisation.

To determine the effect of the mutations on catalytic efficiency and compare them directly with FDH_{wt}, steady-state kinetic analysis was performed on each mutant. The rate-dependence of each mutant on the concentrations of the substrate, L-lactate, and the electron acceptor, $[Fe(CN)_6]^{3-}$, were determined. The rate of reduction of $[Fe(CN)_6]^{3-}$ was measured for each by following the rate of decrease in $[Fe(CN)_6]^{3-}$ absorbance at 420 nm over a period of 1 min (Figure 3.5.). The observed rate constant, k_{obs}, was calculated as described (Section 2.3). and plotted against substrate concentration. The resulting curves were fitted to the Michaelis-Menten equation (Figure 3.6.) generating values of k_{cat} and K_m. The kinetic parameters obtained in this manner for each of the mutants and FDH_{wt} are shown in Table 3.2.

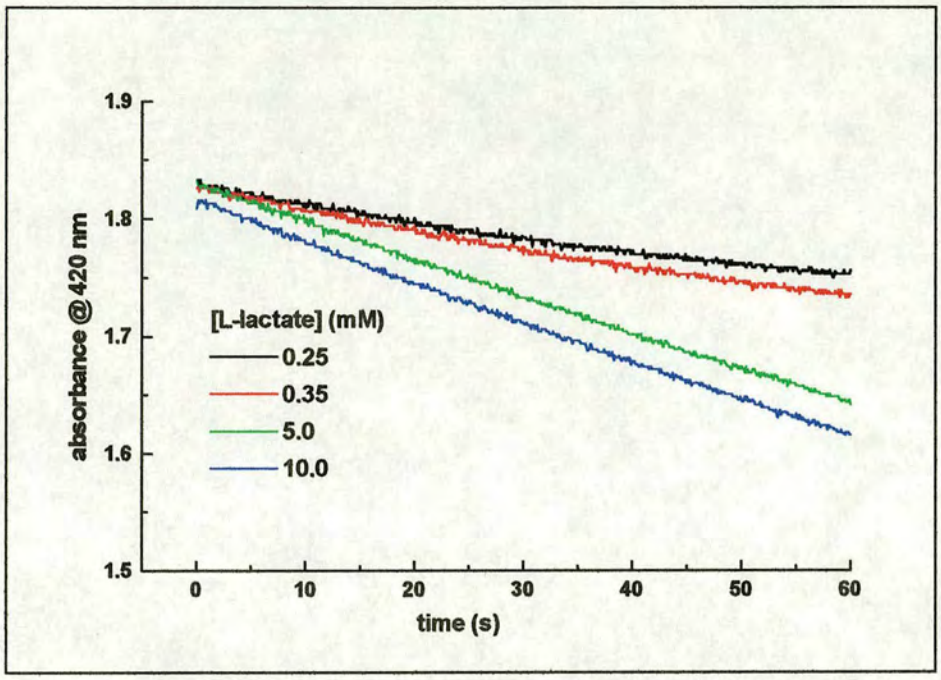

Figure 3.5. *Steady-state traces for the reduction of $[Fe(CN)_6]^{3-}$ (10 mM) by FDH_{wt} ($2x10^{-7}$ M) at 420 nm, p.l. = 0.2 mm, [L-lactate] = 2 mM, t = 1 min. All experiments were performed at 25°C in Tris.HCl pH 7.5, I=0.1 M.*

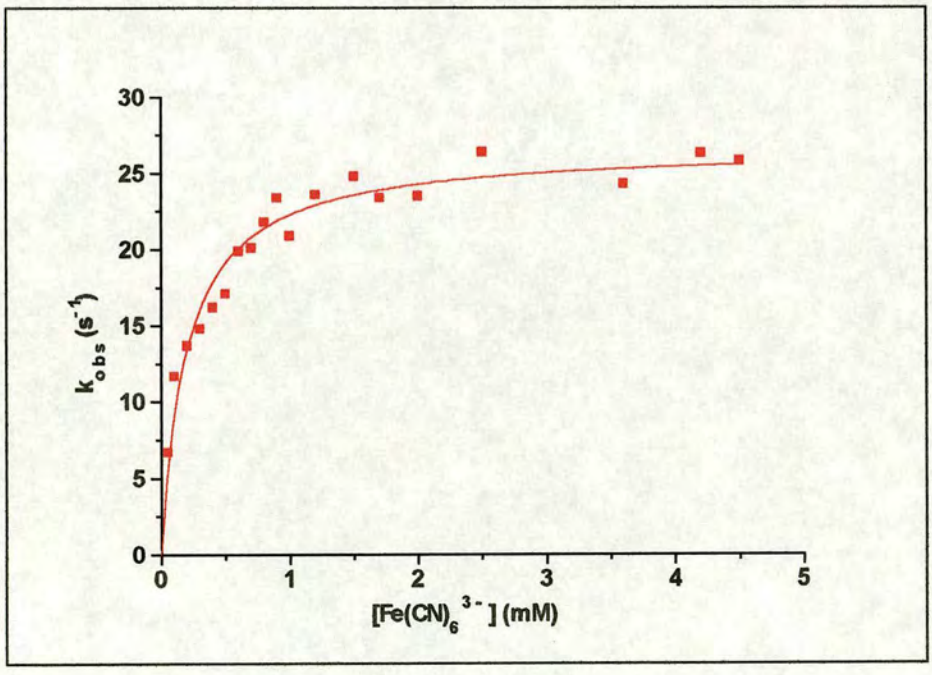

Figure 3.6. *The $[Fe(CN)_6^{3-}]$ dependence of L199E ($1.8x10^{-7}$ M). These data have been fitted to a Michealis-Menten curve. All experiments were performed at 25°C in Tris.HCl pH 7.5, I=0.1 M. [L-lactate] = 2 mM, λ = 450 nm, p.l. = 1 cm, time = 1 min*

The values of k_{cat} for L199E/K201E and L199E/K201E/K324A/F325E are in agreement with the proposal that the double mutation L199E/K201E seriously impairs flavodehydrogenase activity. It can be seen from Table 3.2. that only enzymes where these two mutations occur together suffer almost total loss of activity. The value of k_{cat} for L199E/K201E is almost 400-fold less than that for FDH_{wt} but its K_m for L-lactate is only 2-fold increased. This suggests that substrate binding is essentially unaffected by the mutations and that altered transition-state stability is the major contributor to a value of k_{cat}/K_m, being 860-fold lower than for FDH_{wt}. However, it may be that low FMN content, suggested by fluorescence experiments (Section 3.2.3.2.), contributes to such low activities

FDHwt & Mutants.	k_{cat} s^{-1}	K_m lactate mM	k_{cat}/K_m M^{-1} s^{-1} lactate.	K_m $Fe(CN)_6^{3-}$ mM
FDH_{wt}	273 ± 6	0.2 ± 0.1	1.24×10^6	0.58
L199E	29.4 ± 2	2.0 ± 0.5	1.47×10^4	0.2 ± 0.04
K201E	~250	7.2 ± 1.4	3.47×10^4	~0.5
F325E	321 ± 7	0.4 ± 0.03	8.4×10^5	-
L199E/K201E	0.7	0.5	1.4×10^3	-
L199E/K296E	20.9 ± 0.8	1.7 ± 0.2	1.2×10^4	0.1 ± 0.02
K201E/K324A/F325E	14.6 ± 0.3	4.8 ± 0.4	3×10^3	1.6 ± 0.1
L199E/K201E/K324A/F325E	~3.5	-	-	-

Table 3.2. *Steady-state kinetic data for FDH_{wt} and mutants using L-lactate as substrate and $[Fe(CN)_6]^{3-}$ as the electron acceptor. All experiments were performed at 25°C in Tris.HCl pH 7.5, I = 0.1M.*

The very low activity exhibited by the quadruple mutant produced poor quality traces resulting in irreproducible data. The approximate value of k_{cat} was almost 80-fold lower than for FDH_{wt}. The enzyme showed no detectable dependence on the concentration of either L-lactate or $[Fe(CN)_6]^{3-}$. The single mutant K201E, although having a value of k_{cat} similar to FDH_{wt}, produced unreliable data. All steady-state traces exhibited severe curvature with the rate of reduction of $[Fe(CN)_6]^{3-}$ decreasing rapidly during the assay. Thus, there were no linear portions on the traces making steady-state analysis difficult. It was proposed that the cause of this phenomenon was

FMN loss. Fluorescence experiments were performed following the increase in FMN fluorescence during steady-state turnover (data not shown). Assays were similar to those for steady-state analysis but were allowed to run for up to 20 mins. At intervals of 1-2 mins assay solutions were excited at 450 nm and the resulting fluorescence measured at ~520 nm. It was observed that the rate of loss of FMN in K201E was significantly faster during turnover than in a non-catalytic control solution. However, eventually both solutions reached a similar final fluorescence value suggesting that the K201E mutant has significantly weakened FMN binding and this disruption is accentuated by catalytic turnover. This is not a unique observation for flavocytochrome b_2. Similar observations have been made with a C-terminal tail deletion mutant in intact flavocytochrome b_2. This mutant also exhibited increased FMN loss during turnover (White *et al.*, 1989) indicating that the C-terminal tail plays an important role in FMN binding in flavocytochrome b_2. None of the remaining four mutants showed any indications of being less stable than FDH_{wt} and all possessed reasonable L-lactate dehydrogenase activity. Although the single mutant F325E has a slightly higher k_{cat} value than FDH_{wt} its increased K_m value means the catalytic efficiency, k_{cat}/K_m, is 1.4-fold lower than that of FDH_{wt}. The remaining mutants L199E, L199E/K296E and K201E/K324A/F325E all have much lower k_{cat} values than FDH_{wt} but also higher values of K_m suggesting that the negative charges introduced may have perturbed substrate binding. Notably, the triple mutant has a K_m value for $[Fe(CN)_6]^{3-}$ considerably higher than FDH_{wt}, perhaps indicating that $[Fe(CN)_6]^{3-}$ is repelled by the two additional glutamates. By neutralising K324, the negative charge on F325E will have a much greater effect on $[Fe(CN)_6]^{3-}$ thus enhancing the repulsion.

3.2.5. Redox potentiometry.

The introduction of negative charges close to the FMN could have an effect on its reduction potential and so the driving force for an electron transfer from the FMN to an acceptor. Such an effect could explain any decreased activity with $[Fe(CN)_6]^{3-}$. This possibility was investigated by measuring the reduction potential of the triple mutant K201E/K324A/F325E (Section 2.5.). Excluding those mutants which

effectively destroyed catalysis, the triple mutant had the most mutations whilst retaining reasonable catalytic properties. It was assumed that should the triple mutant exhibit a reduction potential similar to that of FDH_{wt} then it was unlikely that any single or double mutant would have a more dramatic effect. Figure 3.7 shows the UV/Vis spectra of the enzyme generated during reductive and oxidative titrations using L-lactate and $[Fe(CN)_6]^{3-}$ respectively. Turbidity and evaporation are often observed during these experiments due to the length of time the enzyme remains at 25°C. They are manifested by an increase in absorbance across the entire UV/Vis spectrum and were found to be particularly pronounced during the later oxidative titrations. To correct for these phenomena the spectra were normalised to zero absorbance at 700 nm, where no absorbance would be expected, and corrected by multiplying by (1-(1/λ)). Each spectrum was converted to a percentage of oxidised FMN based on the FMN absorbance at 452 nm. The fully reduced spectrum being 0 % oxidised and the fully oxidised spectrum being 100 % oxidised.

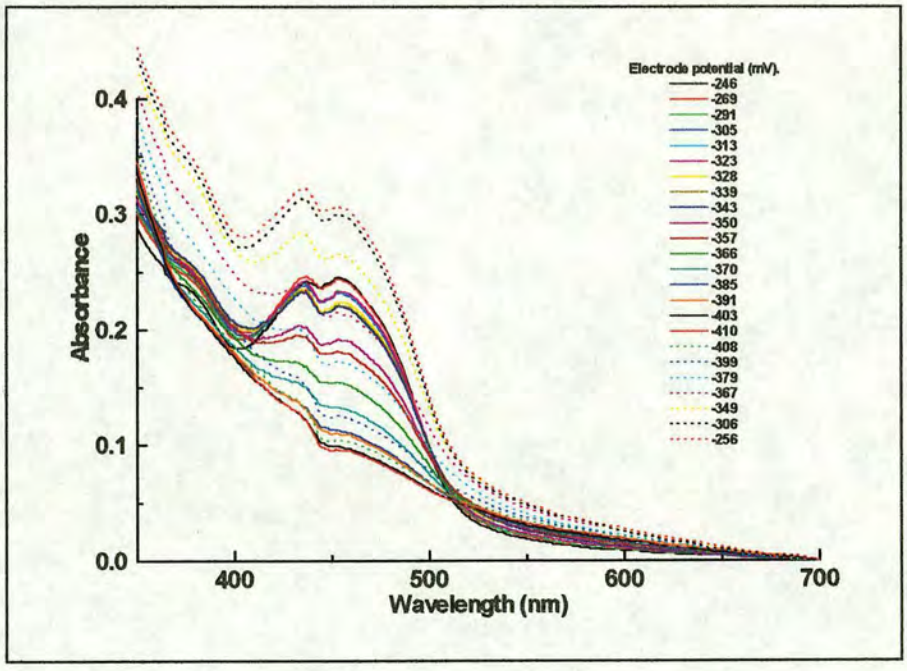

Figure 3.7. *UV/Vis spectra of the redox titration of K201E/K324A/F325E by L-lactate (solid lines) and* $[Fe(CN)_6]^{3-}$ *(dashed lines). The typical FMN absorbance can be seen at 452nm. The increase in absorbance over the entire spectrum due to turbidity and evaporation can be seen for the oxidation traces. All experiments were performed at 25°C in a* N_2 *atmosphere.*

The measured reduction potentials for each spectrum, corrected relative to the standard hydrogen electrode (Section 2.5), were plotted against the corresponding value of % oxidised FMN and fitted to a single Nernst curve (Figure 3.8.).

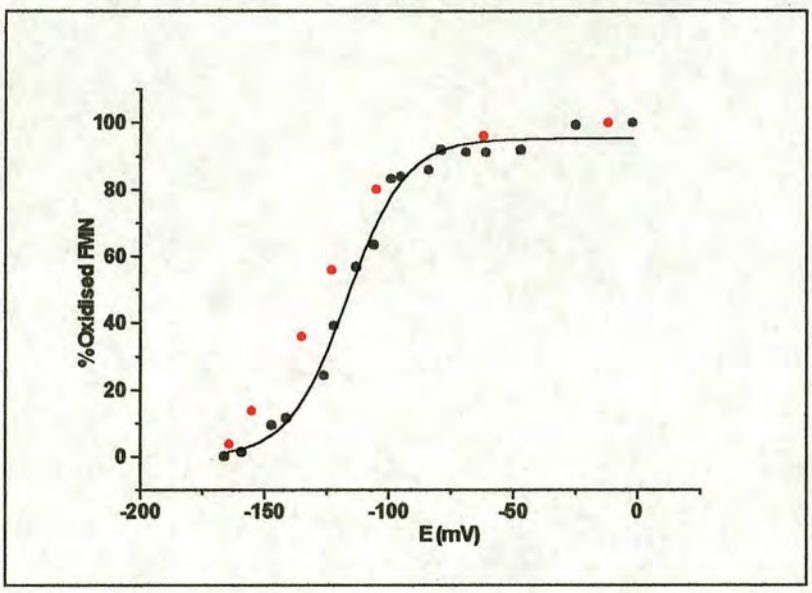

Figure 3.8. *A Nernst plot for the triple mutant K201E/K324A/F325E. Reduction titration with L-lactate (●) and oxidation titration with* $[Fe(CN)_6]^{3-}$ *(●). The reduction data points have been fitted to a single Nernst curve (black line).*

The Nernst plot indicates a slight amount of hysteresis during the oxidation of the enzyme. This effect may be due to the presence of some free FMN. The reduction fits well to a single Nernst curve giving a reduction potential for the FMN of -116 ± 10 mV (vs NHE). This is a difference of -36 mV from FDH_{wt} (-80 mV). Although this is a significant alteration to the midpoint potential it actually increases the driving force for an electron transfer with $[Fe(CN)_6]^{3-}$ (+410 mV) and so cannot be responsible for any decrease in activity which is observed with this electron acceptor.

3.2.6. Stopped-flow oxidation of FDH by inorganic complexes.

3.2.6.1. Introduction.

The aim of this work was to alter the specificity of FDH for electron acceptors. To determine if this had been achieved the ability of inorganic complexes to oxidise FDH was studied using stopped-flow spectrophotometry. Each of the mutants was tested for its affinity for three inorganic molecules with the charges -3, -1 and +3. These

molecules are listed in Table 3.3. along with their associated charges and redox potentials. Such analysis should indicate which of the mutations or combinations of mutations has the greatest influence over electron acceptors.

Complex	Redox Potential mV.	Charge.	Reference.
$[Fe(CN)_6]^{3-}$	+410	-3	Chapman *et al.*, 1983b
$[Co(dipicolinato)_2]^-$	+400	-1	Mauk *et al.*, 1979
$[Co(phen)_3]^{3+}$	+370	+3	Paglia *et al.*, 1957

Table 3.3. *Inorganic complexes used during stopped flow oxidation of FDH_{wt} and mutants along with their reduction potentials (vs NHE) and charge.*

Table 3.3. shows that the reduction potentials of the inorganic complexes do not vary dramatically so that there are no large differences in driving force for the reactions. These complexes react with FDH according to the following equation.

$$FDH\text{:} + 2[Fe(CN)_6]^{3-} \rightarrow FDH + 2[Fe(CN)_6]^{4-}$$

The rates of oxidation of fully reduced FDH by the electron acceptors were studied. The rate of reduction of FDH by L-lactate is in the millisecond time-scale. Thus, re-reduction of FDH by L-lactate would interfere with FDH oxidation experiments. Instead, FDH was fully reduced with excess glycolate. Glycolate has been shown to be a poor substrate for flavocytochrome b_2, taking seconds to reduce the enzyme fully. This allows oxidation of FDH to be observed over the millisecond time-scale with no significant interference from re-reduction.

3.2.6.2. FDH oxidation by $[Fe(CN)_6]^{3-}$.

The electron acceptor $[Fe(CN)_6]^{3-}$ was used to determine the efficiency of the mutants as electron donors to negatively charged molecules. The stopped-flow measurements were performed as described in Section 2.4. using $[Fe(CN)_6]^{3-}$ in the concentration range 10 μM-1.5 mM . FDH_{wt} and mutants were used at a concentration of 2 μM. Thus, at all times $[Fe(CN)_6]^{3-}$ was in excess of the enzyme. Each experiment was repeated at least five times, then averaged to give a trace similar to the examples

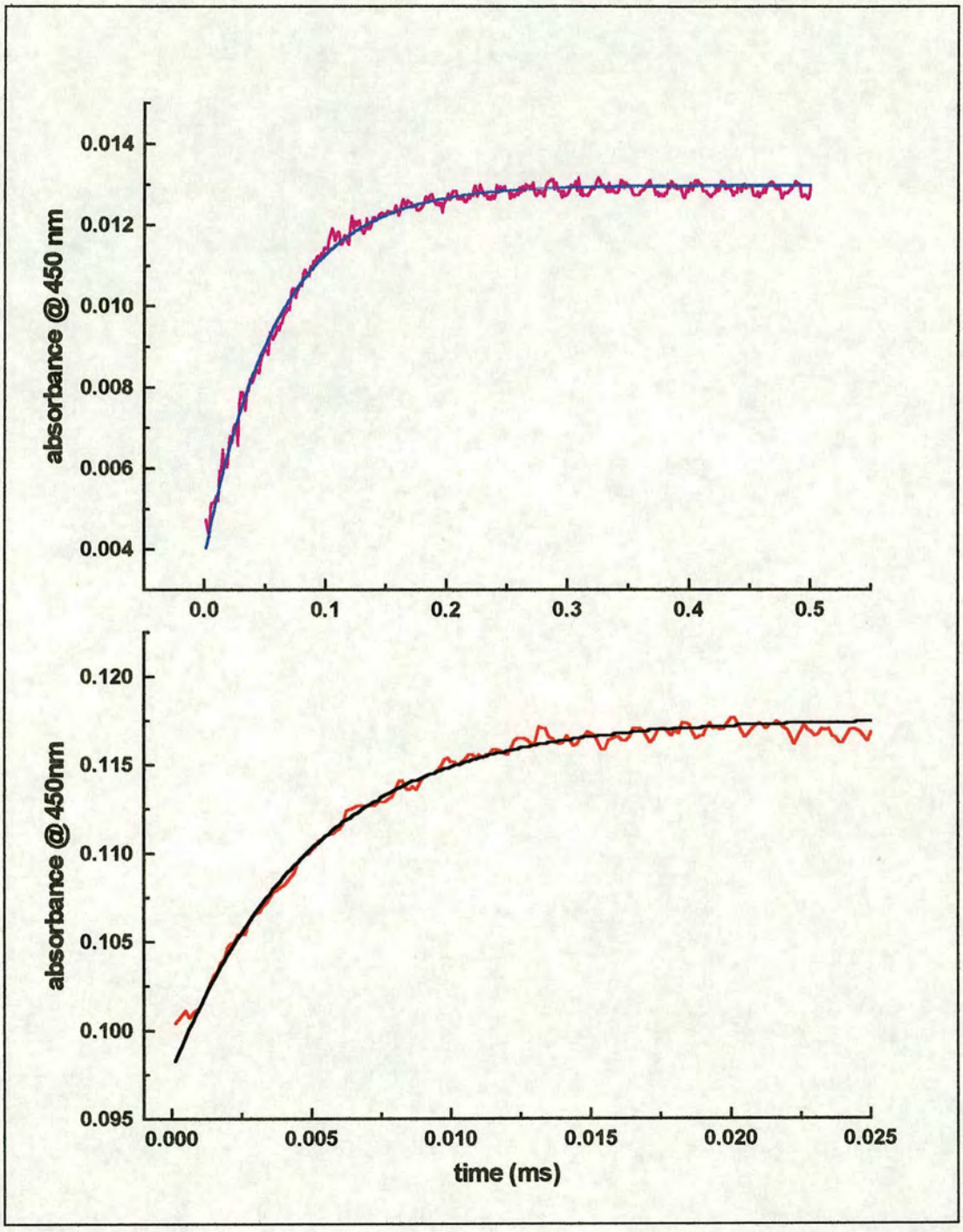

Figure 3.9. *Stopped-flow traces showing the oxidation of FMN by $[Fe(CN)_6]^{3-}$, 200 μM, for FDH_{wt}, (bottom) and by $[Fe(CN)_6]^{3-}$, 500 μM, the triple mutant K201E/K324A/F325E (top). These data have been fitted to single exponentials (black and blue lines). All experiments were performed at 25°C in Tris.HCl pH 7.5, I = 0.1 M.*

shown in Figure 3.9. The figure shows that traces fitted well to single exponentials giving reliable values for k_{obs}. These values of k_{obs} were plotted against electron acceptor concentration to give the plot shown in Figure 3.10. The points fit well to straight lines allowing the calculation of second-order rate constants for each of the enzymes.

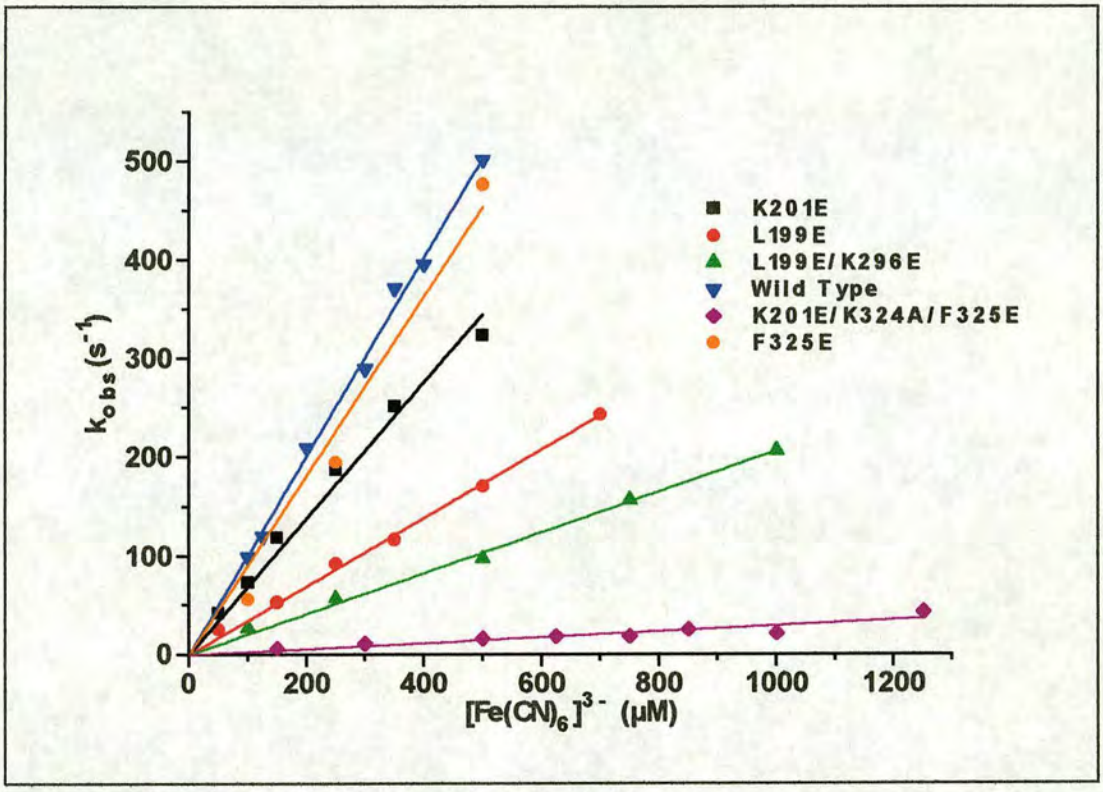

Figure 3.10. *k_{obs} (s^{-1}) vs $[Fe(CN)_6^{3-}]$ (μM) for FDH_{wt} and mutants. Data points for each enzyme have been fitted to a straight line.*

Figure 3.10 shows the dramatic effect these point mutations have had on the ability of FDH to transfer electrons to $[Fe(CN)_6]^{3-}$. None of the mutants exhibit Michaelis-Menten type kinetics at these concentrations. FDH_{wt} with a bimolecular rate constant, k_2, of 1 x 10^6 $M^{-1}s^{-1}$ is the most efficient and at 500μM $[Fe(CN)_6]^{3-}$ is approaching the limitations of the apparatus with a value for k_{obs} of $500s^{-1}$. What is most striking about Figure 3.10 is the much slower rates of FDH oxidation exhibited by $[Fe(CN)_6]^{3-}$ for the triple mutant. The enzyme has the lowest k_2 value at only 3 x 10^4 $M^{-1}s^{-1}$, approximately 34-fold lower than that for FDH_{wt}. The values of k_2 for the remaining mutants follow a trend with increasing mutations causing a decrease in

activity with $[Fe(CN)_6]^{3-}$. This is most probably due to the increase in electrostatic repulsion for $[Fe(CN)_6]^{3-}$ by the glutamate residues. It was assumed that the quadruple mutant and the double mutant L199E/K201E would continue the series, but consistent data could not be obtained, due to their very low activities, and these were not pursued. Although the number of mutations is important, so are their positions on the enzyme surface. The k_2 values suggest that certain point mutations are having a greater influence on the interaction with $[Fe(CN)_6]^{3-}$ than others, and this can be rationalised by looking at the surface of the enzyme close to the FMN group (Figure 3.1.). The most effective single mutation is L199E, which seems reasonable since it is easily the closest residue to the exposed FMN molecule. It is unlikely that $[Fe(CN)_6]^{3-}$ would be able to get close enough to the FMN for electron transfer due to the presence of this new repulsive force. The next most effective single mutation is K201E which is also not far from the FMN. Looking at Figure 3.1. the position of the side-chain at the right hand side of the FMN molecule perhaps allows easier access for $[Fe(CN)_6]^{3-}$, explaining why the k_2 value is twice that of L199E. What is interesting is that, individually, both mutations have marked effects on the enzyme but still allow it to function as a dehydrogenase. However, in combination they effectively destroy $[Fe(CN)_6]^{3-}$ reduction, although reduction by L-lactate remains possible. The F325E mutation is a little further from the FMN than either of the previous single mutations and so likely to have less influence on approaching acceptors. It is also immediately next to K324 and so at best will be neutralised by the lysine, thus decreasing its effect still further. In this case the two lysines (K201 and K296) will probably be sufficient to attract $[Fe(CN)_6]^{3-}$ towards the FMN group. The mutant with the largest effect after the triple mutant is L199E/K296E, with a k_2 value of 2.1×10^5 $M^{-1}s^{-1}$. This is not much bigger than the k_2 value for L199E and may be explained by the proximity of K296E to the 4 lysines in the proteolytically sensitive loop. An interesting experiment would be to construct a K296E single mutant to determine if the effect produced by the double is the sum of the two singles.

These data have shown that only three, well placed, mutations are required to destroy the interaction of FDH with $[Fe(CN)_6]^{3-}$. However, this is only half the aim

when trying to alter the specificity of an enzyme. Can these mutations not only repel electron acceptors but attract them and promote the interaction with positively charged molecules such as $[Co(phen)_3]^{3+}$?

3.2.6.3. FDH oxidation by $[Co(phen)_3]^{3+}$.

The stopped-flow experiments were repeated to determine the reactions of the mutant enzymes with the positively charged electron acceptor Cobalt trisphenanthroline, $[Co(phen)_3]^{3+}$. The stoichiometry of this reaction is the same as that for the $[Fe(CN)_6]^{3-}$ reaction. The results indicate how successful we have been in altering the electron acceptor specificity of FDH. The concentration of $[Co(phen)_3]^{3+}$ used was 10 μM-2 mM. The concentrations were determined as described in Section 2.4. The rate of oxidation of FMN was followed as for the $[Fe(CN)_6]^{3-}$ experiment at 450 nm over a time-scale from 100 ms-5s. Again at least five traces were generated at each concentration and the average of these fitted to single exponentials giving values for k_{obs} (Figure 3.11.).

The plot of k_{obs} vs $[Co(phen)_3^{3+}]$ is shown in Figure 3.12. Looking first of all at the two extreme cases, *i.e.* FDH_{wt} and the triple mutant, the effect of the mutations is clear. The plots show that the relationship which these two exhibited with $[Fe(CN)_6]^{3-}$ has been reversed, with FDH_{wt} having very little reductase activity for $[Co(phen)_3]^{3+}$ whereas the triple mutant, with its negatively charged docking site, has much better reactivity with $[Co(phen)_3]^{3+}$ than with $[Fe(CN)_6]^{3-}$. This proves immediately that not only has the original binding site, specific for negatively charged molecules, been seriously impaired but also that a new binding site, specific for small, positively charged complexes, has been created.

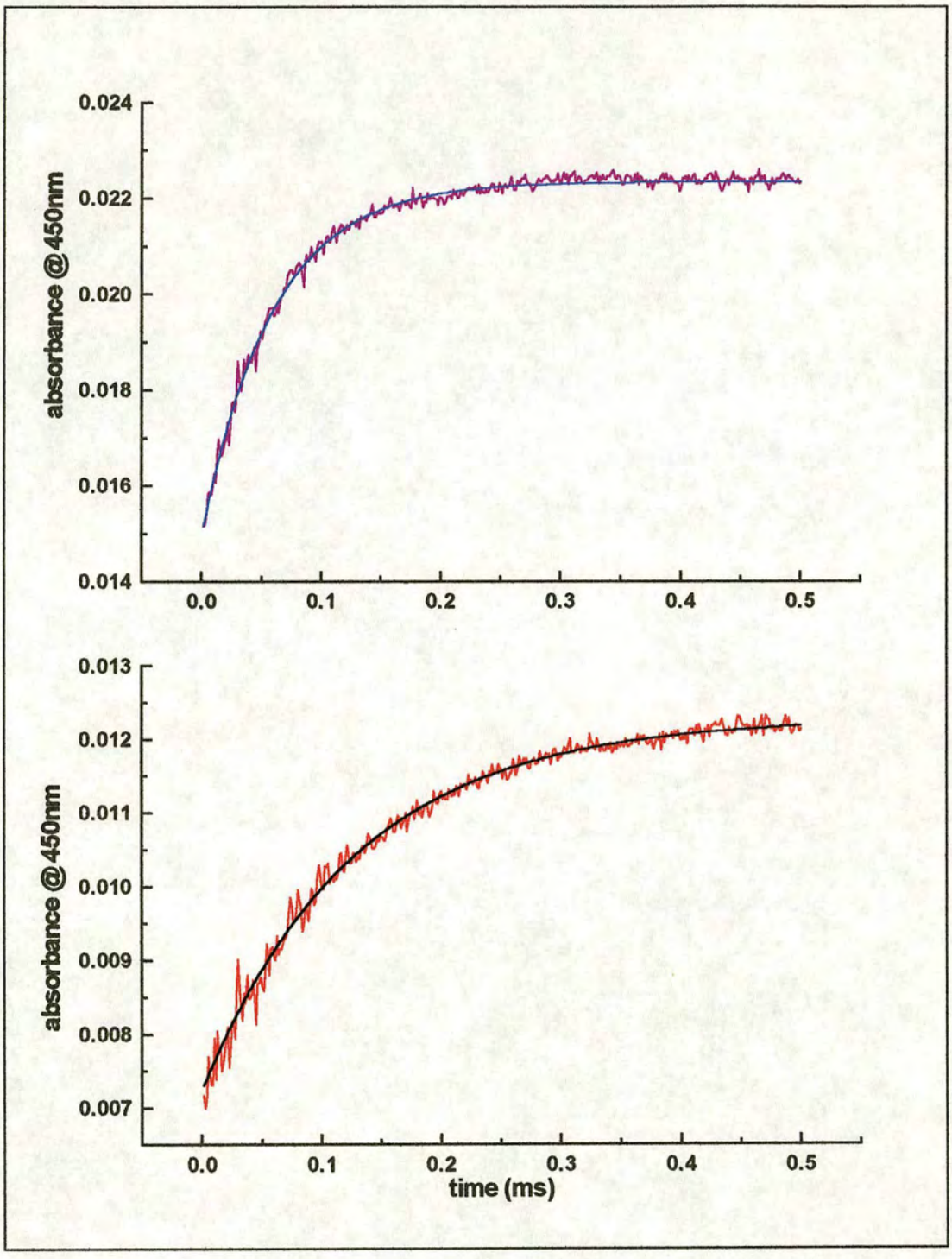

Figure 3.11. *Stopped-flow traces for the oxidation of FMN by $[Co(phen)_3]^{3+}$, 1 mM, for FDH_{wb} (bottom) and by $[Co(phen)_3]^{3+}$, 125 μM, for the triple mutant K201E/K324A/F325E (top). These data have been fitted to single exponentials (black and blue lines). All experiments were performed at 25°C in Tris.HCl pH 7.5, I = 0.1 M.*

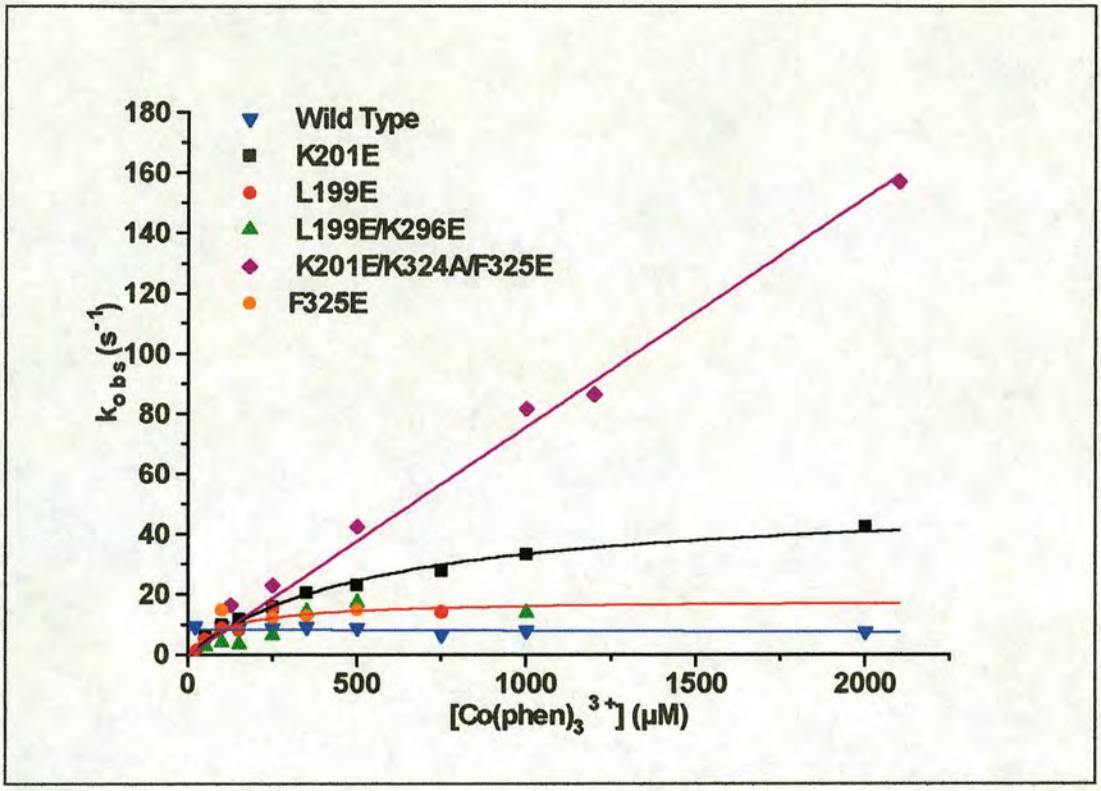

Figure 3.12. *k_{obs} s^{-1} vs [Co(phen)$_3$$^{3+}$] for the oxidation of FDH_{wt} and mutants. Data points have been fitted to straight lines (FDH_{wt} and K201E/K324A/F325E) and Michaelis-Menten curves (L199E and K201E).*

FDH_{wt} shows no dependence on the concentration of $[Co(phen)_3]^{3+}$, over the range analysed, with a maximum rate of electron transfer of ~10s^{-1}. It is possible that the positive charges close to the FMN repel $[Co(phen)_3]^{3+}$ to another position much further from the FMN. Thus, distance from FMN to acceptor would limit the rate of electron transfer. The triple mutant exhibits by far the best reductase activity with $[Co(phen)_3]^{3+}$ and shows no signs of saturation having a bimolecular rate constant of $7.6x10^4$ $M^{-1}s^{-1}$. This is ~2.5-fold faster than with $[Fe(CN)_6]^{3-}$. At 2 mM $[Co(phen)_3]^{3+}$, the k_{obs} for oxidation of the triple mutant is 16-fold faster than for FDH_{wt}. These data show that the re-design project has brought about a dramatic switch in the specificity of FDH for electron acceptors. The values of k_{obs} for the triple mutant with $[Co(phen)_3]^{3+}$ suggest that electron transfer is not as efficient as between FDH_{wt} and $[Fe(CN)_6]^{3-}$. This could be due to the relative sizes of the two acceptor molecules. The $[Co(phen)_3]^{3+}$ molecule is significantly larger than $[Fe(CN)_6]^{3-}$ and may not be able to get as close to the FMN. Molecular modelling studies were undertaken to

estimate the distances involved, and these are discussed in detail in Chapter 5. An interesting point to note is that the double mutant L199E/K296E, with the second poorest activity with $[Fe(CN)_6]^{3-}$, also has a slow rate of oxidation with $[Co(phen)_3]^{3+}$. This may be explained by the position of the K296 residue, which is very close to the proteolytically sensitive loop. The bulk of the loop could well cause more steric problems for the large $[Co(phen)_3]^{3+}$ than for the much smaller $[Fe(CN)_6]^{3-}$. Thus, the effect of K296E on $[Co(phen)_3]^{3+}$ would be less pronounced than for $[Fe(CN)_6]^{3-}$. Therefore, the repulsion for $[Fe(CN)_6]^{3-}$ is significantly more than that from L199E alone, but the attraction for $[Co(phen)_3]^{3+}$ is, at most, only that from L199E. The remaining two mutants K201E and L199E both exhibit what looks like saturation kinetics, giving reasonable fits to the Michaelis-Menten equation. However, on studying the bimolecular rate constants (k_{cat}/K_m) for these compared to the triple mutant it becomes clear that they are essentially the same. This suggests that electron transfer is being limited by distance from the FMN *i.e.* the rate of electron transfer is much slower than the association rate and so is rate limiting. Thus, the concentration of acceptor is irrelevant as the electron transfer rate can get no faster (Figure 3.13.)

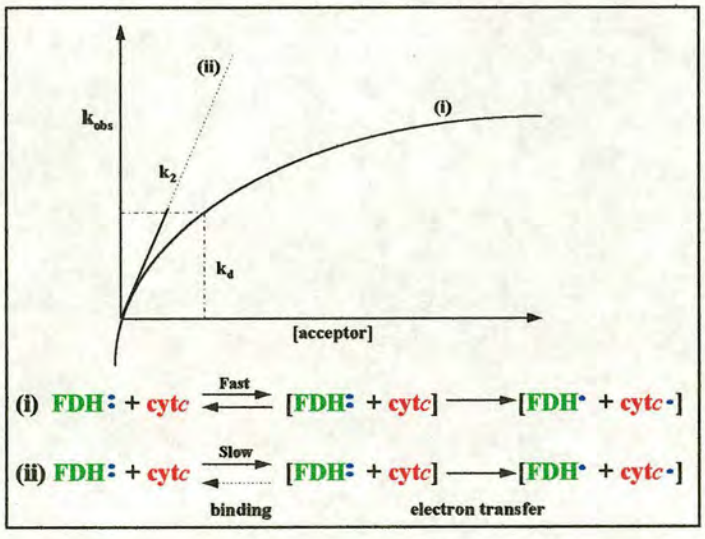

Figure 3.13. *Pre-steady-state oxidation of FDH by cytochrome c (or an artificial electron acceptor). Under standard conditions FDH oxidation follows a single exponential function. This is only possible if one of the two schemes shown above is satisfied by the reaction mechanism. Therefore, either (i) binding is fast and reversible but electron-transfer slow by comparison or (ii) binding is slow and electron-transfer is fast by comparison.*

In L199E the introduced negative charge must work against the positive K201 and is unlikely to be allowed to exert its full charge on $[Co(phen)_3]^{3+}$. The long trailing, positively charged side chain of K201 is probably enough to repel $[Co(phen)_3]^{3+}$. With K201E, the nearest positive charge to FMN has been replaced, so there is little electrostatic repulsion for $[Co(phen)_3]^{3+}$. However, the bulk of the two methyl groups on L199 will create a steric barrier for the acceptor molecule. Thus, there is a minimum distance, from FMN, that $[Co(phen)_3]^{3+}$ can reach in both mutant enzymes which limits the rate of electron transfer. In the triple mutant as well as the K201E mutation, the steric bulk of F325 has been replaced by a more flexible glutamate residue, revealing a new approach route for $[Co(phen)_3]^{3+}$ which avoids L199 altogether. As well as removing steric hindrance, the F325E mutation will also exert some coulombic attraction on $[Co(phen)_3]^{3+}$. This attraction should be enhanced considerably by mutating K324 to an alanine. These three mutations remove steric bulk and introduce significant coulombic attractions for $[Co(phen)_3]^{3+}$, thus improving its rate of electron transfer with FDH.

3.2.7. The Ionic strength dependence of FDH oxidation.

To investigate further the binding of inorganic complexes to FDH_{wt} and the triple mutant the stopped-flow experiments were repeated over a range of ionic strengths from 0.05-0.5 M (Section 2.4). Again five traces were averaged for each experiment and these also fitted well to single exponentials. Values of k_{obs} were converted to second-order rate constants, k_2, and $\log k_2$ was plotted against the square root of ionic strength as shown in Figure 3.14.

Looking first of all at the plot for the reaction of the enzymes with $[Fe(CN)_6]^{3-}$. These data have been fitted to the extended Debye-Hückel equation (Section 7.3.) which allows calculation of the product of charges involved at a bimolecular interface. The equation was intended for use with small molecules and caution should be exercised when interpreting such data for protein interactions, where the charge contribution at a protein interface may be difficult to calculate.

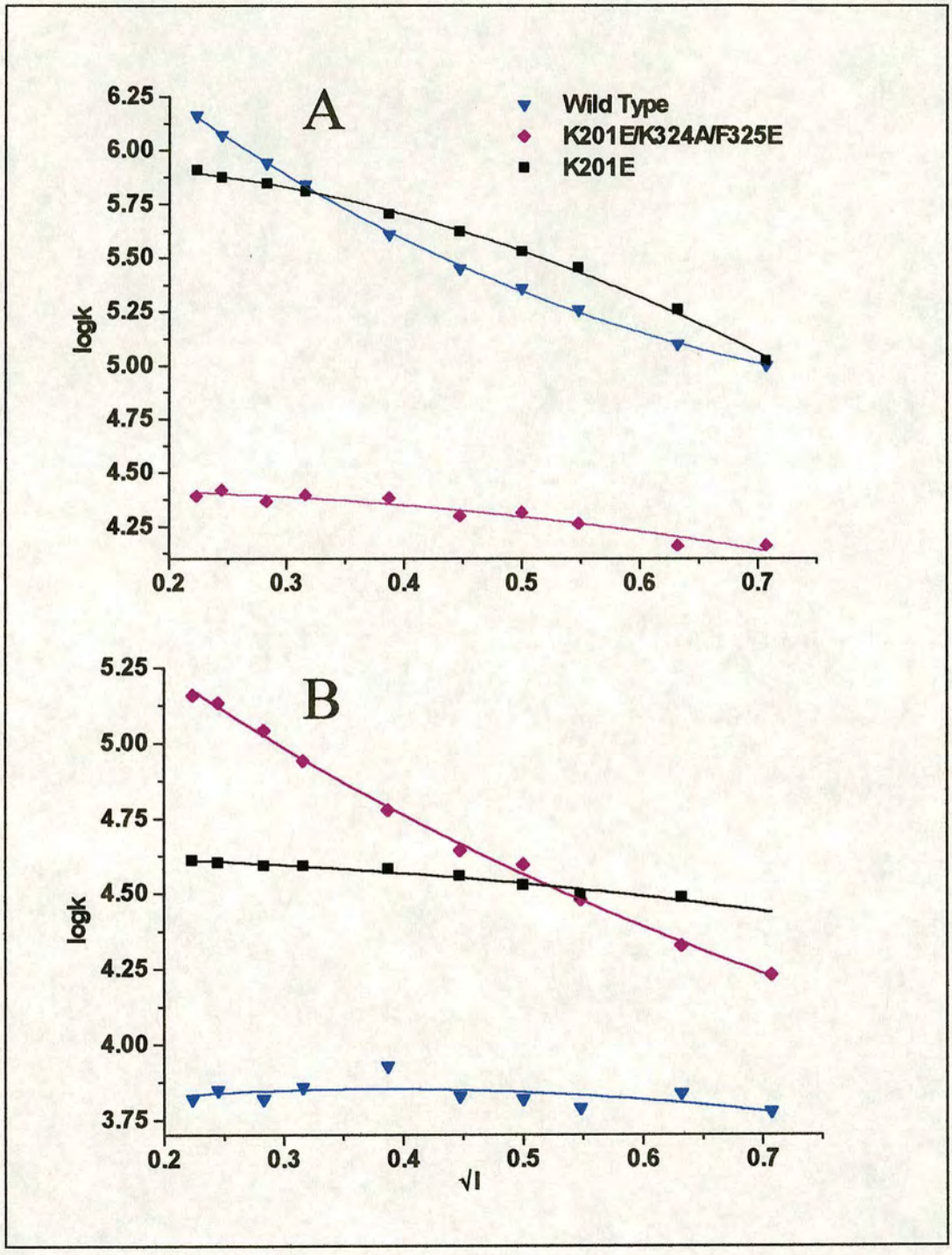

Figure 3.14. *Ionic strength plots of FMN oxidation for FDH_{wt} (100 μM $[Fe(CN)_6]^{3-}$, 1 mM $[Co(phen)_3]^{3+}$), K201E (400 μM $[Fe(CN)_6]^{3-}$, 2 mM $[Co(phen)_3]^{3+}$) and K201E/K324A/F325E (1 mM $[Fe(CN)_6]^{3-}$, 1 mM $[Co(phen)_3]^{3+}$). All enzymes were 2 μM. Glycolate = 25 mM. $[Fe(CN)_6]^{3-}$ data plot A and $[Co(phen)_3]^{3+}$ data plot B. These data have been fitted to the extended Debye-Hückel equation providing values for z_+z_-, the product of the charges interacting at the protein:electron acceptor interface.*

However, in this case, where $[Fe(CN)_6]^{3-}$ and $[Co(phen)_3]^{3+}$ are of known charge, a good indication of the electrostatic nature of the docking site on the enzyme can be obtained as well as an estimate of the charge being contributed by the enzyme. The ionic strength plot for the interaction with $[Fe(CN)_6]^{3-}$ shows firstly that increasing the ionic strength has a much larger effect on the interaction with FDH_{wt} than with the triple mutant, indicating that the charges introduced by mutagenesis definitely affect the binding of $[Fe(CN)_6]^{3-}$. This is confirmed when looking at the product of the interaction charges (z_+z_-) as calculated from the gradient of the ionic strength plots (Table 3.4.). For FDH_{wt} z_+z_- has a value of -7.7. Knowing that the charge on $[Fe(CN)_6]^{3-}$ is -3 then the charge on the enzyme surface with which the acceptor is interacting can be estimated at around +2.6. This is a reasonable value considering the residues close at hand, although it would be difficult to calculate the exact contribution from each residue.

	$[Co(phen)_3]^{3+}$	**$[Fe(CN)_6]^{3-}$**
FDH_{wt}	+0.296	+2.56
K201E	-0.016	-0.156
K201E/K324A/F325E	-1.65	-0.08

Table 3.4. *The charges exerted on the electron acceptors by the enzyme during interaction between the 2, as determined from ionic strength plots.*

In K201E where a positive residue has been replaced by a negative residue, the charge contribution from the enzyme is estimated at -0.156. This is a dramatic drop compared to FDH_{wt}. This coupled with its negative nature suggests two possible explanations: (i) This residue has a powerful influence on the overall charge of the $[Fe(CN)_6]^{3-}$-docking site, but the net charge produced is not enough to repel $[Fe(CN)_6]^{3-}$ entirely; or (ii) $[Fe(CN)_6]^{3-}$ is forced to dock at an entirely different site where it is influenced less by the mutated residue. The former explanation looks more promising when the value for the triple mutant is taken into account. If $[Fe(CN)_6]^{3-}$ were using the same docking site on both mutant enzymes, then the estimated charge contribution by the triple mutant would be more negative than that for K201E because of the greater number of mutations. However, as can be seen the charge on

the triple mutant is only half of that exhibited by K201E. This suggests that in the case of the triple mutant $[Fe(CN)_6]^{3-}$ experiences too much repulsion and is forced to use an alternative site where the repulsive forces are less. The fact that another site must be further from the exposed FMN explains why the rate of electron transfer with $[Fe(CN)_6]^{3-}$ is so low.

Data for the interaction of the enzymes with $[Co(phen)_3]^{3+}$ is also in Table 3.4. The estimated charge contribution from the triple mutant (-1.65) indicates the change in docking environment created by the mutations. Again this is a reasonable value considering the charges which have been introduced. If both $[Co(phen)_3]^{3+}$ and $[Fe(CN)_6]^{3-}$ were using the same docking site on the mutant then the charge contributions from the enzyme would be similar. The fact that they are quite different supports the conclusion that $[Co(phen)_3]^{3+}$ is utilising the negatively charged engineered site and $[Fe(CN)_6]^{3-}$ is being repelled to a less negatively charged site. The charge contribution from the single mutant K201E is less negative. This can be explained by the bulk of F325 which sterically hinders the approach of $[Co(phen)_3]^{3+}$. The large $[Co(phen)_3]^{3+}$ molecule cannot get close to K201E due to the bulky phenylalanine side-chain. The much smaller $[Fe(CN)_6]^{3-}$ gets much closer to K201E and so the charge contribution it experiences is correspondingly much more negative. This supports the earlier suggestion that the "saturation" exhibited by K201E oxidation by $[Co(phen)_3]^{3+}$ is actually due to electron transfer being rate limited by distance. In the triple mutant the F325 residue has been replaced by the less bulky glutamate group. Thus, $[Co(phen)_3]^{3+}$ can get close enough to the FMN such that: (i) Distance no longer limits the electron transfer rate and (ii) the estimated charge contribution from the enzyme is correspondingly much more negative. Finally the estimated charge contribution from FDH_{wt} during the interaction with $[Co(phen)_3]^{3+}$ is approximately +0.3. This is significantly less positive than that observed with $[Fe(CN)_6]^{3-}$ suggesting that $[Co(phen)_3]^{3+}$ is repelled by the positive charges close to FMN and forced to utilise an alternative site. This site must be further from the FMN molecule resulting in significantly lower electron transfer rates. Again there was no

concentration dependence for this interaction suggesting that, as seen previously, the long distance between FMN and $[Co(phen)_3]^{3+}$ rate limits the reaction.

3.2.8. Alternative electron acceptor.

The final experiment in this series was to repeat the stopped-flow FDH oxidation using the electron acceptor $[Co(dipic)_2]^{1-}$. This molecule has a weaker charge (-1) than the previous electron acceptors (Table 3.3). This allows further investigation of the electrostatic nature of the docking sites on FDH_{wt} and the triple mutant K201E/K324A/F325E. Values for k_{obs} were obtained as for previous experiments. Figure 3.15. shows a stopped-flow trace fitted to a single exponential and the resulting plot of k_{obs} vs $[Co(dipic)_2^{1-}]$ for the interaction between the FDH_{wt} and the triple mutant with $[Co(dipic)_2]^{1-}$.

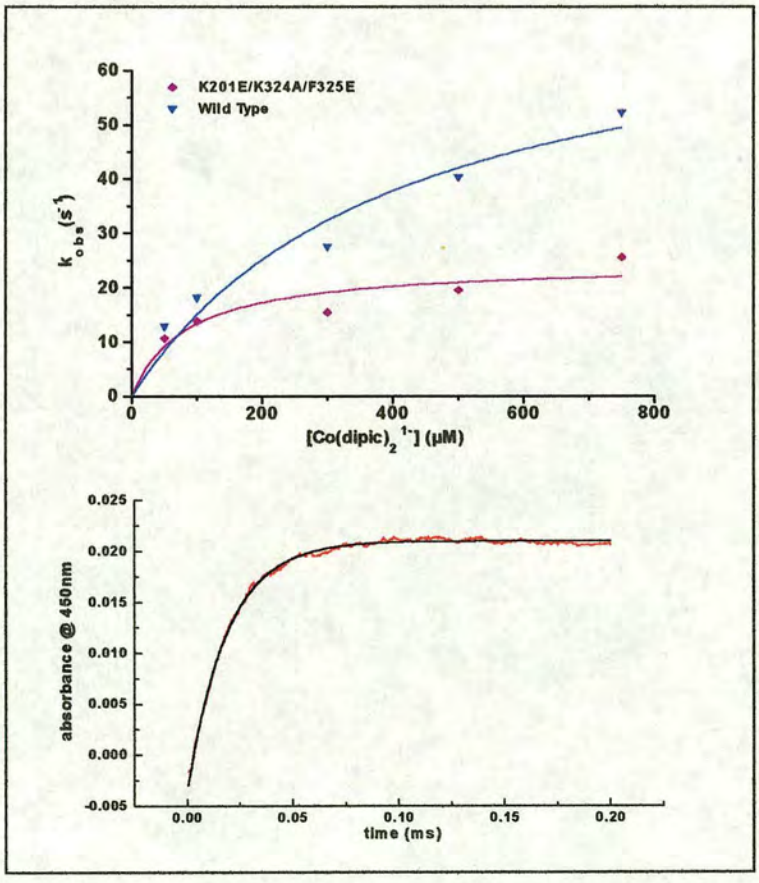

Figure 3.15. *Stopped-flow trace for the oxidation of FDH_{wt} (2 μM) by $[Co(dipic)_2]^{-1}$ (750 μM). These data have been fitted to a single exponential (black line). Also shown is the resulting plot of k_{obs} vs $[Co(dipic)_2^{1-}]$ for the oxidation of FDH_{wt} and K201E/K324A/F325E. All experiments were performed at 25°C in Tris.HCl pH 7.5, I = 0.1 M.*

For FDH_{wt} the bimolecular rate constant, k_2, ($1.88x10^5$ $M^{-1}s^{-1}$) is 5-fold slower with $[Co(dipic)_2]^{1-}$ than it was with $[Fe(CN)_6]^{3-}$. The k_2 value for the triple mutant with $[Co(dipic)_2]^{1-}$ ($2.93x10^5$ $M^{-1}s^{-1}$) is 10-fold faster than that with $[Fe(CN)_6]^{3-}$. This suggests that $[Co(dipic)_2]^{1-}$ can get closer to the FMN in the triple mutant. However, although this is also only 2-fold lower than k_2 with $[Co(phen)_3]^{3+}$ the maximum k_{obs} of $\sim 20s^{-1}$ indicates that the distance between $[Co(dipic)_2]^{1-}$ and FMN remains large and limits the rate of electron transfer. This suggests that $[Co(dipic)_2]^{1-}$ is not utilising fully the designed docking site but one further from the introduced negative charges.

3.3. Conclusion.

Site-directed mutagenesis was used to construct 7 mutant enzymes in order to study the recognition processes between independently expressed FDH from flavocytochrome b_2 and a range of inorganic complexes. Prominent positively charged and hydrophobic residues close to the exposed FMN molecule were replaced with negatively charged glutamate residues and neutral residues. The aim was to re-design the docking site on FDH, thus altering its electron acceptor specificity in favour of positively charged molecules such as $[Co(phen)_3]^{3+}$. The remaining mutants were studied using stopped-flow kinetics to determine the rate of FDH oxidation by the electron acceptors $[Fe(CN)_6]^{3-}$, $[Co(phen)_3]^{3+}$ and $[Co(dipic)_2]^{1-}$. These data indicate that FDH_{wt} was most efficient with $[Fe(CN)_6]^{3-}$ and most inefficient with $[Co(phen)_3]^{3+}$. The triple mutant (K201E/K324A/F325E), which had the most mutations while retaining acceptable catalytic activity, was shown to be the least efficient with $[Fe(CN)_6]^{3-}$ and the most effective with $[Co(phen)_3]^{3+}$. These results confirmed our theory that by altering the electrostatic nature of an enzyme docking site it is possible to alter its specificity for electron acceptors. Taking this a stage further, ionic strength studies showed that in FDH_{wt} the $[Co(phen)_3]^{3+}$ complex was forced to use an alternative site for electron transfer due to electrostatic repulsion. A similar situation arose between the triple mutant and $[Fe(CN)_6]^{3-}$. The kinetic data also suggested that the bulky F325 may sterically hinder binding of $[Co(phen)_3]^{3+}$ and $[Co(dipic)_2]^{1-}$, which are considerably larger than $[Fe(CN)_6]^{3-}$.

The electron-acceptor specificity of independently expressed FDH from flavocytochrome b_2 has been reversed. Three mutations have been shown as sufficient to decrease the rate of electron transfer with $[Fe(CN)_6]^{3-}$ by 50-fold at the same time significantly increasing that with $[Co(phen)_3]^{3+}$. At the highest concentration of $[Co(phen)_3]^{3+}$ studied the triple mutant has an observed rate of electron transfer 16-fold faster than FDH_{wt}. However, the triple mutant shows no signs of saturation at this acceptor concentration whereas FDH_{wt} has already reached a maximum. This suggests that the actual difference in rates of electron-transfer is significantly larger.

4.Cytochrome *c* reductase activity in the flavin binding domain of flavocytochrome b_2.

4.1. Introduction.

As described in Chapter 1 the flavin binding domain of flavocytochrome b_2 (FDH_{wt}) has been independently expressed in *E. coli* allowing its characterisation without the influence of the cytochrome domain or the strong spectral absorbance associated with its haem. Kinetic parameters have been determined which show that FDH_{wt} retains most of the L-lactate dehydrogenase activity exhibited by the intact enzyme, using the artificial electron acceptor ferricyanide, $[Fe(CN)_6]^{3-}$, (Balme *et al.*, 1995) (Table 4.1.). What is surprising is the total inability of FDH_{wt} to transfer electrons to the independently expressed b_2-cytochrome domain (Pallister *et al.*, 1990).

	k_{cat} s^{-1}	K_m mM	k_{cat}/K_m M^{-1} s^{-1}
flavocytochrome b_2	400 ± 10	0.49 ± 0.05	(8.2 ± 1.1) x 10^5
FDH_{wt}	273 ± 6	0.22 ± 0.05	(1.2 ± 0.4) x 10^6

Table 4.1. *Kinetic parameters for the interaction of FDH_{wt} and intact flavocytochrome b_2 with the $[Fe(CN)_6]^{3-}$. All experiments were performed at 25°C in Tris.HCl pH 7.5, I = 0.1 M.*

Table 4.1. shows that, under standard conditions, with $[Fe(CN)_6]^{3-}$ as electron acceptor, FDH_{wt} is an efficient L-lactate dehydrogenase with a k_{cat} value two thirds of that exhibited by intact flavocytochrome b_2. FDH_{wt} also shows a K_m value almost half that of intact flavocytochrome b_2.

The hinge region, which tethers the cytochrome domain to FDH_{wt} in intact flavocytochrome b_2, is of vital importance for efficient intra-protein electron transfer (White *et al.*, 1993). By shortening or lengthening the hinge, the rate of intra-protein electron transfer is seriously affected (Sharp *et al.*, 1996a & b). The two independently expressed domains exhibit no detectable inter-protein electron transfer. However, electrostatic attractions between the two domains are favourable, suggesting that there is perhaps a steric factor preventing the two forming a complex.

What is particularly intriguing is the dramatic loss of cytochrome *c* reductase activity on removal of the cytochrome domain. The kinetic parameters of this reaction for both intact flavocytochrome b_2 and FDH_{wt} are shown in Table 4.2.

	k_{cat} s^{-1}	K_m μM	k_{cat}/K_m M^{-1} s^{-1}
flavocytochrome b_2	207 ± 2	10 ± 1	(2.1 ± 0.2) x 10^7
FDH_{wt}	0.02 ± 0.002	23 ± 7	(8.7 ± 5.3) x 10^2

Table 4.2. *Kinetic parameters for the interaction of FDH_{wt} and intact flavocytochrome b_2 with cytochrome c. All experiments were performed at 25°C in Tris.HCl pH 7.5, I = 0.1 M.*

The kinetic parameters show that removal of the cytochrome domain causes a huge loss of cytochrome *c* reductase activity. The k_{cat} value for the reaction of FDH_{wt} with cytochrome *c* is 10^4-fold lower than that for intact flavocytochrome b_2. This is the major contribution to a catalytic efficiency which is $2.4x10^4$-fold lower for FDH_{wt}. This is a remarkable loss of electron transferase activity for a catalytically sound enzyme. The ability of FMN to exist as both semiquinone and hydroquinone suggest that FDH_{wt} should be able to transfer electrons individually to cytochrome *c* without a mediator. Why then does flavocytochrome b_2 require a cytochrome domain to mediate electron transfer? This requirement is even more surprising when other factors are taken into consideration. The thermodynamic driving force for electron transfer between FDH_{wt} and cytochrome *c* has been measured from reduction potentials and found to be 340 mV. This is a considerable driving force in biological terms indicating that thermodynamics cannot be the cause of such low activity. Molecular modelling experiments were undertaken to estimate the closest edge-to-edge distance possible between the FMN group of FDH_{wt} and the haem from cytochrome *c*. The co-ordinates of the FDH_{wt}, from the intact flavocytochrome b_2 crystal structure, and the structure of Horse Heart cytochrome *c* were used. The minimum distance between the prosthetic groups was estimated at ~13Å. This is close to the edge-to-edge distance between the FMN and haem groups in intact flavocytochrome b_2 which is 9.7 Å (Xia *et al.*, 1990). This suggests that the distance between the prosthetic groups will not limit the rate of electron transfer. It must be stressed at this point that these estimates were crude in the sense that no energy minimisation was performed and the structure of FDH_{wt} was assumed to be that of intact flavocytochrome b_2 minus that of the cytochrome domain. If this distance is achievable then it is unlikely that the intervening medium would limit electron transfer

significantly. As the two proteins approach, solvent molecules will be forced out of the interface region and electron transfer ought to become more feasible.

Distance and medium can be controlled by a third factor, that of recognition. In a solution of two physiological redox partners random collisions are likely to bring the two together and may even result in complexation. However, it is unlikely that the prosthetic groups of the proteins will come close enough together, often enough, to promote efficient electron transfer. If the two proteins have surface patches of complementary charge then the chances of complexation are improved. Furthermore if these patches are close to, or surrounding the prosthetic groups then the chances of the complex promoting electron transfer are also significantly enhanced. It is our proposal that FDH_{wt} and cytochrome *c* do not have complementary recognition sites and so consequently cannot form an efficient electron-transfer complex. This leads to the very low rates of inter-protein electron transfer which have been observed.

As described in Chapter 3. it is possible to alter the electron acceptor specificity of a protein for inorganic complexes using the principles of electrostatic interactions. The aim of the work described in this chapter was to create specificity where there is none *i.e.* to build a recognition site on FDH_{wt} which is specific for cytochrome *c* such that the rate of inter-protein electron transfer is improved.

4.2. Results and discussion.

4.2.1. The cytochrome *c*:FDH_{wt} interface.

If cytochrome *c* and FDH_{wt} are to form an efficient electron-transfer complex then the respective prosthetic groups must be as close to one another as possible. To achieve this it is necessary to bring the two proteins together where their prosthetic groups are exposed. Figure 4.1. shows the surface of cytochrome *c*, where the haem molecule is exposed to solvent and the most prominent residues surrounding it.

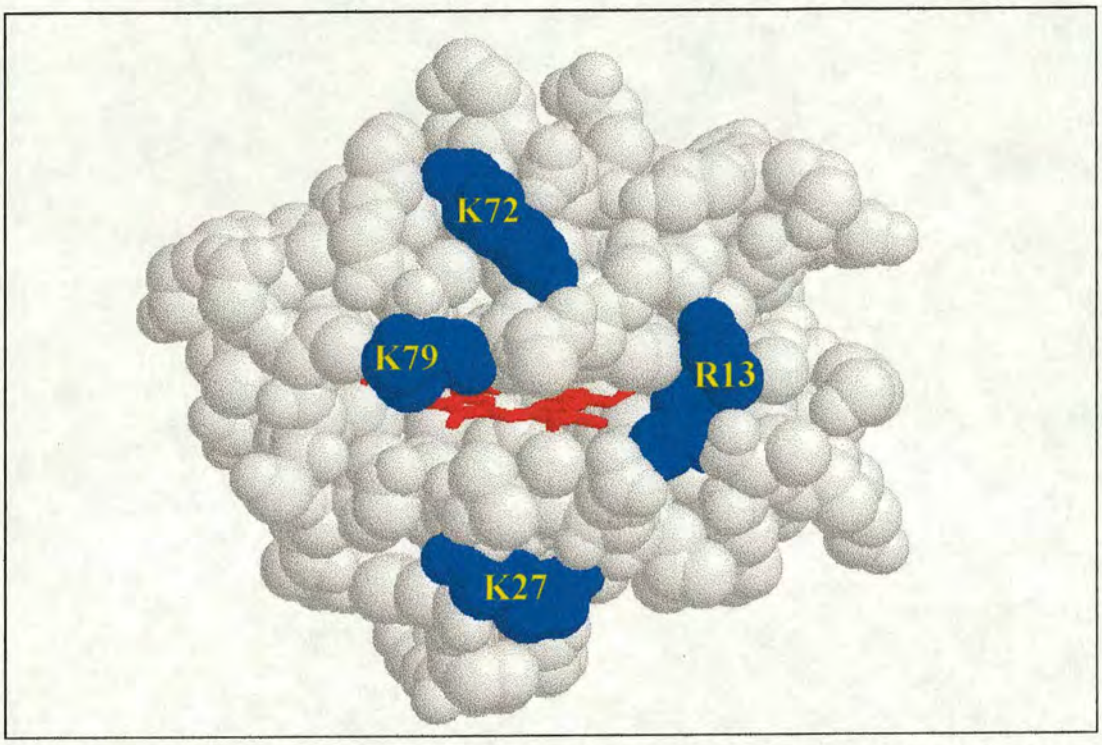

Figure 4.1. *The surface of cytochrome c (yeast) involved in electrostatic attractions and electron transfer (Koppenol et al., 1982). The exposed Haem molecule (red) and prominent, positively charged residues (blue) are highlighted.*

As described in Chapter 1. the charge distribution on cytochrome *c* has been studied in great detail (Koppenol *et al.*, 1982). The highlighted lysine and arginine residues are some of the positively charged amino acids that contribute to the asymmetric distribution of charge around the protein. They are also believed to be important in the binding of cytochrome *c* to cytochrome b_5 (Salemme, 1976). To interact with this surface, FDH_{wt} requires a complementary surface of negative residues close to the exposed FMN. Figure 4.2. shows the face of FDH_{wt} around the exposed edge of the FMN molecule. The prominent residues have been highlighted. Only three atoms from the FMN isoalloxazine ring are actually exposed to solvent C-4A, N-5 and C-5A. These are shown in yellow at the centre of the figure. The residues which have been highlighted demonstrate the predominantly positive and hydrophobic nature of the surface in the vicinity of the FMN. It should be noted that although the proteolytically sensitive loop cannot be seen, it is present and contains another four positively charged lysine residues.

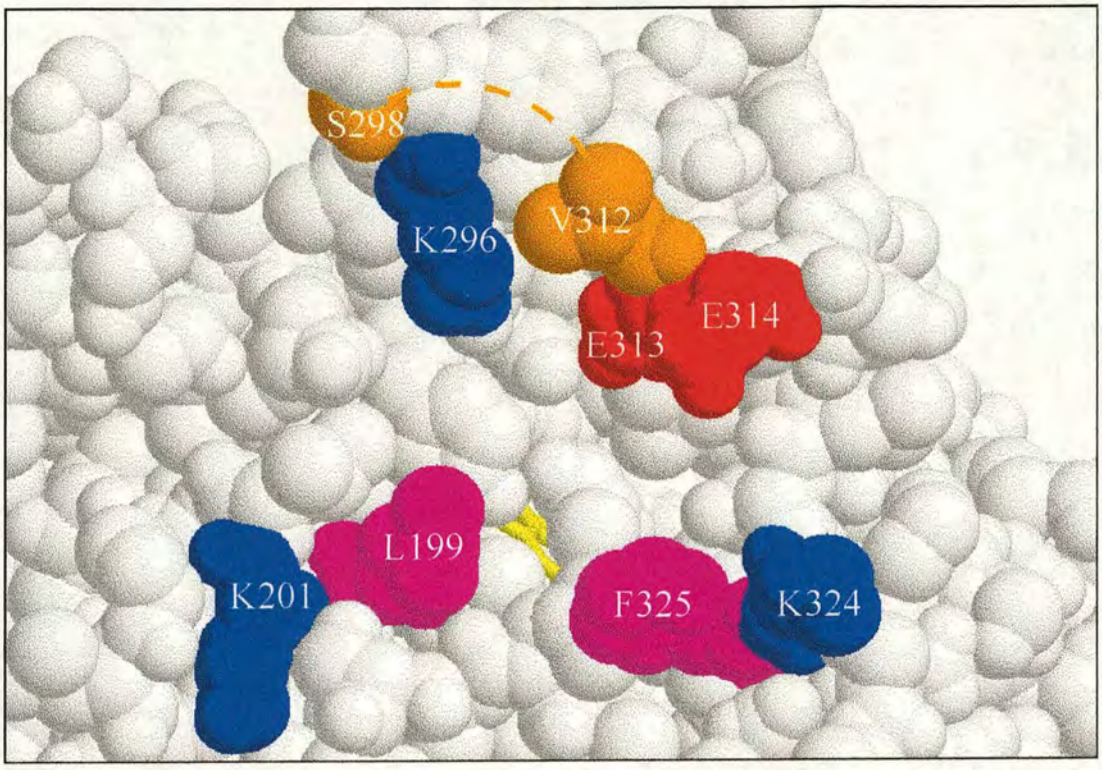

Figure 4.2. *The surface of FDH_{wt} close to the exposed FMN (yellow). Highlighted regions are: basic residues (blue); acidic residues (red) and hydrophobic residues (pink). The approximate position of the proteolytically sensitive loop, which is highly disordered and so invisible in the crystal structure, is indicated by a dashed line from Ser 298-Val 312 (orange).*

In fact apart from the two glutamate residues (313 and 314) this surface can be looked upon as the exact opposite of that required to interact with cytochrome *c*.

4.2.2. The nature of the FDH_{wt}:cytochrome *c* interaction.

It has been demonstrated that the faces on cytochrome *c* and FDH_{wt}, which would allow optimum electron transfer in terms of distance between the prosthetic groups, are electrostatically incompatible. However, the two proteins do exhibit an extremely slow rate of electron transfer consistent with an interaction between them some distance from the exposed FMN group. To determine the nature of this site steady-state analysis was carried out over a range of ionic strengths. The rate of reduction of cytochrome *c* was followed by the increase in absorbance at 550 nm (Section 2.3) generating traces such those in Figure 4.3. Values of k_{obs} were calculated as described in Section 2.3. Figure 4.4. shows a plot of k_{obs} vs [cytochrome *c*].

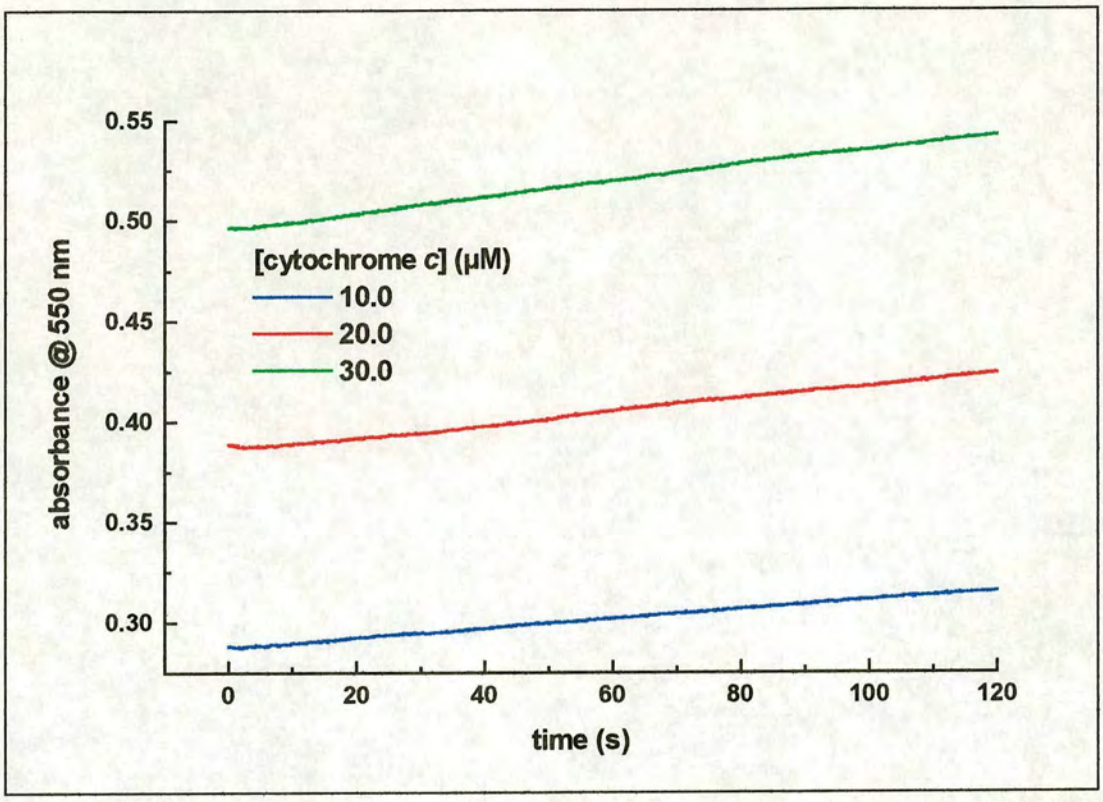

Figure 4.3. *Steady-state assay traces for the reduction of cytochrome c at 550 nm by FDH_{wt} (I = 0.1M). All experiments were performed at 25°C in Tris.HCl pH 7.5, I = 0.1 M.*

Kinetic data was fitted to the Michaelis-Menten equation providing values of k_{cat}, K_m and k_{cat}/K_m (Table 4.1.).

Ionic strength M	k_{cat} x$10^{-3}s^{-1}$	K_m μM	k_{cat}/K_m $M^{-1}s^{-1}$
0.05	11±1	23±4	460.9
0.06	10±2	28±7	362.7
0.08	7±1	22±5	318.6
0.1	6±0.3	17±1.0	379.5
0.2	6±2	38±13	169.3
0.3	3±0.6	26±8	128.9
0.4	3±0.7	35±12	95.1
0.5	2±0.2	22±5	98.2

Table 4.1. *Kinetic parameters for the interaction of FDH_{wt} with cytochrome c at varying ionic strengths (0.05-0.5 M).*

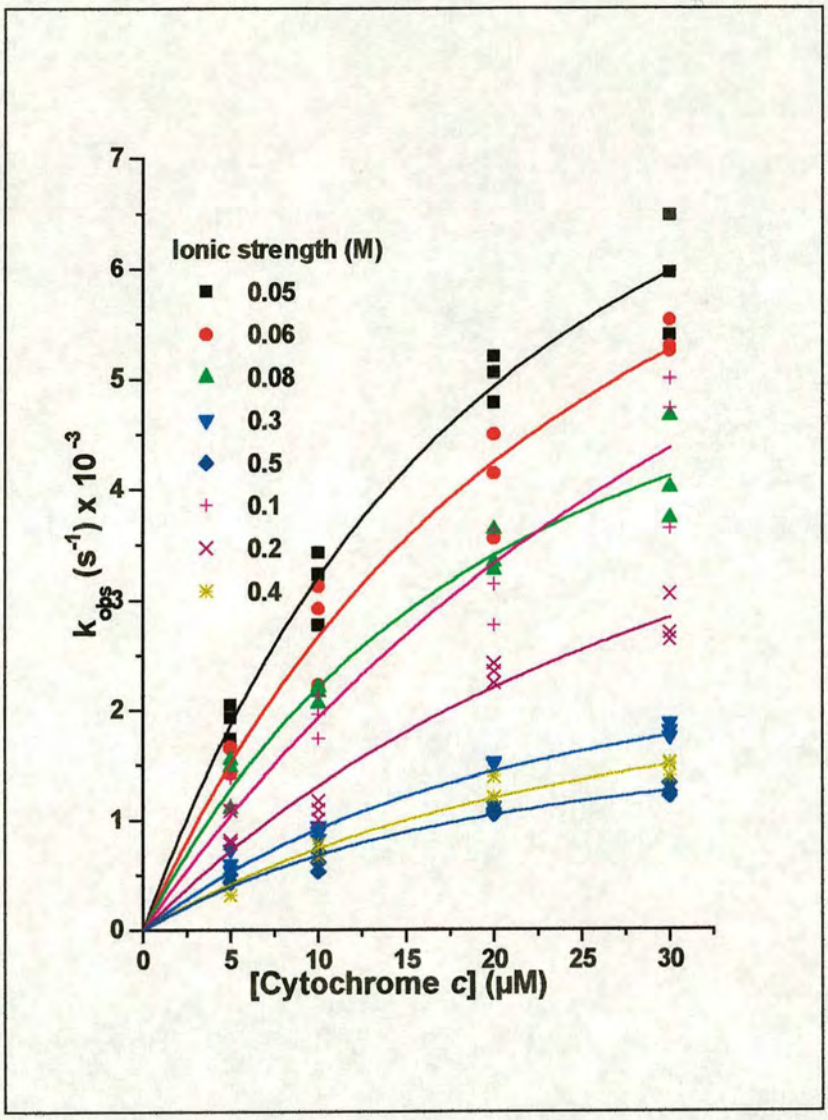

Figure 4.4. *A plot of k_{obs} vs [cytochrome c] over the ionic strength range 0.05 M-0.5 M. Assays at each ionic strength were performed in triplicate and data points have been fitted to the Michaelis-Menten equation*

As the ionic strength is increased it can be seen that the rate of reduction of cytochrome *c* drops steadily. Between 0.05 M and 0.5 M the value of k_{cat}/K_m has dropped by approximately 5-fold. Such a decrease in activity caused by increasing ionic strength is indicative of an electrostatic interaction between oppositely charged bodies. Thus it is likely that the predominantly positively charged cytochrome *c* is interacting with an area of negative charge on the surface of FDH_{wt}. The rate of electron transfer suggests that, at this site, the prosthetic groups are too far apart to allow efficient electron transfer. Values of k_2 were plotted against $\sqrt{I}$, to produce the

ionic strength plot shown in Figure 4.5. These data have been fitted to the extended Debye Hückel equation (Appendix 2). From the gradient of this fit a value of z+z- can be deduced where z_+z_- is the product of the charges at the interface of the two proteins. The equation was intended for use with small molecules. For proteins where the charges interacting at the interface are difficult to determine, its results can only be interpreted qualitatively. In this case z_+z_- has a value of -6. If we assume that the charge contribution from cytochrome *c* is +3 then it can be estimated that the contribution from FDH_{wt} is -2. Therefore, cytochrome *c* and FDH_{wt} utilise electrostatics in their present, albeit poor, interaction. The suggestion from this is that the engineering of a recognition site on FDH_{wt} should incorporate this type of interaction.

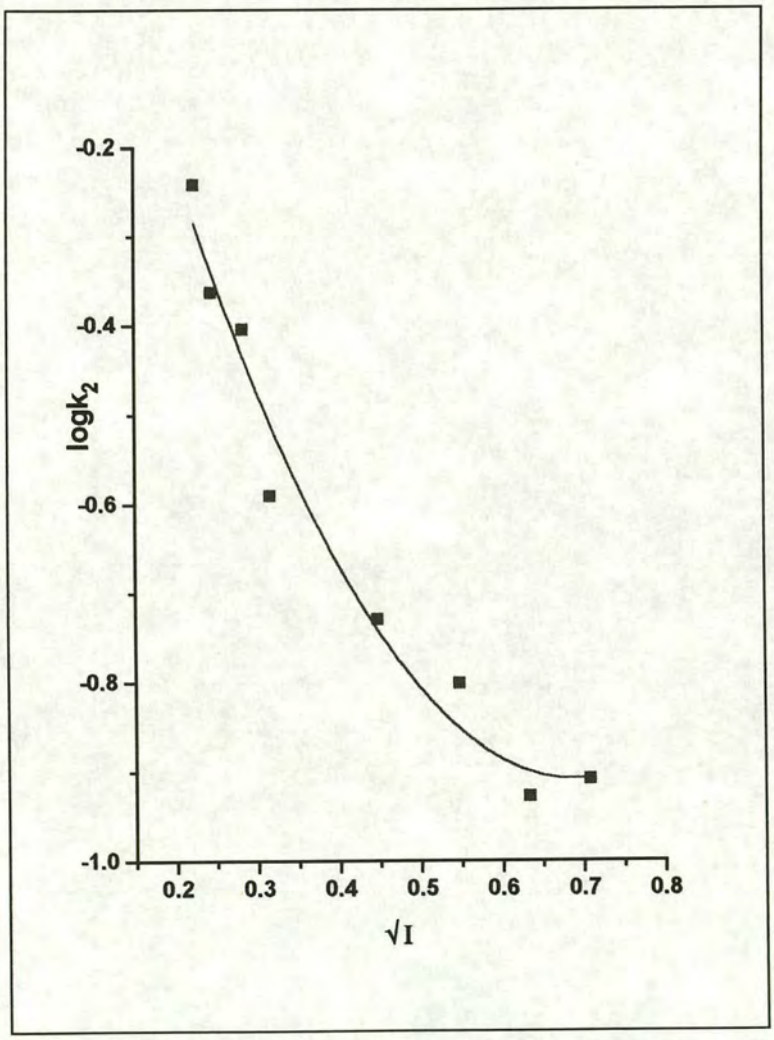

Figure 4.5. *The ionic strength plot for the interaction of FDH_{wt} with cytochrome c. These data have been fitted to the extended Debye-Hückel equation producing a value for z_+z_- of -6.*

The evidence obtained suggests that to improve recognition between FDH_{wt} and cytochrome *c* a negatively charged docking site must be constructed on the surface of FDH_{wt} close to the exposed FMN molecule. As described in Chapter 3. a range of mutant FDH enzymes have already been constructed using site-directed mutagenesis and shown to have significant effects on the electrostatic interactions between FDH and inorganic complexes such as $[Fe(CN)_6]^{3-}$ and $[Co(phen)_3]^{3+}$. Prominent positive and hydrophobic residues on FDH_{wt} (Figure 4.2.) were replaced with negatively charged glutamates. The electron acceptor specificity of FDH was altered in favour of the positively charged $[Co(phen)_3]^{3+}$. As this is the type of site required for interaction with the positively charged cytochrome *c* it was decided to test these mutants for improved cytochrome *c* reductase activity.

4.2.3. Steady-state analysis of cytochrome *c* reductase activity.

Steady-state assays following the reduction of cytochrome *c* by the mutant enzymes were performed as described in Section 2.3. Traces similar to those in Figure 4.6. were generated showing the rate of increase of absorbance at 550 nm over a period of 2 mins.

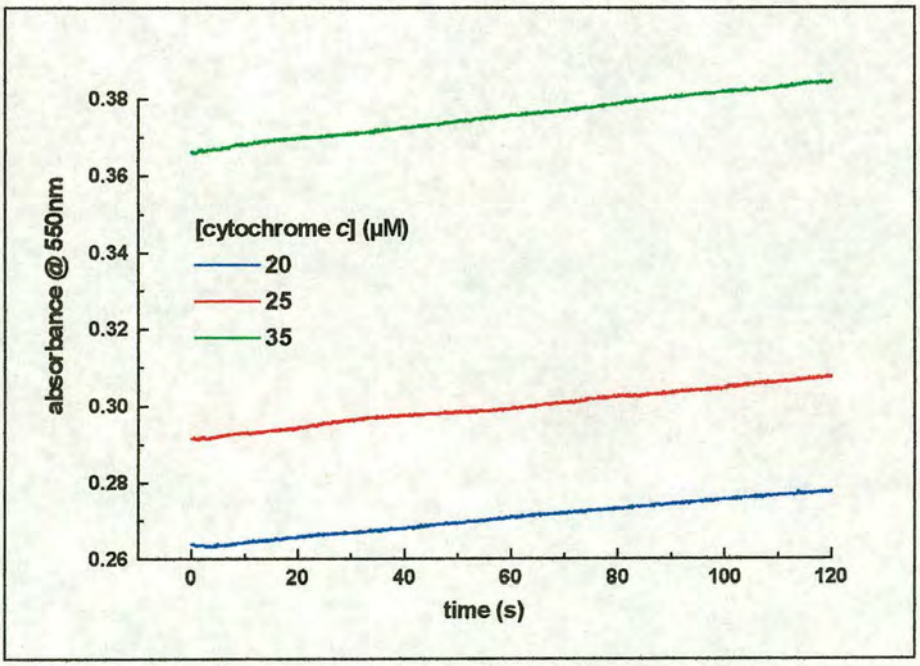

Figure 4.6. *Steady-state traces for the reduction of cytochrome c by L199E at 550 nm. All experiments were performed at 25°C in Tris.HCl pH 7.5 I = 0.1 M.*

Values of k_{obs} were calculated from these traces and plotted against [cytochrome *c*] to generate a Michaelis-Menten curve such as the one in Figure 4.7. The kinetic parameters for all the mutants are compared with those for FDH_{wt} in Table 4.2.

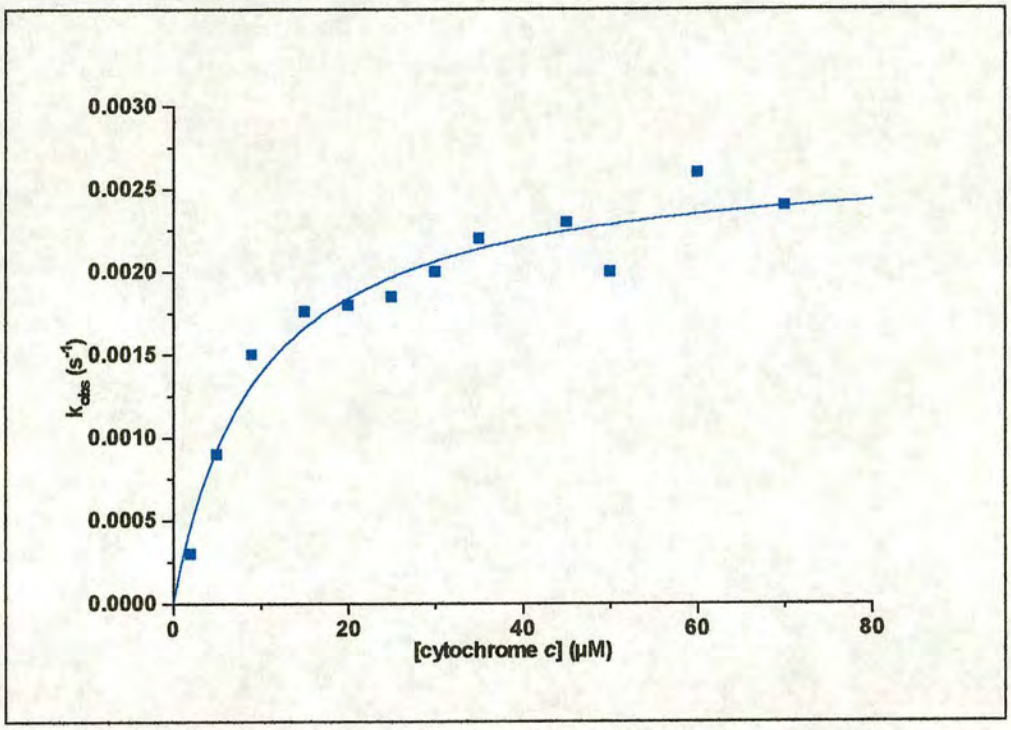

Figure 4.7. *A Michaelis-Menten plot, k_{obs} vs [cytochrome c], for the reduction of cytochrome c at 550 nm by L199E. Assays were performed at 25°C in Tris.HCl pH 7.5, I = 0.1 M.*

	k_{cat} s^{-1}	K_m μM	k_{cat}/K_m M^{-1} s^{-1}
FDH_{wt}	0.02 ± 0.002	23 ± 7	8.7×10^2
L199E	0.0027 ± 0.0001	9.7 ± 1.9	2.8×10^2
K201E	0.02	15	1.3×10^3
F325E	0.01	-	-
L199E/K296E	0.02 ± 0.003	57 ± 20	3.5×10^2
L199E/K201E	0.0024 ± 0.0001	6.2 ± 1	3.9×10^2
K201E/K324A/F325E	0.006	15	4×10^2
L199E/K201E/K324A/F325E	-	-	-

Table 4.2. *Kinetic parameters for the reduction of cytochrome c by FDH_{wt} and mutant enzymes. All experiments were performed at saturating concentrations of L-lactate, at 25°C, in Tric.HCl pH 7.5, I = 0.1 M.*

Looking initially at the values of k_{cat} it is obvious that, at best, the mutants have a similar cytochrome *c* reductase activity to that of FDH_{wt}. In most cases in fact the rate of cytochrome *c* reduction is considerably slower than for FDH_{wt}. The mutants L199E and L199E/K201E have k_{cat} values 10-fold lower than FDH_{wt}. The triple mutant (K201E/K324A/F325E) has a k_{cat} value 3-fold lower than FDH_{wt}. This, in particular, was a disappointing result after such promising results with the inorganic complexes. Oxidation of FMN by cytochrome *c* was measured using stopped-flow kinetics for the triple mutant (Section 2.4.). The rate was identical to that measured by steady-state analysis confirming the lack of reaction between the two proteins. Bearing in mind the very poor L-lactate dehydrogenase activity of the quadruple mutant (Section 3.2.4), its similarly poor cytochrome *c* reductase activity was not unexpected.

At this stage the single mutant K201E was observed to have improved cytochrome *c* reductase activity. However, the enzyme also exhibited FMN loss during turnover making the acquisition of reliable data difficult. On repetition of the experiments in the presence of free FMN the data quality was much improved (Figure 4.8.). This reproducible data shows that K201E is actually no better a cytochrome *c* reductase than FDH_{wt} having an identical value of k_{cat}. A control experiment showed no unusual effects on the FDH_{wt}:cytochrome *c* reaction due to the presence of free FMN.

The kinetic parameters in Table 4.2. simply confirm that, compared to intact flavocytochrome b_2, FDH_{wt} and all the mutants are very inefficient cytochrome *c* reductases. This shows that the mutations were not sufficient to improve the rate of inter-protein electron transfer. However, it may be that they have improved inter-protein recognition but some other factor is limiting the rate of electron transfer. This possibility was investigated by studying the binding of cytochrome *c* to FDH_{wt} and the mutant enzymes.

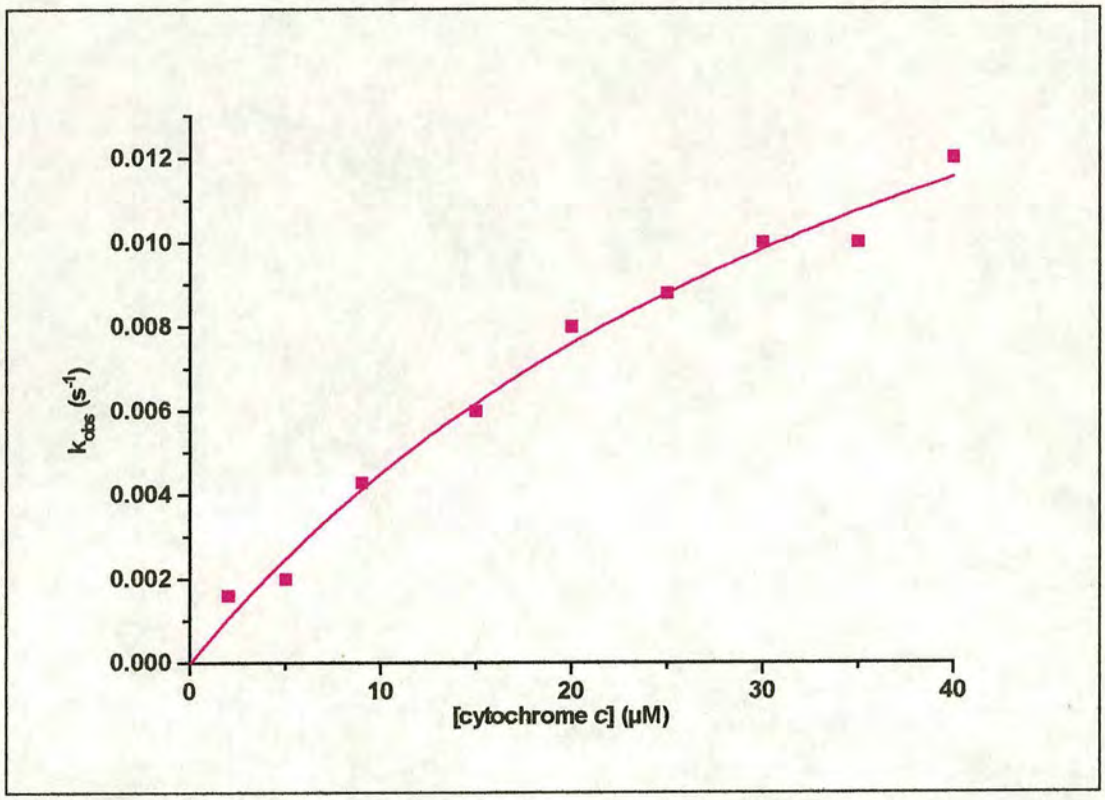

Figure 4.8. *A Michaelis-Menten plot for cytochrome c reduction by K201E in the presence of free FMN. The assays were performed as previously described, at 25°C, in Tris.HCl pH7.5, I =0.1M.*

4.2.4. Binding studies.

4.2.4.1. Circular dichroism.

Circular dichroism is a commonly used technique for the study of structural properties of proteins and enzymes (Section 2.8.). It can be used to study binding of proteins in solution. This is observed as discrepancies in the spectra of a mixture of two proteins compared to an algebraic mixture of the two. An algebraic mixture is created by summing the spectra of the individual proteins. The extent of binding between cytochrome *c* and the enzymes FDH_{wt}, K201E and L199E/K201E/K324A/F325E was studied. It was expected that the quadruple mutant, with the most mutations, would exhibit the strongest binding to cytochrome *c*. An experiment with FDH_{wt} and the independently expressed cytochrome domain was also performed to study the binding between two proteins which ought to have an inherent attraction for each other.

Circular dichroism was measured over both the Far UV (180-260 nm)(FUV) and the Near UV/Visible (260-600 nm)(NUV/Vis) as described in Section 2.8.

Spectra were recorded for the individual proteins *e.g.* FDH_{wt} and cytochrome *c*. These spectra were added together to give a theoretical "algebraic" mixture. These predicted spectra were then compared with physical mix spectra obtained by measuring the circular dichroism of the two proteins together.

Starting with the FDH_{wt}:b_2 cytochrome domain mixture. Figure 4.9. shows both the FUV and NUV/Vis spectra for these two.

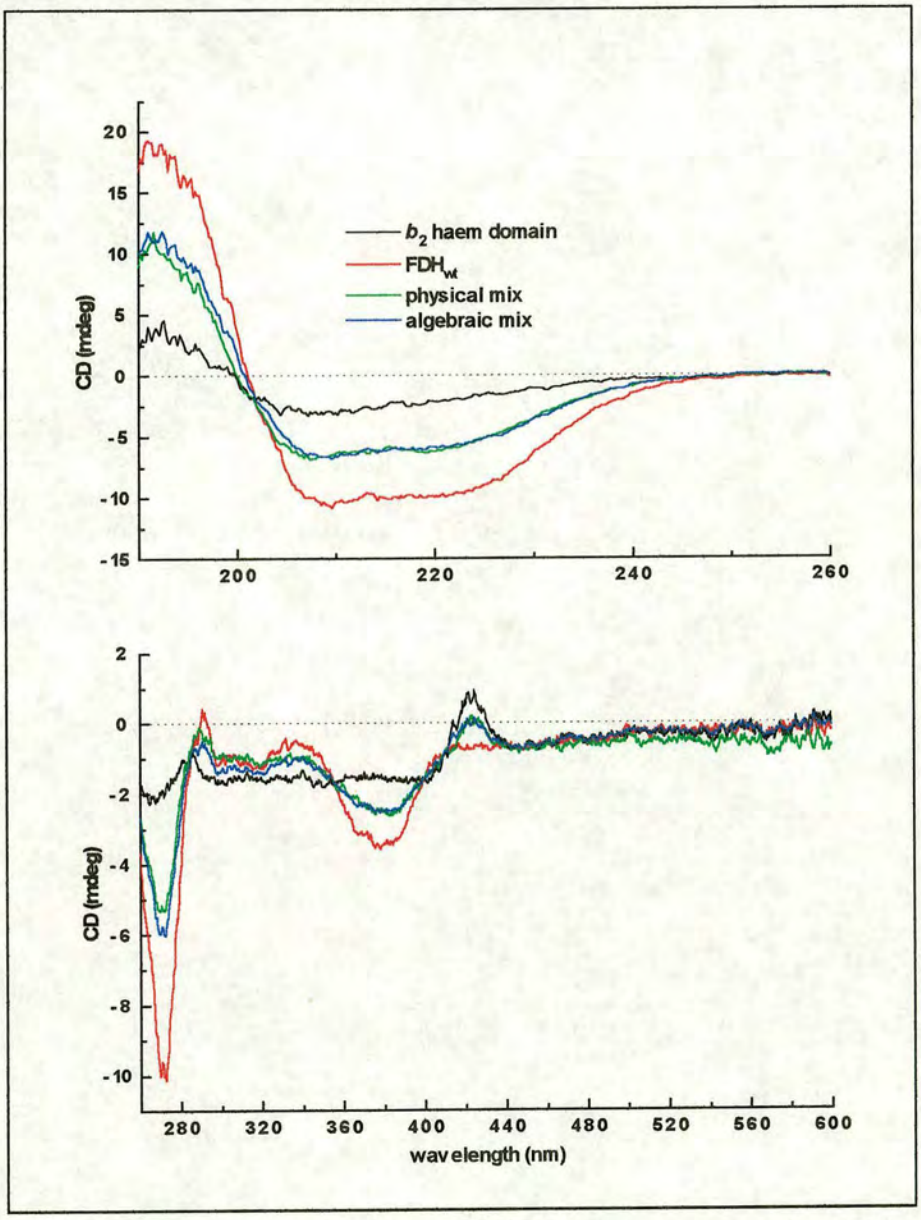

Figure 4.9. *The Far UV (top) and the Near UV/Visible (bottom) spectra for FDH_{wt} (red), b_2 cytochrome domain (black), a physical mixture of the two (green) and a predicted algebraic mixture of the two (blue). Experiments were performed at room temperature in Tris.HCl pH 7.5, I = 0.01 M.*

The FUV spectra show the differences in secondary structure possessed by the two proteins. They also indicate, by the almost superimposed physical and algebraic mixes, that there is no perturbation of this structure by inter-protein binding. The CD spectra of the FMN and haem chromophores can be seen in the NUV/Vis spectra in the region 350-500 nm. Also visible are the large differences in the region 260-280 nm caused by the different tertiary structure of the two proteins and the presence of many more tyrosine and phenylalanine residues in FDH_{wt} which give a strong signal in this region. Again, although the individual spectra are quite different, the physical and algebraic mixtures are essentially identical confirming that there is no binding between the two. This suggests that without being covalently attached, via the hinge, then the two domains have no inherent attractions for each other (Sharp *et al.*, 1994; Sharp *et al.*, 1996a & b).

The same experiment was performed with cytochrome *c* and FDH_{wt} producing similar results (Figure 4.10.). The small discrepancies between the physical and algebraic mixtures in the FUV spectra and the chromophore region of the NUV/Vis perhaps indicate a weak interaction between FDH_{wt} and cytochrome *c*. This is the standard to which the spectra of mutant enzymes was compared. The single mutant K201E was studied in the same manner and the resulting spectra are shown in Figure 4.11.

Again only small discrepancies can be seen between the spectra of the two mixtures. As with FDH_{wt} these occur around the chromophore signals in the NUV/Vis spectrum and to a lesser extent in the FUV spectrum. This suggests K201E binds very weakly to cytochrome *c*, in a similar manner to FDH_{wt}. The quadruple mutant L199E/K201E/K324A/F325E, where three glutamates have been introduced and a lysine neutralised, was expected to exhibit the strongest binding with positively charged molecules. The resulting C.D. spectra are shown in Figure 4.12.

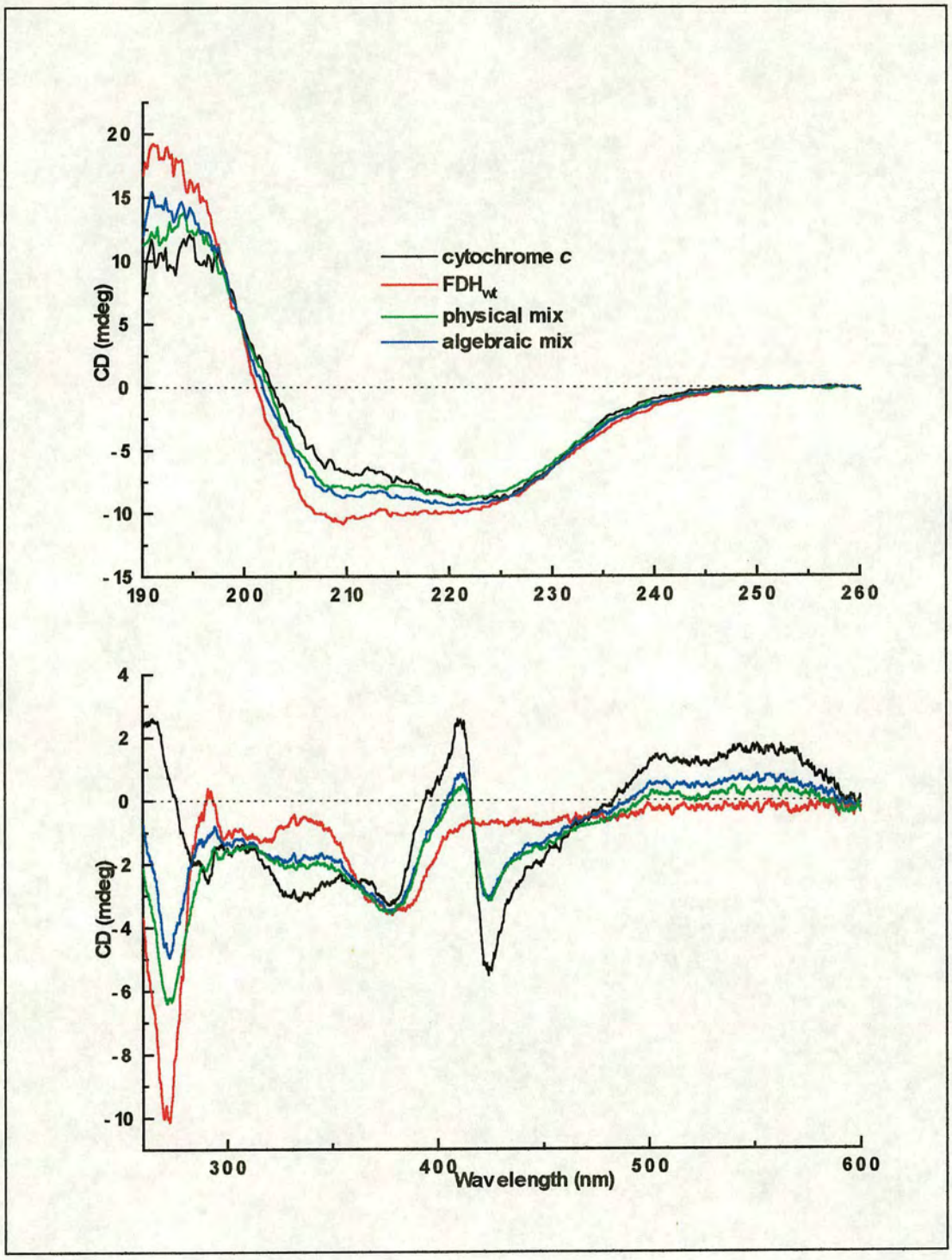

Figure 4.10. *The Far UV (top) and the Near UV/Visible (bottom) spectra for FDH$_{wt}$ (red), cytochrome c (black), a physical mixture of the two (green) and a predicted algebraic mixture of the two (blue). Experiments were performed at room temperature in Tris.HCl pH 7.5, I = 0.0 1M.*

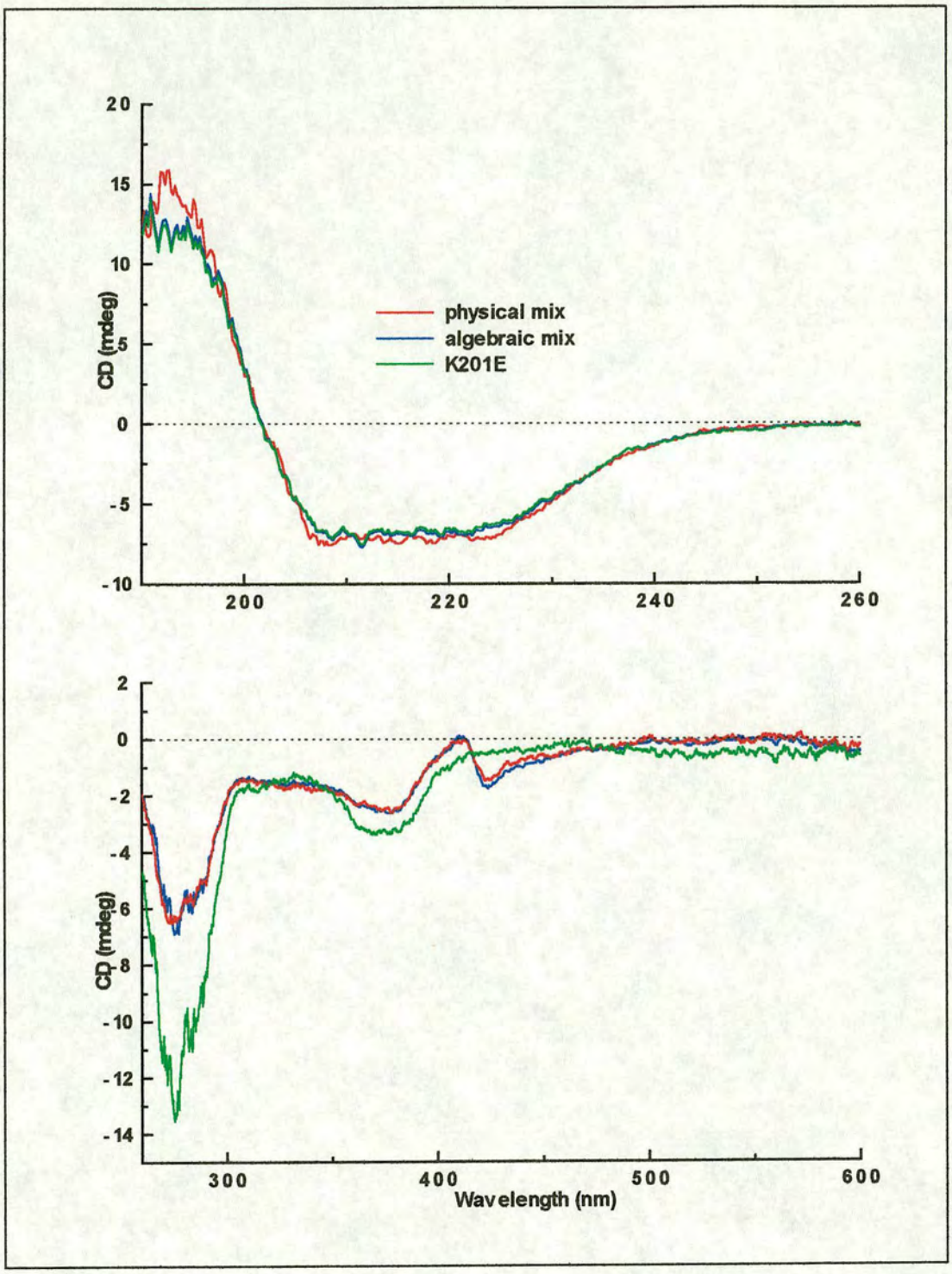

Figure 4.11. *The Far UV (top) and the Near UV/Visible (bottom) spectra for K201E (red), a physical mixture of K201E and cytochrome c (green) and a predicted algebraic mixture of the two (blue). Experiments were performed at room temperature in Tris.HCl pH 7.5, I = 0.01 M.*

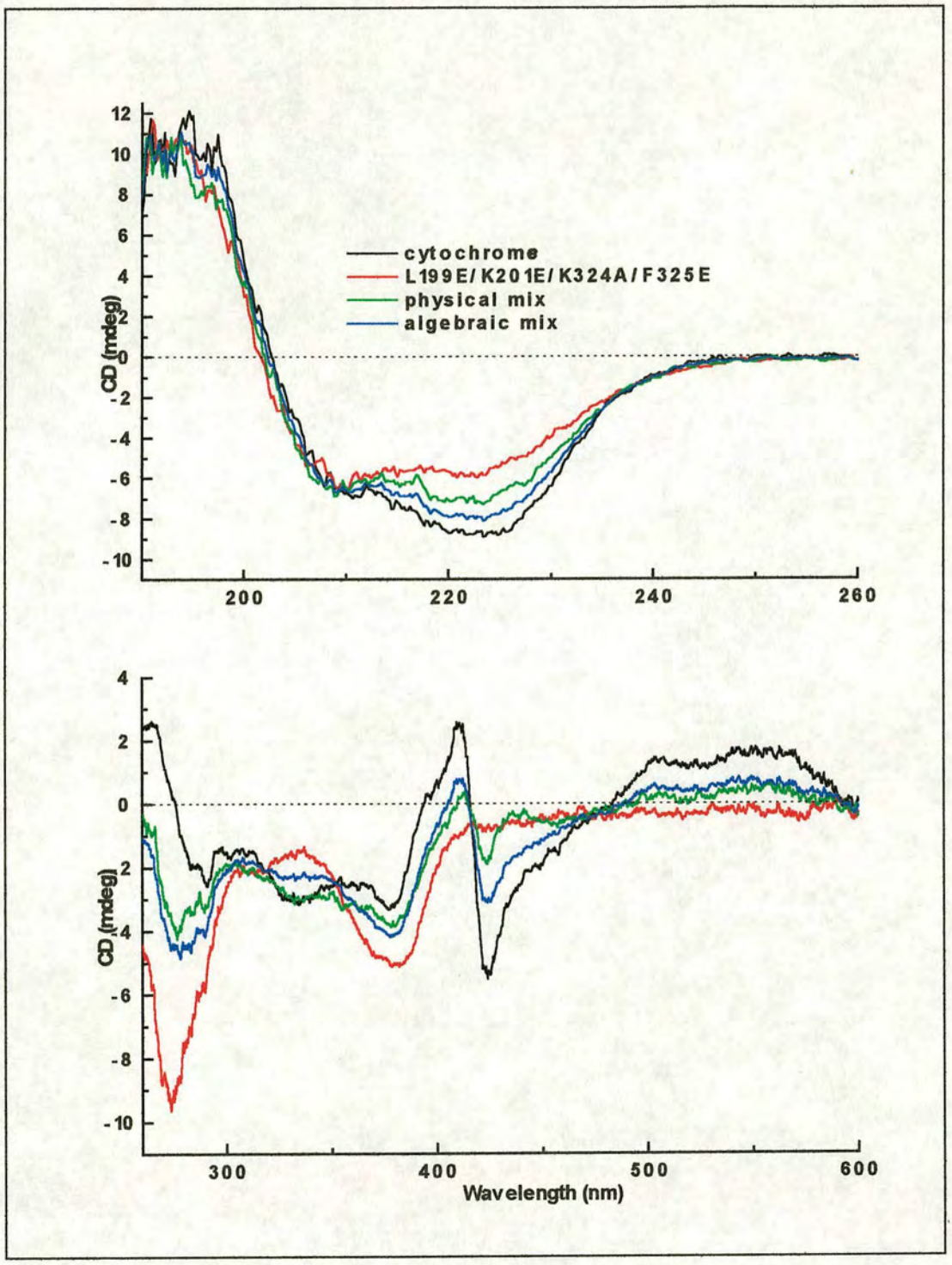

Figure 4.12. *The Far UV (top) and the Near UV/Visible (bottom) spectra for L199E/K201E/K324A/F325E (red), cytochrome c (black), a physical mixture of the two (green) and a predicted algebraic mixture of the two (blue). Experiments were performed at room temperature in Tris.HCl pH 7.5, I = 0.01 M.*

The spectra indicate that, compared to FDH_{wt} and K201E, the quadruple mutant exhibited the largest discrepancies between the spectra of the physical and predicted mixtures. The differences were observed throughout the two measured regions suggestive of significant structural changes on mixing of the two proteins. These experiments suggest that four mutations are sufficient to induce a binding interaction between cytochrome *c* and the flavin binding domain. However, because of the mutant's almost total lack of cytochrome *c* reductase activity it is hard to envisage this interaction being directly over the exposed FMN molecule of FDH.

4.2.4.2. Isothermal calorimetry.

The second technique used to study the binding between cytochrome *c* and FDH was Isothermal titration. By this method the heat energy from the titration of one protein into another is measured very accurately and used to determine; (i) if there is any interaction, and (ii) the physical parameters of the interaction. The experiments were conducted as described in Section 2.9. Cytochrome *c* at a stock concentration of 1.05 mM was titrated into solutions of FDH_{wt} or mutant enzyme and the heat of reaction was measured. Control experiments were made to determine the heat of dilution on titration of cytochrome *c* into buffer and buffer into protein mixture. Some of the traces obtained from these experiments are shown in Figure 4.13. The traces shown are for the titrations of cytochrome *c* into FDH_{wt}, K201E, K201E/K324A/F325E and L199E/K201E/K324A/F325E. The FDH_{wt} trace has been corrected for baseline drift but the others have not. These data reveal that all the titrations exhibit only the exothermic events associated with the dilution effects. There is no indication that any of the enzymes display enhanced binding with cytochrome *c*. It is surprising that the quadruple mutant did not show some effect considering its C.D. spectra. However, it is possible that aggregation of cytochrome *c* in the titration chamber interfered with the measurements.

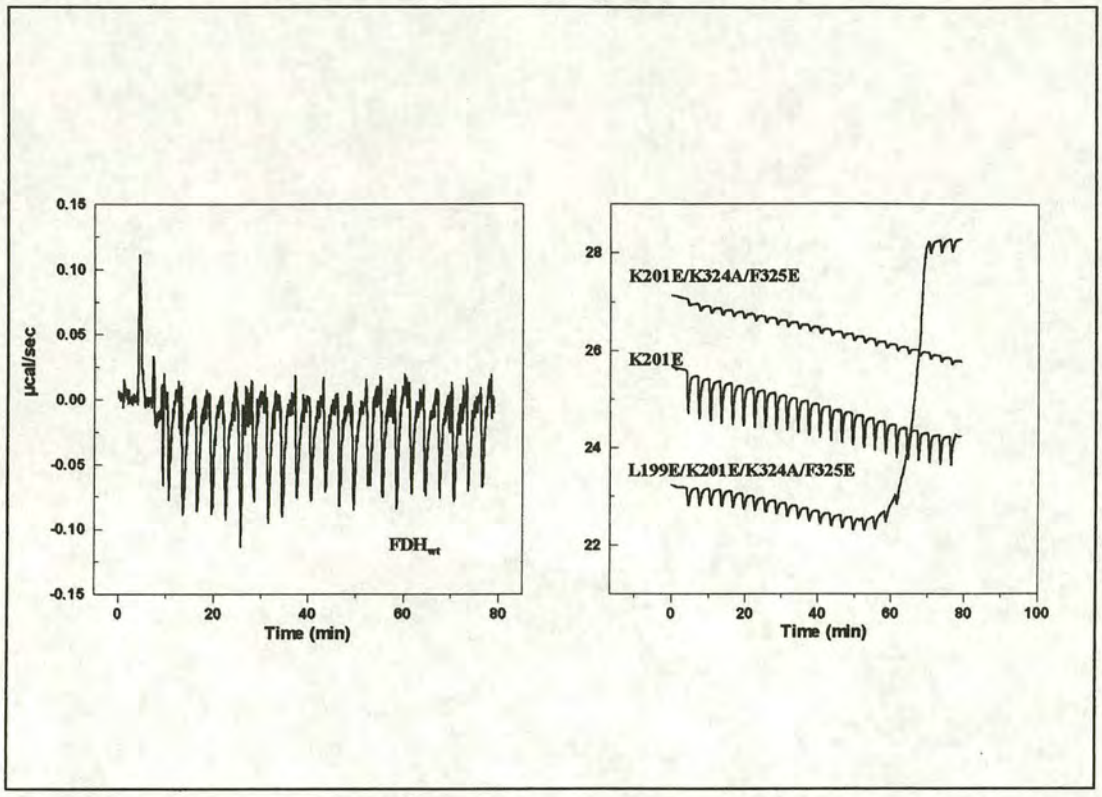

Figure 4.13. *Traces for the isothermal titrations of cytochrome c into FDH_{wt} and mutant enzymes Traces show the rate of change of heat per titration. All experiments were performed at 25°C, in Tris.HCl pH 7.5, I=0.1 M.*

4.3. Conclusion.

The thermodynamics for the electron-transfer between cytochrome *c* and FDH_{wt} are highly favourable and yet the rate of electron transfer is 10^4-fold lower than that for intact flavocytochrome b_2 to cytochrome *c*. Looking at the residues around the exposed prosthetic groups it is apparent that the positively charged and hydrophobic surface of FDH_{wt} is the complete opposite of that required to interact with the predominantly positively charged surface of cytochrome *c*. It was proposed that this electrostatic incompatibility prevents the two proteins forming an efficient electron-transfer complex. Such an energetically favourable system is ideal for a recognition-site re-design project. To improve inter-protein recognition between the proteins the positive and hydrophobic residues on FDH_{wt} were mutated to negatively charged glutamate and neutral alanine residues. These should interact more favourably with the positively charged lysine residues on cytochrome *c*. Although

these mutants have been shown to bind and react with positively charged molecules, such as $[Co(phen)_3]^{3+}$, they showed no improvement in interaction with cytochrome *c*. Steady-state and stopped-flow experiments were performed to determine the rate constants of electron-transfer but indicated that, at best, the mutants equalled the cytochrome *c* reductase activity exhibited by FDH_{wt}. Circular dichroism and isothermal calorimetry were used to study the binding of the mutant enzymes to cytochrome *c*. Neither of these methods proved conclusively that cytochrome *c* binding had been significantly improved by the mutations.

It has been shown that the electron acceptor specificity of FDH_{wt} can be altered for small inorganic complexes but not for cytochrome *c*. This suggests that a steric factor may hinder the binding of cytochrome *c* but not that of the much smaller inorganic complexes. One possible source of steric hindrance is the proteolytically sensitive loop. This loop is highly disordered in the crystal structure and so its structure and position remain unknown. It may be that the loop folds down onto the surface of FDH_{wt} when the b_2-cytochrome domain is not present. It may also be possible that the negative charge introduced in the multiple mutants actually attracts the predominantly positively charged loop. In both situations access to the FMN molecule is likely to be severely limited for cytochrome *c* whereas the smaller inorganic complexes may be much less affected. In the absence of a crystal structure for FDH_{wt}, molecular modelling techniques have been employed to investigate the position of the loop and the docking of electron acceptors on FDH_{wt} and the triple mutant. The results predict that cytochrome *c* is indeed sterically hindered by the loop and that the inorganic complexes can get significantly closer to the FMN molecule. These results are discussed in detail in Chapter 5.

5. Crystallisation and molecular modelling of the flavin binding domain.

5.1. Protein crystallisation.

5.1.1. Introduction.

To date, all structural studies of the flavin binding domain (FDH_{wt}) have assumed that the structure of this independently expressed domain will essentially be the same as that in the crystal structure of intact flavocytochrome b_2 (Xia *et al.*, 1990). The main reason for this assumption is that the structure of FDH_{wt} is that of an $\alpha 8\beta 8$-TIM barrel. This common fold, which is found in a number of other enzymes *e.g.* triose phosphate isomerase, Spinach glycolate oxidase, pyruvate kinase and trimethylamine dehydrogenase, should be stable enough to withstand the removal of the cytochrome domain. However, it seems unlikely that this is possible without at least some minor effect on the structure of FDH_{wt}, perhaps to the surface loops outside the main barrel structure. One area in particular which has been a source of much speculation is the proteolytically sensitive loop (residues 299-311 inclusive). This stretch of peptide is highly disordered and so invisible in the crystal structure of flavocytochrome b_2. A functional role for this loop has yet to be determined although it has been the focus of much recent research (Østergaard., 1997). The likelihood is that, in intact flavocytochrome b_2, the loop is held away from the exposed FMN by the presence of the cytochrome domain. Removing the cytochrome domain may allow the loop to fold back over the flavin domain obstructing the previously exposed FMN. It is possible in this scenario that the loop will be more ordered thus, providing an opportunity to determine its structure. The loop has been implicated as a steric barrier for the interaction of cytochrome *c* with FDH_{wt} (Chapter 4). A crystal structure could provide evidence for such behaviour.

5.1.2. Crystal growth and X-ray diffraction.

It has been a long term aim of the Chapman, Reid and Mathews groups to determine the crystal structure of FDH_{wt}. Until recently this has proved a formidable challenge due mainly to poor expression and consequently low purity of the enzyme, making crystal growth difficult. However, the expression system pJF118/TG1, developed by Østergaard (1997), provides a much increased yield of FDH_{wt}. This allows enzyme of high purity to be isolated using a very simple purification procedure (Section 2.2). In

a concerted effort to obtain crystals of FDH_{wt} the author joined the Mathews group for three weeks to provide them with the pJF118/TG1 expression system and to purify FDH_{wt} protein. As well as purifying FDH_{wt} a number of crystallisation experiments were set up which were performed under the supervision of Prof. F. Scott. Mathews, Washington University, St Louis, USA.

FDH_{wt} was purified from the expression system pJF118/TG1 as described in Section 2.2. Since no diffraction quality crystals had been previously produced, trials were conducted as though from scratch. With this in mind FDH_{wt} was used in conjunction with a series of preliminary crystallisation screens from Hampton Research. In this situation, where large amounts of pure protein are available, these screens allow a huge range of crystallisation conditions to be sampled based on variations in pH, salt, precipitant and buffer. The hanging drop method of crystallisation was adopted as a fast and efficient technique for this preliminary study. Section 2.6. describes in detail the approach taken. The initial results from these screens were promising, showing precipitation in many of the hanging drops and occasional "showers" of tiny crystalline fragments. Following these trials, custom made trays were prepared varying the conditions and other factors such as temperature, drop size and concentration of enzyme. By this process conditions were obtained which allowed the growth of very small crystals suitable for X-ray diffraction. The conditions in which this was achieved are described below. These were based on preliminary results from the Hampton screen Membfac™ which was originally designed for crystal growth of membrane bound proteins.

Crystal growth conditions: 175 mM Na Citrate buffer, pH 4.9.
17-18.25% PEG 4K.
8.86 mg/ml FDH_{wt}.
3µl protein + 3µl mother liquor.
4°C, undisturbed for 36 hrs.

The largest crystals at this point were approximately 0.1 x 0.3 mm. Figure 5.1. shows a photograph of two such crystals. A typical 6µl droplet produced 20 or so similar

crystals but not all of these were suitable for diffraction with some severe twinning occurring. The yellow crystals are stable at room temperature for approximately 30-60 mins before they deteriorate, rapidly losing their colour and dissolving.

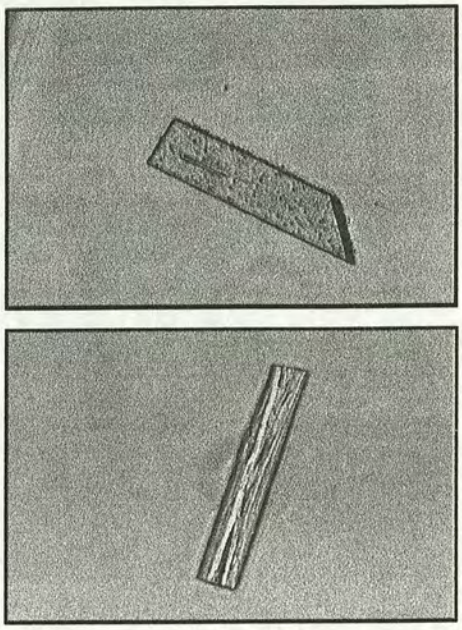

Figure 5.1. *Two FDH_{wt} crystals similar to those used for X-ray diffraction.*

Due to this instability the crystals must be frozen in liquid nitrogen prior to diffraction experiments. A good data set has been collected on a synchrotron source diffracting to 2.75Å. It is believed that this will be sufficient to solve the structure by molecular replacement with the intact flavocytochrome b_2 structure (Mathews, 1998). Refinement of this molecular replacement is ongoing and it is hoped that a solution for the structure of FDH_{wt} is close.

5.2. Molecular modelling studies.

5.2.1. Introduction.

In the absence of a crystal structure for FDH_{wt} molecular modelling techniques were employed in an attempt to predict the position of the loop. This work was carried out with Rhiannon Macfie and Prof Malcolm Walkinshaw, Institute for Cell and Molecular Biology, Edinburgh University. The modelling procedures were performed as described in Section 2.10. These studies had a number of aims:

- To suggest a structure for the proteolytically sensitive loop (N299-N311) which is disordered in the crystal structure of intact flavocytochrome b_2.
- To investigate the binding of cytochrome *c* to FDH_{wt} in order to help explain the very slow rate of electron transfer between the two.
- To perform a feasibility study on replacement of the loop by shorter stretches of peptide with the aim of removing any steric hindrance caused by the loop during interaction with electron acceptors.
- To visually explore the binding of artificial electron acceptors and correlate this with kinetic data obtained in Chapter 3.

5.2.2. Modelling of the loop.

Preliminary modelling of the loop was based on a similar loop from a yeast protein, 3GRS, which is 60% homologous to the flavocytochrome b_2 loop. The resulting structure was energy minimised but it was found that a number of the residues were in energetically unfavourable positions or illegal conformations. To improve this situation the loop was subjected to simulated annealing. This procedure produced 10 new conformations. The conformation with the lowest energy was selected for further studies. Figure 5.2. shows this model with the loop region highlighted. It forms a large outcrop over the face of FDH_{wt} blocking access to the exposed area of the FMN group. These results suggest that the loop will sterically hinder electron accepting proteins such as cytochrome *c*.

Although a good prediction of the loop's position and structure, the model is of course theoretical and so carries with it the constraints imposed upon it during the modelling process. In this case the positions of solvent molecules have not been taken into account during the energy minimisation procedure.

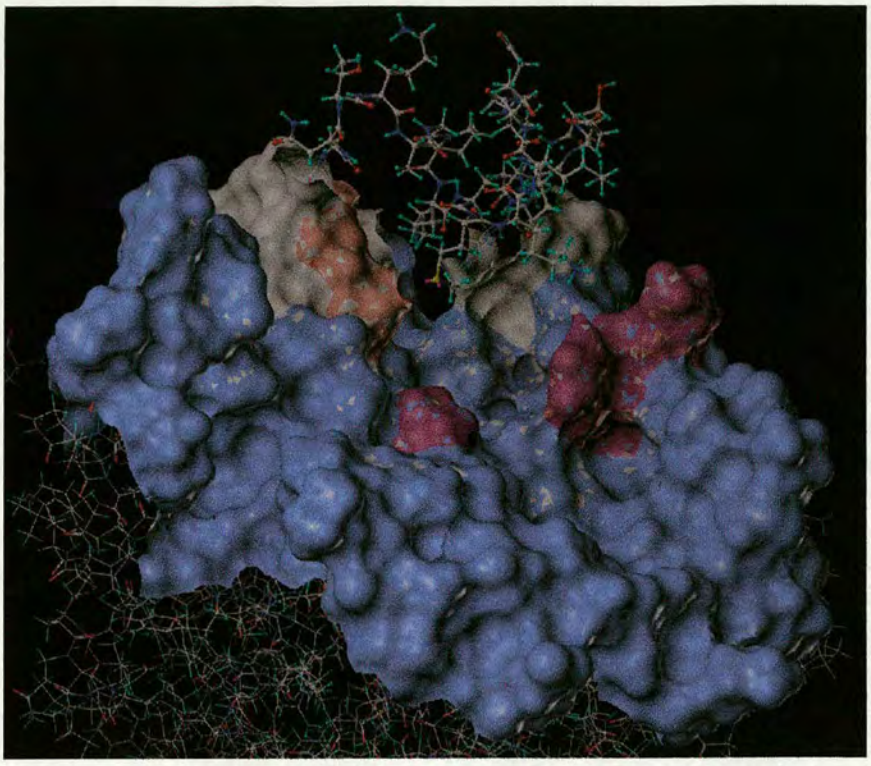

Figure 5.2. *The flavin binding domain of flavocytochrome b_2 showing the modelled position of the loop highlighted in stick representation. The residues around the loop are shown as a Connolly surface. The three mutated residues of the triple mutant (K201E/K324A/F325E) are highlighted in red.*

In effect, this means the simulations are taking place in a vacuum and cause the peptide bonds to curl up into compact structures. What the model does show however, is that it is energetically feasible for the loop to adopt a conformation which impedes the docking of cytochrome *c* at what ought to be the optimum position for electron transfer.

It was suggested that the presence of so many positively charged residues in the loop may attract it to the negatively charged face of the triple mutant. To determine if this was the case, simulated annealing was carried out on the loop in the mutant protein to study the most favourable conformations. Rigorous simulations had no effect on the conformation. Only by severely constraining the molecule could any effects be observed. As it was felt that this situation did not reflect the natural behaviour of the protein it was pursued no further.

5.2.3. Loop replacement: A feasibility study.

The modelling of the loop suggests that its conformation hinders the approach of cytochrome *c* to FDH_{wt}. A study was undertaken to determine the feasibility of replacing the loop (residues 298-317) with short stretches of polyglycine or polyalanine peptides. Although it was desirable that these should be unobtrusive, the new loop must not distort the folding or stability of the protein. The modelled loop was varied from 3 to 7 residues in length, containing alanines, glycines or an alternating mixture of the two. After initial energy minimisation (residues 291-335) it was noticed that R320 protruded from the surface of FDH into the interaction interface. The deletion was therefore extended (D298-R320) to remove this problem and energy minimisation was carried out on the various alanine and glycine peptides. The results of these experiments indicate that as the length of the loop is decreased the energy of the bond stretching and angle bending initially decreases. However, these energies increase significantly for very short peptides as the loop becomes more strained. Thus a 3 residue peptide caused a large distortion of the surrounding geometry. The optimum loop length, with minimum distortion of geometry, was found to be 7 residues. (Figure 5.3.)

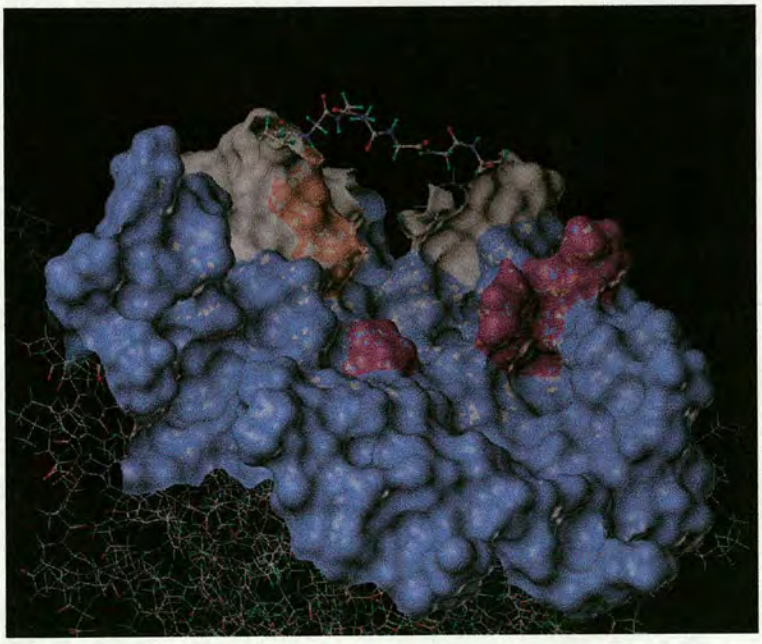

Figure 5.3. *The flavin binding domain of flavocytochrome b_2 showing the loop replaced by a 7 glycine peptide. Again the residues around the loop are part of a Connolly surface and the mutated residues, K201E/K324A/F325E, are highlighted in red.*

The energetics of this were made more favourable by using glycine residues rather than alanines or a mixture. The glycine loops were consistently shown to have a lower energy than the others. Thus molecular modelling predicts that by replacing the loop of FDH (D298-R320) with a 7 glycine peptide the protein will fold correctly. The absence of the bulk of the loop should allow the unhindered approach of cytochrome *c*. To test this hypothesis oligonucleotides are currently being made with the aim of using site-directed mutagenesis to replace the loop in the triple mutant (K201E/K324A/F325E) with a 7 glycine loop. It is expected that the combination of the loop replacement and the engineered binding site will promote the binding of cytochrome *c* and dramatically increase the cytochrome *c* reductase activity exhibited by FDH. However, if the loop swap were performed on FDH_{wt} it is possible that removal of this steric bulk would be sufficient to improve its cytochrome *c* reductase activity even in the absence of electrostatic attractions. If this is the case then it would seem that steric repulsion has been more influential than electrostatic interactions all along.

5.2.4. Cytochrome *c* binding.

Docking experiments were undertaken to determine how close cytochrome *c* could approach FMN in both FDH_{wt} and the triple mutant with the loop replacement. Figure 5.4. shows a model of the closest possible edge-to-edge distance (FMN to haem) between cytochrome *c* and FDH_{wt} with the original loop modelled in. The model suggests that the two prosthetic groups can be no closer than 22Å explaining the very slow rate of electron-transfer under these circumstances and confirming that the steric bulk of the loop does hinder the approach of cytochrome *c*. During the modelling process, as the number of residues in the loop is decreased so the edge-to-edge distance between the two prosthetic groups also decreases. By replacing the loop with 7 glycine residues this distance is decreased by 9Å to only 13Å (Figure 5.5.).

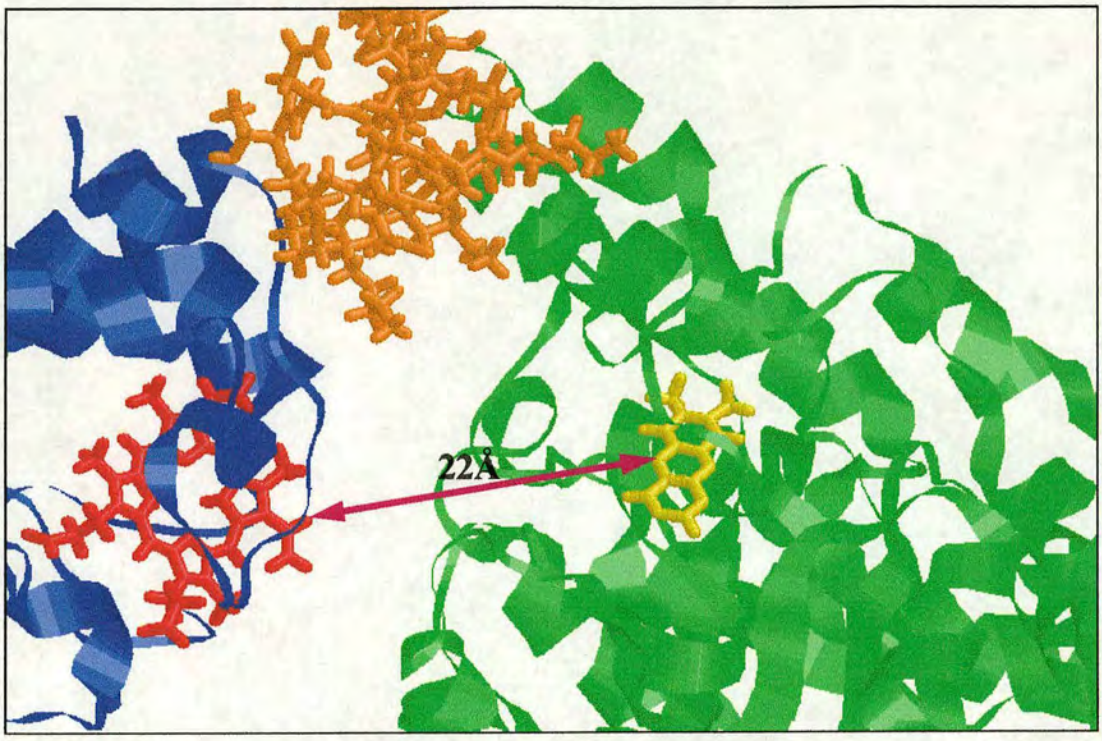

Figure 5.4. *The closest approach of cytochrome c (blue) to FDH_{wt} (green) allowed by the modelled loop (orange). The magenta arrow indicates the closest FMN (yellow) to haem (red) distance of 22Å.*

This decrease in distance of 9Å will have a significant effect on the rate of electron-transfer from haem to FMN. Estimating that, in an optimised situation, a 1.7Å change in distance between prosthetic groups could have a 10-fold effect on the rate of electron transfer (Chapman *et al.*, 1995) it is easy to see that 9Å is sufficient to significantly increase the $0.02s^{-1}$ achieved by FDH_{wt} with cytochrome *c*. Further mutagenesis experiments to incorporate the new loop in both FDH_{wt} and the triple mutant will help to determine whether distance or recognition is the most important factor in this interaction. Should cytochrome *c* reductase activity be improved equally in both cases then it is likely that steric factors are most influential.

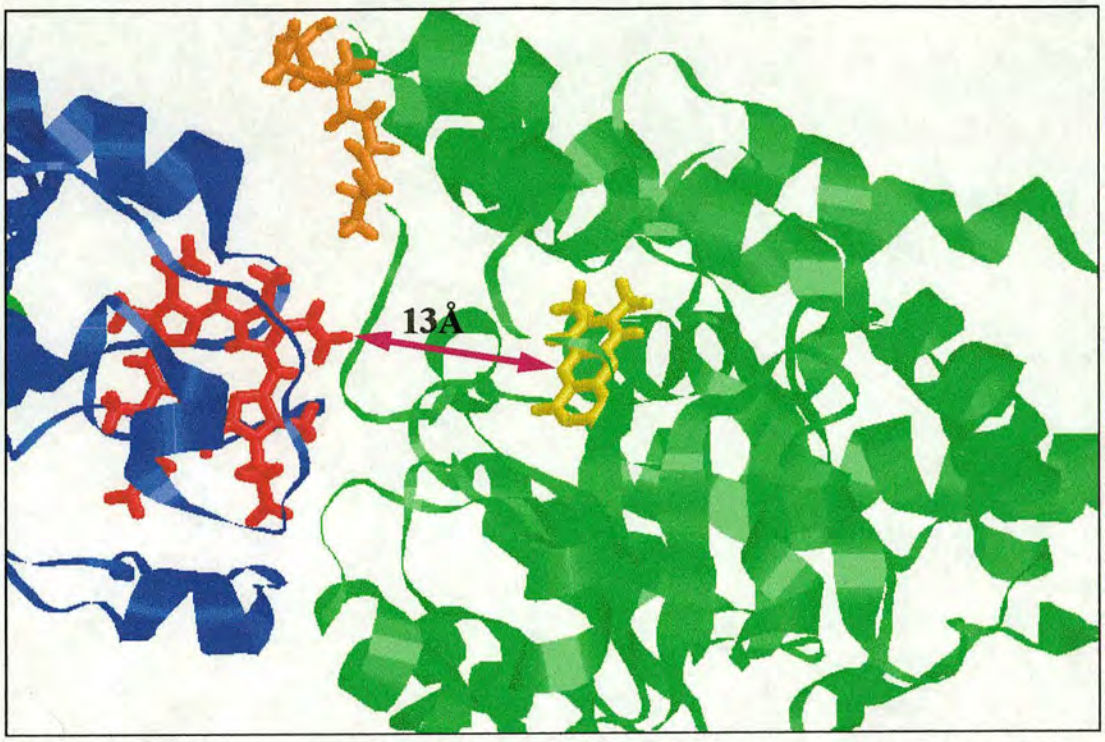

Figure 5.5. *The closest approach of cytochrome c (blue) to the triple mutant (K201E/K324A/F325E) (green) with 7 glycines (orange) replacing the proteolytically sensitive loop. The magenta arrow indicates the closest FMN (yellow) to haem (red) distance of 13Å.*

Studies of the complexation energy of the modelled interaction indicate unfavourable electrostatic repulsions between FDH_{wt} residues and those on cytochrome *c*. By creating the negatively charged binding site on the triple mutant these repulsive forces have been dramatically lowered. However, significant electrostatic repulsion remains suggesting that the binding site could be improved by introduction of further negative residues.

5.2.5. Electron acceptor binding.

The final part of the molecular modelling project was to correlate kinetic data for FMN oxidation, by inorganic molecules, with structural models. Table 5.1. shows the distance from the edge of the acceptor molecule to the edge of FMN for FDH_{wt} and the triple mutant, K201E/K324A/F325E. The table also gives values for the total energy of the docked complex as calculated during the modelling. These are not the true energies of the complexes. However, the difference between these values (ΔG) does indicate the stability of each complex relative to each other.

	FMN to acceptor. (Edge-to-edge distance)	**Total energy.** (kcal mol^{-1})
FDH_{wt} + $[Fe(CN)_6]^{3-}$	6.43Å	-32606
FDH_{wt} + $[Co(phen)_3]^{3+}$	6.67Å	20415
K201E/K324A/F325E + $[Co(phen)_3]^{3+}$	6.5Å	37.29

Table 5.1. *The closest edge-to-edge distances between the artificial electron acceptor complexes and FDH_{wt} or the triple mutant. Also shown are the comparative total energies of the docking complexes. These give an indication of the most stable complex (lowest energy) and the most unstable complex (highest energy).*

Both electron acceptors can get to within the same distance from the FMN in FDH_{wt} and the triple mutant. However, looking at the comparative energies of these complexes it is clear that electrostatics will play a part in attracting them to their minimum distance or repelling them to an intermediate distance. The most favourable interaction is for $[Fe(CN)_6]^{3-}$ with FDH_{wt} (Figure 5.6.) which has a highly negative energy due to the many electrostatic attractions present.

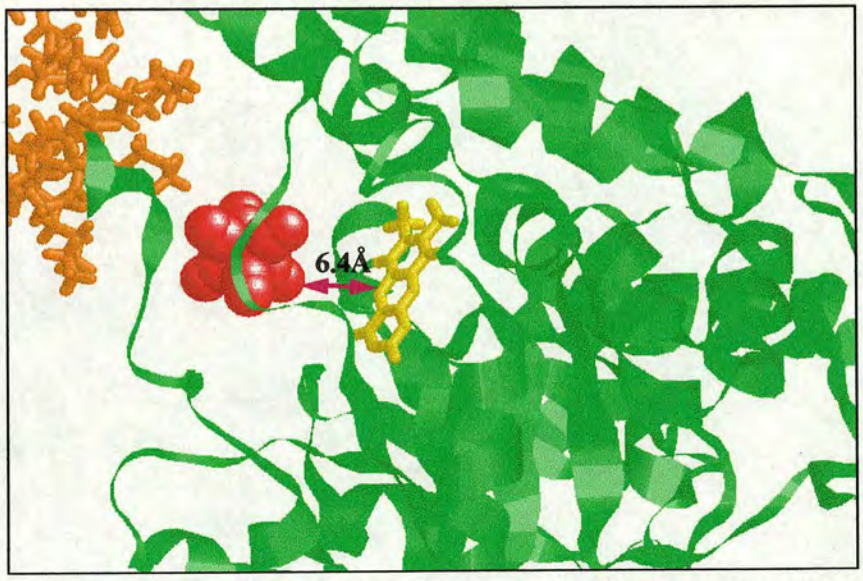

Figure 5.6. *The closest approach of $[Fe(CN)_6]^{3-}$ (red) to the FMN (yellow) of FDH_{wt} (green) as predicted by molecular modelling studies. The proteolytically sensitive loop is highlighted in orange.*

The least favourable is for $[Co(phen)_3]^{3+}$ with FDH_{wt} where many repulsive interactions exist. This very positive energy is decreased dramatically by the mutated

residues of the triple mutant giving a much less positive energy, consisting mainly of steric components, suggesting that most of the electrostatic repulsions have been removed. It would seem that there is improved binding of $[Co(phen)_3]^{3+}$ to the triple mutant (Figure 5.7.) but that it is still not as strong as the binding of $[Fe(CN)_6]^{3-}$ to FDH_{wt}.

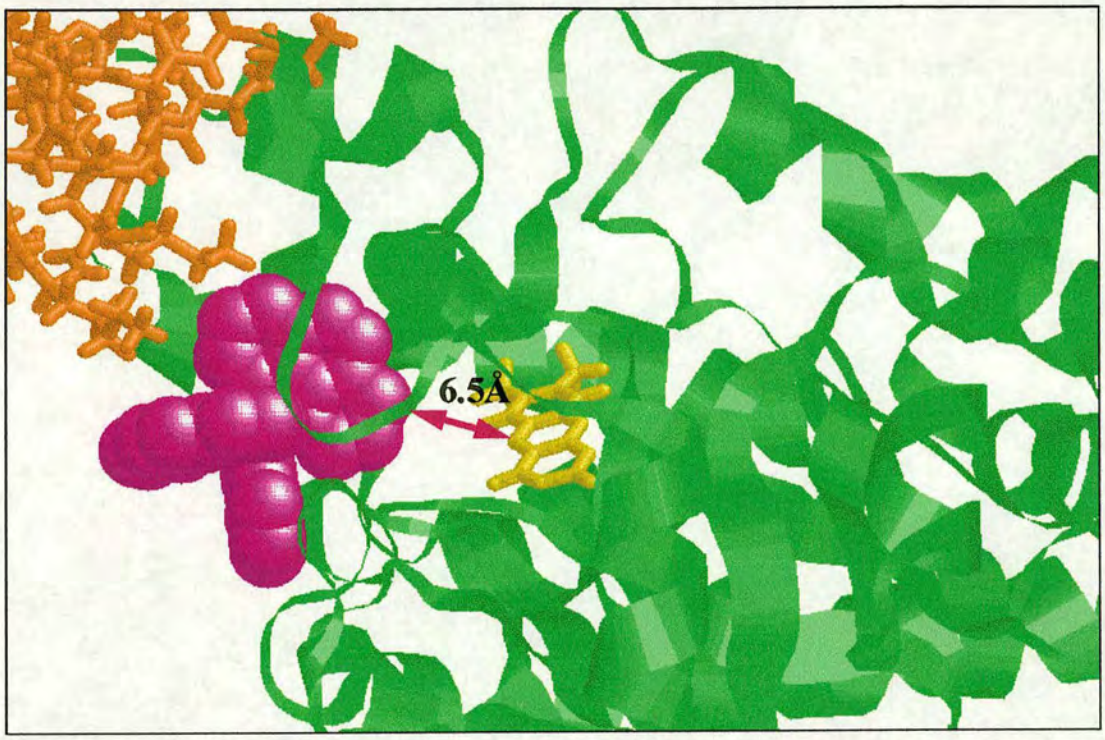

Figure 5.7. *The closest approach of* $[Co(phen)_3]^{3+}$ *(magenta) to the FMN (yellow) of K201E/K324A/F325E (green) as predicted by molecular modelling studies. The proteolytically sensitive loop is highlighted in orange.*

The distances between residues and the electron acceptor molecules shown in Table 5.2. suggest the extent to which individual residues influence docking with $[Fe(CN)_6]^{3-}$ and $[Co(phen)_3]^{3+}$.

Distances from FDH residue to electron acceptor molecule, Å		
Residue	**$[Fe(CN)_6]^{3-}$**	**$[Co(phen)_3]^{3+}$**
K201	15.0	11.1
K324	11.3	9.3
F325	5.1	3.3
K296	4.3	3.7
E201	-	6.9
A324	-	8.2
E325	-	3.4
E296	-	5.7

Table 5.2. *The distances between mutated residues on FDH and the artificial electron acceptors $[Fe(CN)_6]^{3-}$ and $[Co(phen)_3]^{3+}$ as calculated from molecular modelling experiments.*

The distances between these mutated residues and the electron acceptors indicates that some of the residues play a more important role than others. It is prudent to remember that these distances have been calculated from one predicted conformation of a complex which may have many other possible conformations. The first point to note is that the distances to $[Co(phen)_3]^{3+}$ are always shorter than those to $[Fe(CN)_6]^{3-}$ for all of the residues. This is most likely due to the greater bulk of $[Co(phen)_3]^{3+}$. In the triple mutant, K201E/K324A/F325E, it is clear that these residues are close enough to both electron acceptors to repel $[Fe(CN)_6]^{3-}$ and attract $[Co(phen)_3]^{3+}$. In particular the effect of F325E should be noted. At 5.1Å from $[Fe(CN)_6]^{3-}$ it is one of the closest residues to the acceptor and ought to repel the molecule. In the single mutant F325E the neighbouring K324 probably neutralises the glutamate. However, in the triple mutant, where K324 is mutated to an alanine, this neutralisation is overcome. It is possible then that F325 is one of the most influential residues close to the active site but only when the positive charge of K324 has been removed. The short distance from K296 to the acceptor complexes may also implicate this side-chain in protein:complex interactions. This residue is only 4.3Å from $[Fe(CN)_6]^{3-}$ and 3.7Å from $[Co(phen)_3]^{3+}$. In the double mutant, L199E/K296E, it would seem not to have a dramatic effect on rates of electron-transfer but this may be

caused by its proximity to the loop and the 4 lysine residues therein. In conjunction with the triple mutant it may yet prove to have a significant effect on the attraction of positively charged molecules.

5.3. Conclusion.

Much of the work surrounding FDH_{wt} has been based on the assumption that its crystal structure will be essentially identical to that of intact flavocytochrome b_2. Expression of large amounts of high quality protein by the system pJF118/TG1 has enabled the growth of diffraction grade crystals for the first time. A diffraction pattern has been obtained, from a synchrotron source, resolving to 2.75Å. This should enable the structure to be solved by molecular replacement with the flavin domain from the intact flavocytochrome b_2 structure. Refinements are currently under way.

In the absence of a crystal structure molecular modelling studies have been used to indicate the structure of the proteolytically sensitive loop and to investigate the binding of electron acceptors to FDH. These studies predict that the loop will sterically hinder the approach of cytochrome *c* to FDH_{wt} allowing a minimum haem-to-FMN distance (edge-to-edge) of 22Å. A theoretical model was constructed whereby the loop was replaced by a 7 glycine peptide. The model predicts that the steric bulk of the loop can be removed while still allowing the protein to fold normally. Such a mutant may allow cytochrome *c* to approach much closer to FDH, the minimum edge-to-edge distance between the haem and the FMN predicted to be only 13Å. Mutants are currently being constructed where this loop is incorporated into the triple mutant. These mutants will be characterised kinetically for cytochrome *c* reductase activity. Theoretical models of the binding conformations of artificial electron acceptors were also produced. These showed that the two molecules $[Fe(CN)_6]^{3-}$ and $[Co(phen)_3]^{3+}$ can approach the FMN group in both FDH_{wt} and the triple mutant to almost the same distance with no steric hindrance from the loop. However, the relative energies of these complexes indicate huge electrostatic repulsions between the positive charges on FDH_{wt} and $[Co(phen)_3]^{3+}$. These are significantly lower in the complex between the triple mutant and $[Co(phen)_3]^{3+}$ where negative charges have been introduced. These studies confirm the kinetic data

obtained in Chapter 3. They also suggest that residues F325 and K296 are placed very close to these inorganic molecules such that they may have a more influential role in the electrostatics of the complexes than some of the other mutated residues.

6. References.

Balme, A., Brunt, C. E., Pallister, R. L., Chapman, S. K. & Reid, G. A. (1995). Isolation and characterisation of the flavin-binding domain of flavocytochrome b_2 expressed independently in *Escherichia coli*. *Biochem. J.* **309**, 601-605.

Bell, C., Uhrinova, S., Barlow, P.N., Chapman, S.K. & Reid, G.A. (1996). Domain Mobility in flavocytochrome b_2: Fact or Fiction?. *Flavins and Flavoproteins*. 12th Int Symposium. Calgary University Press.

Beratan, D. N., Onuchic, J. N., Betts, J. N., Bowler, B. E. & Gray, H. B. (1990). Electron tunneling pathways in ruthenated proteins. *J. Am. Chem. Soc.* **112**, 7915-7921.

Beratan, D. N., Betts, J. N. & Onuchic, J. N. (1991).Protein electron transfer rates set by the bridging secondary and tertiary structure. *Science*. **252**, 1285-1288.

Bernard, H. -U., Remaut, E., Hershfield, M. V., Das, H. K. & Helinski, D. R. (1979). Construction of plasmid cloning vehicles that promote gene expression from the bacteriophage p_L promoter. *Gene*. **5**, 59-76.

Bjerrum, M. J., Casimiro, D, R., Chang, I-J., Di Billio, A. J., Gray, H. B., Hill, M. G., Langen, R., Mines, G. A., Skov, L. K., Winkler, J. R. & Wuttke, D. S. (1995). Electron transfer in ruthenium modified proteins. *J. Bioeng. Biomem.* **27**, 295-302.

Brunt, C. E., Miles, C. S., Pallister, R. L., Reid, G. A. & Chapman, S. K. (1990). Isolation and characterisation of the flavin domain of flavocytochrome b_2 expressed independently in *E. coli*. *Flavins and Flavoproteins*. 10th Int Symposium.

Capeillère-Blandin, C. (1975). Flavocytochrome b_2: Simulation studies of the electron transfer reactions among the prosthetic groups. *Eur. J. Biochem.* **56**, 91-101.

Casimiro, D. R., Wong, L-L., Colón, J. L., Zewert, T. E., Richards, J. H., Chang, I-J., Winkler, J. R. & Gray, H. B. (1993). Electron transfer in ruthenium/zinc porphyrin derivatives of recombinant human myoglobins. Analysis of tunneling pathways in myoglobin and cytochrome *c*. *J. Am. Chem. Soc.* **115**, 1485-1489.

Chapman, S. K., Daff, S. & Munro, A. W. (1997). Haem: The most versatile redox centre in biology? *Structure and Bonding*. **88**, 40-70.

Chapman, S. K. & Mount, A. R. (1995). Electron transfer in proteins. *Natural Product Reports*. 93-100.

Chapman, S. K., Reid, G. A., Daff, S., Sharp, R. E., White, P., Manson, F. D. C. & Lederer, F. (1994). Flavin to haem electron transfer in flavocytochrome b_2. *Biochem. Soc. Trans.* **22**, 713-718.

Chapman, S. K., Reid, G. A., Bell, C., Short, D. & Daff, S. (1996). Flavocytochrome b_2: an ideal system for studying protein-mediated electron transfer. Flavoproteins: Structures and Mechanisms, *Biochem. Soc. Trans.* 73-77.

Chapman, S. K., Watson, A. D. & Sykes, A. G. (1983)a. Kinetic studies on 1:1 electron transfer reactions involving blue copper proteins. Part 6. *J. Chem. Soc. Dalton. Trans.* 2543-2548.

Chapman, S. K., Sanemasa, I. & Sykes, A. G. (1983)b. Kinetic studies on 1:1 electron transfer reactions involving blue copper proteins. Part 7. *J. Chem. Soc. Dalton. Trans.* 2549-2553.

Chapman, S. K., White, S. A. & Reid, G. A. (1991). Flavocytochrome b_2. *Adv. Inorg. Chem.* **36**, 257-301

Chen, L., Durley, R., Poliks, B. J., Hamada, K., Chen, Z., Mathews, F. S., Davidson, V. L., Satow, Y., Huizinga, E., Vellieux, F. M. D. & Hol, W. G. J. (1992). Crystal structure of an electron transfer complex between Methylamine dehydrogenase and Amicyanin. *Biochemistry*. **31**, 4959-4964.

Crowl, R., Seamans, C., Lomedico, P. & McAndrew, S. (1985). Versatile expression vectors for high-level synthesis of cloned gene products in *Escherichia coli*. *Gene*. **38**, 31-38.

Daff, S., Ingledew, W. J., Reid, G. A. & Chapman, S. K. (1996)a. New insights into the catalytic cycle of flavocytochrome b_2. *Biochemistry*. **35**, 6345-6350.

Daff, S., Sharp, R. E., Short, D. M., Bell, C., White, P., Manson, F. B. C., Reid, G. A. & Chapman, S. K. (1996)b. Interaction of cytochrome *c* with flavocytochrome b_2. *Biochemistry*. **35**, 6351-6357.

Daff, S., Manson, F. D. C., Reid, G. A. & Chapman, S. K. (1994). Strategic manipulation of the substrate specificity of *Saccharomyces cereviciae* flavocytochrome b_2. *Biochem. J.* **301**, 829-834.

Fisher, A. J., Raushel, F. H., Baldwin, T. O. & Rayment, I. (1995). Three dimensional structure of bacterial Luciferase from *Vibrio harveyi* at 2.4Å resolution. *Biochemistry*. **34**, 6581-6586.

Fox, K. M. & Karplus, P. A. (1993). Stirring new interest in an old enzyme: crystal structure of old yellow enzyme. *Flavins and Flavoproteins*; Proceedings of the eleventh international symposium on flavins and flavoproteins. (Yagi, K., Ed.). Walter de Gruyter, Berlin, 381-390.

Fürste, J. P., Pansegrau, W., Frank, R., Blöcker, H., Scholz, P., Bagdasarian, M. & Lanka, E. (1986). Molecular cloning of the plasmid RP4 primase region in a multi-host-range *tac*P expression vector. *Gene*. **48**, 119-131.

Ghisla, S. & Massey, V. (1989). Mechanisms of flavoprotein catalysed reactions. *Eur. J. Biochem*. **181**, 1-17.

Ghisla, S. & Massey, V. (1986). New flavins for old: Artificial flavins as active site probes of flavoproteins. *Biochem. J.* **239**, 1-12.

Gondry, M. & Lederer, F. (1996). Functional properties of the histidine-aspartate ion pair of flavocytochrome b_2 (L-lactate dehydrogenase): Substitution of Asp282 with asparagine. *Biochemistry*. **35**, 8587-8594.

Gray, K. A., Davidson, V. L. & Knaff, D. B. (1988). Complex formation between methylamine dehydrogenase and amicyanin from *Paracoccus denitrificans*. *J. Biol. Chem*. **263**, 13987-13990.

Guiard, B. & Lederer, F. (1979). The "cytochrome b_5 fold" : Structure of a novel protein superfamily. *J. Mol. Biol*. **135**, 639-650.

Hake, R., McLendon, G., Corin, A. & Holzschu, D. (1992). Redox dependent molecular recognition in proteins: Site-Directed Mutagenesis suggests that cytochrome *c* oxidation state governs binging and recognition to cytochrome *c* peroxidase. *J. Am. Chem. Soc*. **114**, 5442-5443.

Hazzard, J. T., McDonough, C. A. & Tollin, G. (1994). Intramolecular electron transfer in yeast flavocytochrome b_2 upon $1e^-$ photooxidation of the fully reduced enzyme: Evidence for redox state control of haem-flavin communication. *Biochemistry*. **33**, 13445-13454.

Iwatsubo, M. & Difranco, A. (1965). *Bull Soc Chim Biol*. **47**, 891-910.

Iwatsubo, M., Mevel-Ninio, F. & Labeyrie, F. (1977). Rapid Kinetic Studies of Partial Reactions in the Heme Free Derivative of L-lactate Cytochrome *c* Oxidoreductase (Flavocytochrome b_2); the Flavodehydrogenase function. *Biochemistry*. **16**, 3558-3566.

Janin, J. (1997). The kinetics of protein-protein recognition. *PROTEINS: Structure, Function and Genetics*. **28**. 153-161.

Jucovic, M. & Hartley, R. W. (1996). Protein-protein interaction: A genetic selection for compensating mutations at the barnase-barstar interface. *Proc. Natl. Acad. Sci. USA*. **93**, 2343-2347.

Koppenol, W. H. & Margoliash, E. (1982). The asymmetric distribution of charges on the surface of Horse cytochrome *c*. *J. Biol. Chem*. **257**, 4426-4437.

Kunkel, T. A. (1985). Rapid and efficient site-specific mutagenesis without phenotypic selection. *Proc. Natl. Acad. Sci. USA*. **82**, 488-492.

Labeyrie, F. (1982). Interactions and electron transfer between the flavodehydrogenase and the cytochrome b_2 components of yeast flavocytochrome b_2. *Flavins and flavoproteins*. (Massey, V. & Williams, C. H., ed). Elsevier North Holland Inc, 823-832.

Labeyrie, F., Beloeil, J-C. & Thomas, M-A. (1988). Evidence by NMR for mobility of the cytochrome domain within flavocytochrome b_2. *Biochimica et Biophysica Acta*. **953**, 134-141.

Larsson, S. (1998). Electron transfer in proteins. *BBA*. **1365**, 294-300.

Lederer, F. (1978). Sulphite binding to a flavodehydrogenase, cytochrome b_2 from baker's yeast. *Eur. J. Biochem*. **88**, 425-431.

Lederer, F. (1991). Flavocytochrome b_2. *Chemistry and biochemistry of flavoenzymes*. (Müller, F., ed), vol 2. 479-488.

Lederer, F., Belmouden, A. & Gondry, M. (1996). The chemical mechanism of flavoprotein-catalysed α-hydroxy acid dehydrogenation: a mutational analysis. *Biochem. Soc. Trans*. **24**, 77.

Lederer, F. & Guiard, B. (1980). The protein superfamily of b5 like cytochromes. *Biomedical press. Methods in peptide and protein sequence analysis*. (Chr. Birr, Ed). 433-438.

Lim, L. W., Shamala, N., Mathews, F. S., Steenkamp, D. J., Hamlin, R. & Xuong, N. H. (1986). Three-dimensional structure of the iron-sulphur flavoprotein trimethylamine dehydrogenase at 2.4Å resolution. *J. Biol. Chem.* **261**, 15140-15146.

Lindqvist, Y. & Brändén, C-I. (1989). The active site of Spinach Glycolate Oxidase. *Journal of Biological Chemistry*. **264**, 3624-3628.

Macheroux, P., Massey, P. & Thiele, D. J. (1991). Expression of Spinach Glycolate Oxidase in *Saccharomyces cerevisiae*: Purification and charaterisation. *Biochemistry*. **30**, 4612-4619.

Malatesta, F., Antonini, G., Sarti, P. & Brunori, M. (1995). Structure and function of a molecular machine: cytochrome *c* oxidase. *Biophys. Chem.* **54**, 1-33.

Marcus, R. A. (1956). On the theory of oxidation-reduction reactions involving electron transfer. *J. Chem. Phys.* **24**, 966-978.

Marcus, R. A. (1965). On the theory of electron transfer reactions. VI. Unified treatment for homogeneous and electrode reactions. *J. Chem. Phys.* **43**, 679-701.

Massey, V. (1994). Activation of molecular oxygen by flavins and flavoproteins. *J. Biol. Chem.* **269**, 22459-22462.

Massey, V. & Hemmerich, P. (1980). Active site probes of flavoproteins. *Biochem. Soc. Trans.* **8**, 246-257.

Massey, V. & Palmer, G. (1966). On the existence of spectrally distinct classes of flavoprotein semiquinones. A new method for the quantitative production of flavoprotein semiquinones. *Biochemistry*. **5**, 3181-3189.

Massey, V., Muller, F., Feldberg, R., Schuman, M., Sullivan, P. A., Howell, L. G., Mayhew, S. G., Matthews, R. G. & Foust, G. P. (1969). The reactivity of flavoproteins with sulphite. *The Journal of Biological Chemistry*. **244**, 3999-4006.

Mathews, F. S., Levine, M. & Argos, P. (1972). Three dimensional fourier synthesis of calf liver cytochrome b_5 at 2.8Å resolution. *J. Mol. Biol.* **64**, 449-464.

Mathews, F. S. (1985). The structure, function and evolution of cytochromes. *Progress in Biophysics and Molecular Biology*. **41**, 1-56.

Matthew, J. B., Weber, P. C., Salemme, F. R. & Richards, F. M. (1983). Electrostatic orientation during electron transfer between flavodoxin and cytochrome *c*. *Nature*. **301**, 169-171

Mauk, A. G., Coyle, C. L., Bordingnon, E. & Gray, H. B. (1979). *J. Amer. Chem. Soc*. **101**, 5054-5056.

Mauk, M. R., Barker, P. D. & Mauk, A. G. (1991). Proton linkage of complex formation between cytochrome *c* and cytochrome b_5: Electrostatic consequences of protein-protein interactions. *Biochemistry*. **30**, 9873-9881.

Mauk, M. R., Ried, L. S. & Mauk, A. G. (1982). Spectrophotometric analysis of the interaction between cytochrome b_5 and cytochrome *c*. *Biochemistry*. **21**, 1843-1846.

McLendon, G. (1988). Long-distance electron transfer in proteins and model systems. *Acc. Chem. Res*. **21**, 160-167.

McLendon, G. (1991). *Metal Ions in Biological Systems*. **27**. (Sigel, H. & Sigel, A., Ed). Decker. New York.

McLendon, G. & Hake, R. (1992). Interprotein electron transfer. *Chem. Rev*. **92**, 481-490.

Mevel-Ninio, M., Risler, Y. & Labeyrie, F. (1977). Structural studies of yeast flavocytochrome b_2: Cooperative roles of the a and b globules in the formation of the flavin binding sites. *Eur. J. Biochem*. **73**, 131-140.

Mewies, M., Basran, J., Packman, L. C., Hille, R. & Scrutton, N. S. (1997). Involvement of a flavin iminoquinone methide in the formation of 6-hydroxyflavin mononucleotide in Trimethylamine dehydrogenase: A rationale for the existence of 8a-methyl and C6-linked covalent flavoproteins. *Biochemistry*. **36**, 7162-7168.

Miles, C. S., Rouviere-Fourmy, N., Lederer, F., Mathews, F. S., Reid, G. A., Black, M. T. & Chapman, S. K. (1992). Tyr-143 facilitates interdomain electron transfer in flavocytochrome b_2. *Biochem. J*. **285**, 187-192.

Moir, J. W. B., Baratta, D., Richardson, D. J. & Ferguson, S. J. (1993). The purification of a *cd*-type nitrite reductase from and the absence of a copper-type nitrite reductase from the aerobic denitrifier Thiosphaera pantotropha; the role of pseudoazurin as an electron donor. *Eur. J. Biochem*. **92**, 377-385.

Moir, J. W. B. & Ferguson, S. J. (1994). Properties of a *Paracoccus denitrificans* mutant deleted in cytochrome c_{550} indicate that a copper protein can substitute for this cytochrome in electron transport to nitrite, nitric oxide and nitrous oxide. *Microbiology*. **140**, 389-397.

Moser, C. C., Keske, J. M., Warncke, K., Farid, R. S. & Dutton, P. L. (1992). Nature of biological electron transfer. *Nature*. **355**, 796-802.

Moser, C. C., Page, C. C., Farid, R. & Dutton, P. L. (1995). Biological electron transfer. *J. Bioeng. Biomem*. **27**, 263-274.

Munro, A. W. & Lindsay, J. G. (1996). Bacterial cytochromes P-450. *Mol. Microbiol*. **20**, 1115-1125

Nar, H., Messerschmidt, A., Huber, R., van de Kamp, M. & Canters, G. W. (1991). X-ray crystal structure of the two site specific mutants His35Gln and His35Leu of azurin from *Pseudomonas aeruginosa*. *J. Mol. Biol*. **218**, 427-447.

Østergaard, L. H. (1997). Engineering Oxidase Activity in Flavocytochrome b_2. Ph.D., University of Edinburgh.

Paglia, E. & Sirani, C. (1957). *Gazzetta*. **81**, 1125.

Pelletier, H. & Kraut, J. (1992). Crystal structure of a complex between electron transfer partners, cytochrome *c* peroxidase and cytochrome *c*. *Science*. **258**, 1748-1755.

Pompon, D. (1980). Flavocytochrome b_2 from baker's yeast. Computer simulation studies of a new kinetic scheme for intramolecular electron transfer. *Eur. J. Biochem*. **106**, 151-159.

Reid, G. A., White, S., Black, M. T., Lederer, F., Mathews, F. S., & Chapman, S. K. (1988). Probing the active site of flavocytochrome b_2 by site-directed mutagenesis. *Eur. J. Biochem*. **178**, 329-333.

Robertson, D. E., Farid, R. S., Moser, C. C., Urbauer, J. L., Mulholland, S. E., Pidikiti, R., Lear, J. D., Wand, A. J., DeGrado, W. F. & Dutton, P. L. (1994). Design and synthesis of multi-haem proteins. *Nature*. **368**, 425-432.

Rodgers, K. K., Pochapsky, T. C. & Sligar, S. G. (1988). Probing the mechanism of macromolecular recognition: The cytochrome b_5-cytochrome *c* complex. *Science*. **240**, 1657-1659.

Salemme, F. R. (1976). A cytochrome *c*-b_5 intermolecular complex. *J. Mol. Biol.* **102**, 563-568.

Sambrook, J., Fritsch, E. F. & Maniatis, T. (1989a). *Molecular Cloning, A laboratory manual*. 2nd Edn, (Nolan, C., Ed), 123. 3vols, Cold Spring Harbor Laboratory Press, Cold Spring Harbor.

Scrutton, N. S. (1994). α/β Barrel Evolution and the modular assembly of enzymes:Emerging trends in the Flavin oxidase/dehydrogenase family. *BioEssays*. **16**, 115-122.

Sharp, E. R., Chapman, S. K. & Reid, G. A. (1996)b. Modulation of flavocytochrome b_2 intraprotein electron transfer via an interdomain hinge region. *Biochem. J.* **316**, 507-513.

Sharp, E. R., Chapman, S. K. & Reid, G. A. (1996)a. Deletions in the Interdomain Hinge region of flavocytochrome b_2: Effects on Intraprotein electron transfer. *Biochemistry*. **35**, 891-899.

Sharp, R. E., White, P., Chapman, S. K. & Reid, G. A. (1994). Role of the interdomain hinge of flavocytochrome b_2 in intra- and inter-protein electron transfer. *Biochemistry*. **33**, 5115-5120.

Sharp, K. A. & Honig, B. (1990). Electrostatic interactions in macromolecules: Theory and applications. *Annu. Rev. Biophys. Biophys. Chem*. **19**, 301-332.

Sinclair, R. (1998). The kinetic characterisation of *Rhodotorula graminis* L-mandelate dehydrogenase.. Ph.D., University of Edinburgh.

Smékal, O., Yasin, M., Fewson, C. A., Reid, G. A. & Chapman, S. K. (1993). L-Mandelate dehydrogenase from *Rhodotorula graminis*: comparisons with the L-lactate dehydrogenase (flavocytochrome b_2) from *Saccharomyces cerevisiae*. *Biochem. J.* **290**, 103-107.

Sykes, A. G. (1985). Structure and electron transfer reactivity of the blue copper protein plastocyanin. Chem. Soc. Rev. 14, 283-315.

Sykes, A. G. (1988). Electron transfer in biological systems. *Chemistry in Britain*. **June**, 551-554.

Tegoni, M., Silvestrini, M. C., Labeyrie, F. & Brunori, M. (1984). A temperature jump study of the electron transfer reactions in *Hansenula anomala* flavocytochrome b_2. *Eur. J. Biochem.* **140**, 39-45.

Tiede, D. M., Vashishta, A-C. & Gunner, M. R. (1993). Electron transfer kinetics and electrostatic properties of the *Rhodobacter sphaeroides* reaction center and soluble *c* cytochromes. *Biochemistry*. **32**, 4515-4531.

Tye, B., Chien, J., Lehman, I., Duncan, B. & Warner, H. (1978). Uracil incorporation: A source of pulse-labeled DNA fragments in the replication of *Escherichia coli* chromosome. *Proc. Natl. Acad. Sci. USA*. **75**, 233-237.

van de Kamp, M., Silvestrini, M. C., Brunori, M., Beeumen, J., Hali, F. C. & Canters, G. W. (1990). Involvement of the hydrophobic patch of azurin in the electron transfer reactions with cytochrome c_{551} and nitrite reductase. *Eur. J. Biochem.* **194**, 109-118.

Vergères, G. & Waskell, L. (1995). Cytochrome b_5, its functions, structures and membrane topology. *Biochimie*. **77**, 604-620.

Walsh, C. (1980). Flavin coenzymes: At the crossroads of biological redox chemistry. *Acc. Chem. Res.* **13**, 148-155.

Wendoloski, J. J., Matthew, J. B., Weber, P. C. & Salemme, F. R. (1987). Molecular dynamics of a cytochrome *c*-cytochrome b_5 electron transfer complex. *Science*. **238**, 794-796.

White, S. A., Black, M. T., Reid, G. A. & Chapman, S. K. (1989). The role of the C-terminal tail of flavocytochrome b_2. *Biochem. J.* **263**. 849-853.

White, P., Manson, F. D. C., Brunt, C. E., Chapman, S. K. & Reid, G. A. (1993). The importance of the interdomain hinge in intramolecular electron transfer in flavocytochrome b_2. *Biochem. J.* **291**, 89-94.

Williams, P. A., Fülöp, V., Leung, Y-C., Chan, C., Moir, J. W. B., Howlett, G., Ferguson, S. J., Radford, S. E. & Hadju, J. (1995). Pseudospecific docking surfaces on electron transfer proteins as illustrated by pseudoazurin, cytochrome c_{550} and cytochrome cd_1 nitrite reductase. *Nature Structural Biology*. **2**, 975-982.

Winkler, J. R. & Gray, H. B. (1992). Electron transfer in ruthenium-modified proteins. *Chem. Rev.* **92**, 369-379.

Winkler, J. R. & Gray, H. B. (1997). Electron tunneling in proteins: the role of the intervening medium. *JBIC*. **2**, 399-404.

Winkler, J. R., Malmström, B. G. & Gray, H. B. (1995). Rapid electron injection into multisite metalloproteins: intramolecular electron transfer in cytochrome oxidase. *Biophys. Chem*. **54**, 199-209.

Xia, Z.-x. & Mathews, F.S, (1990). Molecular Structure of Flavocytochrome b_2 at 2.4Å Resolution. *J. Mol. Biol*. **212**, 837-863.

Yasin, M. & Fewson, C. A. (1993). L(+)-Mandelate dehydrogenase from *Rhodotorula graminis*: purification, partial characterisation and identification as a flavocytochrome b_2. *Biochem. J*. **293**, 455-460.

7. Appendix.

7.1. Derivation of the Michaelis-Menten Equation.

$$E + S \underset{k_2}{\overset{k_1}{\rightleftharpoons}} ES \xrightarrow{k_3} E + P$$

E = enzyme, S = substrate, P = product, ES = enzyme:substrate complex.

rate of formation of ES = k_1 [E][S]
rate of dissociation of ES = (k_2 + k_3) [ES]
V = catalytic rate = k_3 [ES]
k_3 = turnover number *i.e.* the number of substrate molecules converted into product by an enzyme molecule in a unit time when under saturating conditions = k_{cat}

Assumption One.
Under steady-state conditions the intermediate concentrations remain unchanged as long as the rates of formation and breakdown remain equal.

$\therefore$ k_1 [E][S] = (k_2 + k_3) [ES]

[ES] = k_1[E][S] / k_2 + k_3

K_m = Michaelis constant = k_2 + k_3 / k_1

[ES] = [E][S] / K_m

[E_o] = [E] + [ES] and so [E] = [E_o] - [ES]

Assumption Two.
[S] >> [E]

$\therefore$ rate is independent of [S] $\therefore$ [S_o] can be ignored and we need only substitute for [E].

[ES] = ([E_o] - [ES]) [S] / K_m solve for [ES] gives

[ES] = [E_o] x ([S] / [S] + K_m)

remembering that V = catalytic rate = k_3 [ES] then,

V = k_3 [E_o] ([S] / [S] + K_m) = Michaelis-Menten Equation.

V_{max} = maximal rate when enzyme sites are saturated with substrate i.e. [S] >> K_m and so [S] / [S] + K_m

$\therefore$ V_{max} = k_3[E_o] = k_{cat}[E_o]

V = k_{cat} [S][E_o] / [S] + K_m

When [S] << Km then,

V = [S] k_{cat} [E_o] / K_m

and so the rate is directly proportional to [S].

When $[S] = K_m$ then,

$$V = V_{max} / 2 \quad = k_{cat} / 2$$

$\therefore$ $K_m =$ (i) [S] at which half the enzyme active sites are full
(ii) $k_2 + k_3 / k_1$

If $k_2 >> k_3$ then dissociation of ES to E + S is more rapid than to E + P

$\therefore$ $K_m = k_2 / k_1$

The dissociation constant for ES is given by,

$$K_{ES} = [E][S] / [ES] = k_2 / k_1$$

$\therefore$ K_m is equal to the dissociation constant of ES

$$K_m = K_{ES}.$$

When this condition is met K_m is a measure of the strength of the ES complex.

A high K_m indicating weak binding i.e. $k_1 << k_2$ with ES tending towards dissociation.

A low K_m indicating strong binding i.e. $k_1 >> k_2$ with ES forming a tight complex.

7.2. Debye-Hückel theory.

The Debye-Hückel limiting law (1) uses the notion of an ionic atmosphere to calculate the activity coefficient of an ion in solution. From this the free energy (ΔG) of the ion can be determined.

$$\textbf{(1)} \qquad \log f_i = -Az_i^2\sqrt{I}$$

z_i = charge on the ion.

f_i = activity coefficient of ion.

I = ionic strength of solution.

A = a temperature and solvent dependent constant;

for water at 25°C A = 0.5115 $mole^{-½}l^{½}$.

combining (1) with the Brønsted kinetic relation produces the Debye-Brønsted equation (2)

$$\textbf{(2)} \qquad \log k_2 = \log k_o + 2Az_+z_-\sqrt{I}$$

k_2 = second order rate constant.

k_o = second order rate constant at I 0

Plotting $\log k_2$ vs $\sqrt{I}$ generates a straight line allowing calculation of the charges involved in the reaction between two species. The limiting law assumes that the ions are point charges and ignores interactions between reactants and solvent. This is particularly important when studying macromolecules. It should also be noted that the equation does not fit satisfactorily to data obtained at high ionic strength being best suited to that range considered suitable for an ideal solution. However, the extended Debye-Brønsted equation (3) introduces a term which is linearly dependent on ionic strength.

$$\textbf{(3)} \qquad \log k_2 = \log k_o + 2Az_+z_-\sqrt{I} - BI$$

In this case a plot of $\log k_2$ vs $\sqrt{I}$ generates a parabola which fits more accurately to high ionic strength data. The coefficient, B, has no simple definition but is designed to compensate for deviations due to short-range solvent interactions and the increasing dominance of the ionic radius at high ionic strength.

(Robinson & Stokes, 1973; Perlmutter-Hayman, 1959)

7.3. Bacterial strains.

Strain.	Genotype.	Reference.
pop2136	F⁻*lac*⁻, λcI857N7N53ΔH1	(Bernard *et al.*, 1979)
BW313	*dut*⁻,*ung*⁻,*thi*-1,*rel*A,*spo*T1/F'lysA	(Tye *et al.*, 1978; Kunkel, 1985)
TG1	*sup*E,Δ(*hsd*M-*mcr*B), *thi*, Δ(*lac-pro*AB), [F', *tra*D36, proAB+, *lacI*^{q}*lac*ZΔM15]	(Sambrook *et al.*, 1989)

7.4. Plasmids.

Plasmid.	Relevant features.	Reference.
pGR401	Gene encoding flavocytochrome b_2 cloned in shuttle vector with a f1 ori (amp^R)	(Reid *et al.*, 1988)
pJF118EH	*tac* promoter and the repressor gene *lacI*^{q} (amp^R)	(Fürste *et al.*, 1986)
pRC23	λp_L promoter (amp^R)	(Crowl *et al.*, 1985)

The resistance conferred by the plasmid is indicated in brackets.

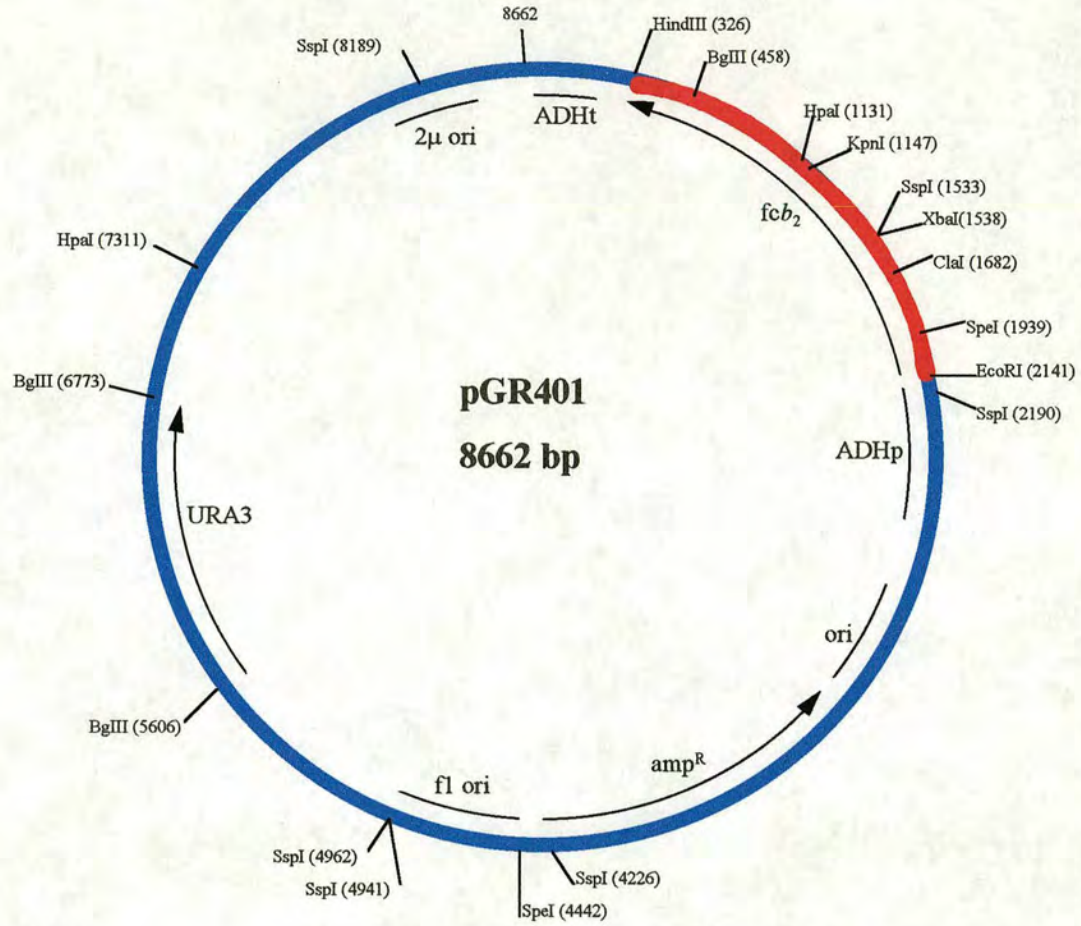

Map of the yeast expression vector pGR401. The flavocytochrome b_2 coding sequence (fcb_2) (red) lies between the promoter (ADH_p) and the terminator (ADH_t) of the *S. cerevisiae* ADH1 gene. The plasmid contains origins of replication and selectable markers for maintenance in *E. coli* (amp^R) and yeast (URA3). The presence of the origin of replication from bacteriophage f1 (f1 ori) allows isolation ssDNA for site-directed mutagenesis and DNA sequence determination. Restriction enzyme sites occurring only once within the fcb_2 gene are indicated with their position on the plasmid (Reid et al., 1988).

The plasmid is used for the production of ssDNA in TG1 under ampicillin selection and for production of uracil-containing ssDNA in BW313 also under ampicillin selection.

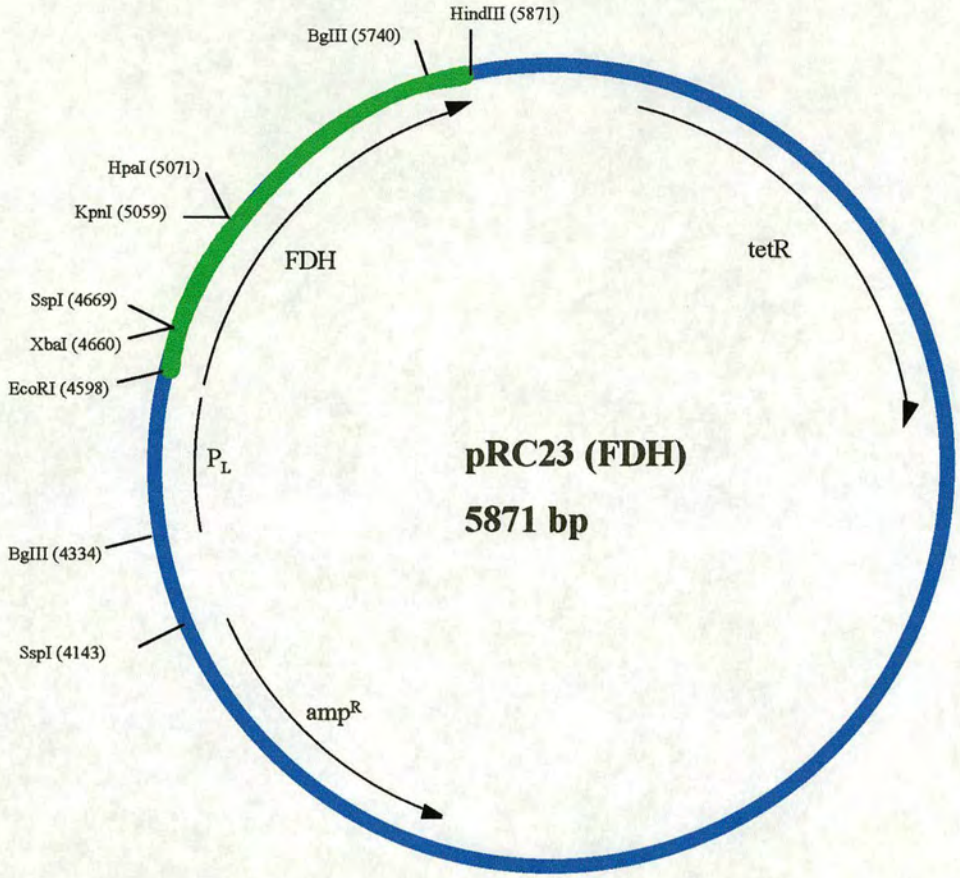

Map of *E. coli* expression vector pRC23(FDH). The coding sequence for the flavin binding domain of flavocytochrome b_2 (FDH) (green) is cloned downstream of the bacteriophage λP_L promoter. The plasmid contains origin of replication and selectable markers for maintenance in *E. coli*. Restriction enzyme sites occurring only once within the FDH gene are indicated with their position on the plasmid (Crowl et al., 1985).

It is used for the expression of FDH in pop2136 or NF1, both of which overproduce the λcI repressor. Expression is induced by growth at 42°C under ampicillin selection.

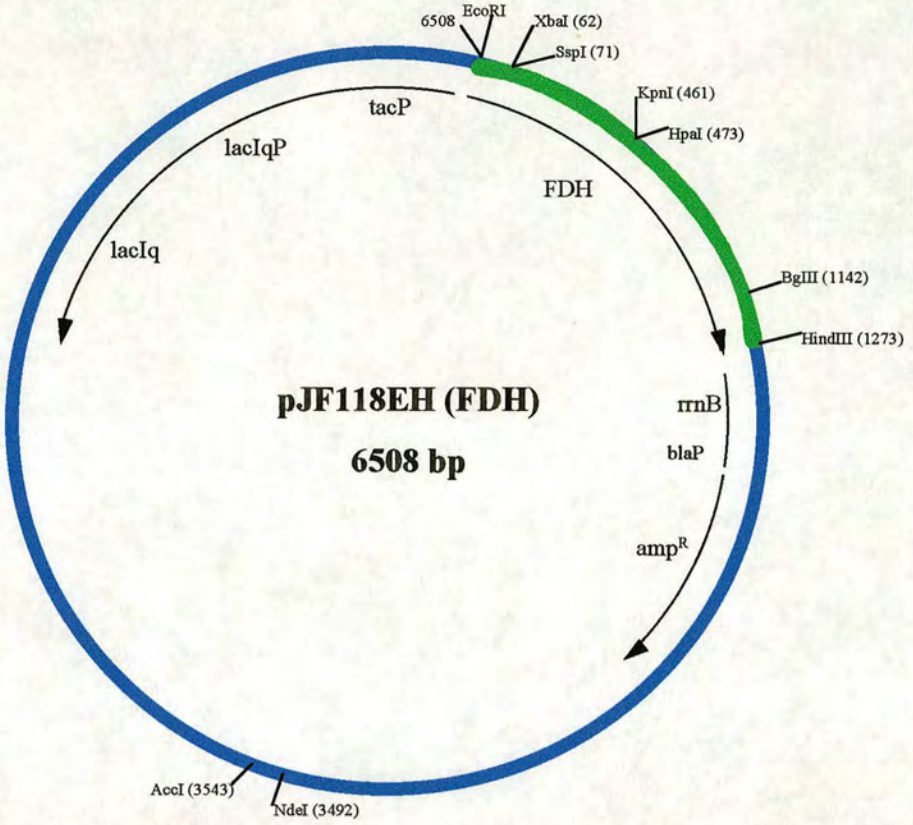

Map of the *E. coli* expression vector pJF118EH(FDH). The FDH coding sequence (green) is cloned downstream of the *tac* hybrid promoter. The plasmid also contains origin of replication and selectable markers for maintenance in *E. coli*. The presence of the *lacI*^{q} gene renders the use of the plasmid independent of repressor overproducing strains. rrnB represents part of the *E. coli* rrnB operon containing the gene for 5S RNA and its 2 transcriptional terminators. This prevents interference between transcription and replication. Restriction enzyme sites occurring only once within the FDH gene are indicated with their position on the plasmid (Fürste et al., 1986).

It is used for expression of FDH in TG1 under ampicillin selection. Expression was induced by addition of 1mM IPTG.

7.5. Conferences and courses attended.

Courses attended.

Post-graduate lectures:

NMR, Intellectual property, Molecular vibrations, Introduction to the crystallographic database, Essentials of EPR.

Department of Chemistry colloquia.

Conferences attended.

Biochemical Society meeting:

University College, Dublin, Ireland (1995).

12th International symposium on Flavins and Flavoproteins:

University of Calgary, Calgary, Canada (1996) (abstract and poster presented).

FLAPS Network meeting:

Dourdan, France (1997).

Inorganic chemistry group meetings:

Firbush point field centre, Scotland (1996-1998) (as speaker and poster presented).

7.6. Publications.

The following publication has resulted from work reported in this thesis:

Forced evolution of a cytochrome *c* recognition site on the flavin binding domain of flavocytochrome b_2.

Welsh, F. E., Kohler, L., Rivers, S. L., Reid, G. A. & Chapman, S. K. (1996). *Flavins and Flavoproteins*. 12th Int Symposium. University of Calgary Press. 587-590.

A Reprint can be found at the back of this thesis.

Forced Evolution of a Cytochrome *c* Recognition Site on the Flavin Domain of Flavocytochrome b_2

F. E. Welsh[1], L. Kohler[2], S.L.Rivers[2], G. A. Reid[2], S. K. Chapman[1]

[1]Department of Chemistry, [2]Institute of Cell and Molecular Biology, University of Edinburgh, Edinburgh, EH9 3JJ, Scotland, UK
email skc08@holyrood.ed.ac.uk

INTRODUCTION

Flavocytochrome b_2 (L-lactate, cytochrome *c* oxidoreductase) from *S.cerevisiae* is a soluble component of the mitochondrial intermembrane space where it catalyses the transfer of electrons from L-lactate to cytochrome *c*. The crystal structure of this homotetramer has been solved (1) and clearly shows that each subunit (M_r=57500) is composed of two distinct domains (fig. 1). The smaller domain contains a b-type haem and the larger a flavin mononucleotide (Flavin domain, FDH). The route of electron transfer in this system is, L-lactate→Flavin→b_2 haem→cytochrome *c*.

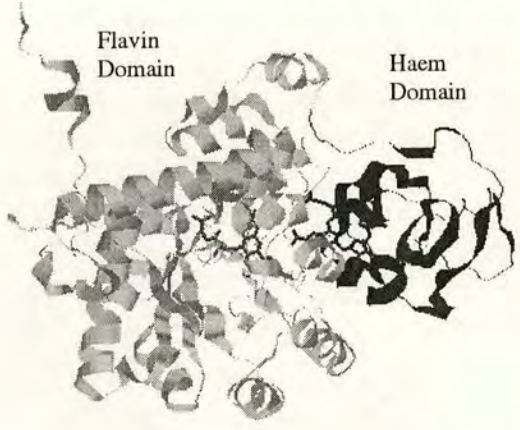

FIG 1. Single subunit of Flavocytochrome b_2.

The Flavin domain has been independently expressed in *E.coli* (2) and characterised kinetically in terms of its behaviour with cytochrome *c* (3). The results from these studies (table 1)

TABLE I. Steady-state kinetic data, 25°C, pH 7.5, Buffer Tris/HCl, I=0.1M.

	k_{cat}/s^{-1}	
	Ferricyanide	Cytochrome c
Flavocytochrome b_2	400	207
FDH	273	0.02

indicate that the rate of electron transfer to the artificial electron acceptor ferricyanide is similar within error to that for intact flavocytochrome b_2. However, electron transfer from FDH to cytochrome *c* (horse heart) is 10^4 fold slower. Thus the haem domain in flavocytochrome b_2 is essential for efficient physiological electron transfer to cytochrome *c*. The driving force for electron transfer between the flavin domain and cytochrome *c*, as deduced from redox potentials, is greater than 1/3 volt. Why then should such an energetically favoured reaction be so slow?

A possible answer is that recognition between the two proteins is practically non-existant preventing the proteins coming together and thus an otherwise rapid electron transfer is impeded. Therefore, the aim of this research is to utilise protein engineering methods to build an enhanced recognition site for cytochrome *c* on FDH and so improve the rate of electron transfer.

Hydrophobic and positively charged surface residues around the exposed flavin mononucleotide face of FDH will be mutated to glutamate residues. This will create a negative triangle of charge complementary to the already well studied positively charged area around the exposed haem edge of cytochrome *c* (fig. 2). This induced interaction should cause the electron transfer rate to

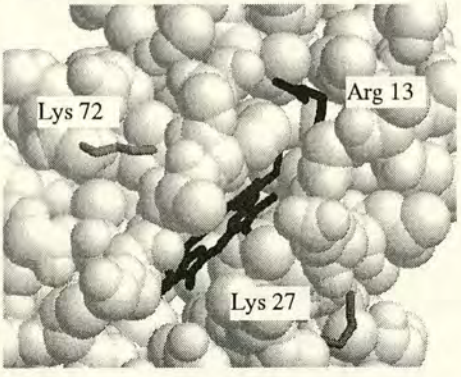

FIG 2. The exposed haem edge of cytochrome c

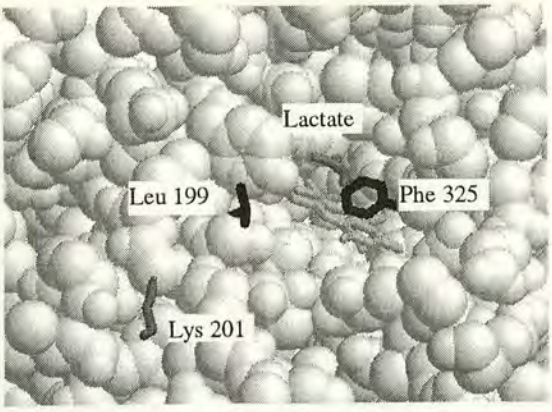

FIG 3. The exposed Flavin of FDH.

increase. Molecular graphics programmes, Rasmol, Sybyl and Frodo, were utilised to determine the residues most suitable for site directed mutagenisis. The three residues, shown in fig. 3, Phe325, Lys201 and Leu199 will be mutated to give the single, double and triple mutants. Obviously the distance between the two prosthetic groups in the complex plays an important role in determining the rate of electron transfer.The face on FDH which exposes the flavin will allow the two to come as close as possible. Estimates from theoretical models suggest that the minimum edge to edge, haem to flavin distance will be 10Å. This is comparable to the internal haem to flavin distance in intact flavocytochrome b_2. Mutant enzymes will be characterised using steady-state kinetic methods to determine the effect on the rate of cytochrome *c* reduction. We believe gross structural changes caused by these mutations are unlikely. However, should they occur they should be detectable by following the rate of electron transfer with ferricyanide and comparing these values to those for the normal FDH domain.

RESULTS

The first mutant, F325E, has been investigated in terms of its steady state behaviour with cytochrome *c* (horse heart), (fig 4). The data suggests that this mutation has no effect on the rate of electron transfer. Analysis of the kinetics is complicated by the reoxidation rate of cytochrome *c* which is similar to its rate of reduction by F325E. Thus all assays must be performed under a nitrogen atmosphere.

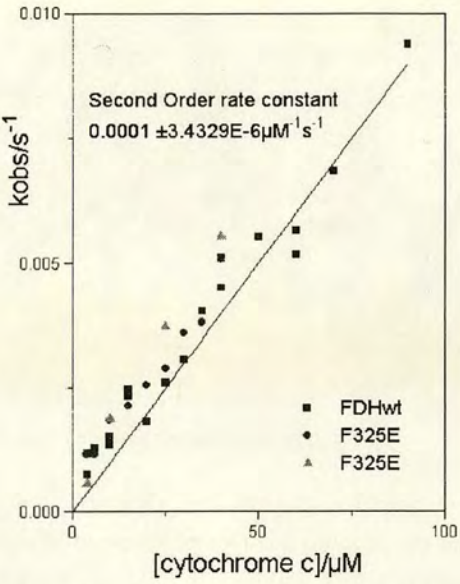

FIG 4. Graph of $k_{cat}(s^{-1})$ vs [cytochrome c]/μM . Experiments were carried out in Tris/HCl buffer, pH 7.5 (I=0.1M), [L-lactate]=5mM.25°C

CONCLUSION

Although F325E has shown no improvement in the rate of electron transfer to cytochrome *c* we believe that recognition between proteins is a major factor in rate determination. Thus the remaining mutants will be fully characterised in an attempt to define its importance.

REFERENCES.

1. Z.X.Mia, F.S.Mathews, 1990, J. Mol. Biol, **212**, 837.

2. C.E.Brunt, C.S.Miles, R.L.Pallister, G.A.Reid, S.K.Chapman, 1990, Flavins and Flavoproteins.

3. A.Balme, C.E.Brunt, R.L.Pallister, S.K.Chapman, G.A.Reid, 1995, Biochem. J, **309**, 601.